GRADING OF FATTY LIVER DISEASE & CLASSIFICATION OF FOCAL LIVER LESIONS USING ULTRASOUND IMAGES

A Dissertation submitted in fulfillment of the requirements for the Degree
of

MASTER OF ENGINEERING

in

Electronic Instrumentation & Control Engineering

Submitted by

Harish Kothari
801451007

Under the Guidance of

Dr. Jitendra Virmani
Assistant Professor, EIED

&

Mr. Nirbhowjap Singh
Assistant Professor, EIED

2016

Electrical and Instrumentation Engineering Department
Thapar University, Patiala
(Declared as Deemed-to-be-University u/s 3 of the UGC Act., 1956)
Post Bag No. 32, Patiala – 147004
Punjab (India)

Declaration

I hereby certify that the work which is presented in dissertation entitled, "Grading of fatty liver disease & classification of focal liver lesions using ultrasound images", in partial fulfillment of the requirements for the award of the degree of Master of Engineering in Electronic Instrumentation & Control, submitted to Electrical & Instrumentation Engineering Department of Thapar University, Patiala is as authentic record of my own work carried under the supervision of Dr. Jitendra Virmani and Mr. Nirbhowjap Singh. It refers others researcher's work which is duly listed in the reference section. The matter contained in this dissertation has not been submitted, neither in part nor in full to any other degree to any other university or institute except as reported in the text and references.

Harish Kothari
801451007

Place: Patiala
Date: 22/08/16

It is certified that the above statement made by the student is correct to the best of my/our knowledge and belief.

Date: 22/8/16

Dr. Jitendra Virmani
Electrical and Instrumentation Engineering Department
Thapar University, Patiala - 147004

Date: 22/08/16

Mr. Nirbhowjap Singh
Electrical and Instrumentation Engineering Department
Thapar University, Patiala - 147004

Countersigned by:

Dr. Ravinder Agarwal
Professor and Head
Electrical and Instrumentation Engineering Department
Thapar University
Patiala – 147004

Dr. S.S. Bhatia
Dean of Academic Affairs
Thapar University
Patiala –147004

Acknowledgement

Foremost of all, I wish to express my gratitude to **Dr. Jitendra Virmani,** Assistant professor, Electrical and Instrumentation Engineering Department, Thapar University Patiala, and **Mr. Nirbhowjap Singh,** Assistant Professor, Electrical and Instrumentation Engineering Department, Thapar University Patiala, who have been a tremendous mentors and teachers. This thesis would not have been possible without their constant encouragement and support. Their constructive criticism and passion for perfection has had a profound impact in my life. I have always enjoyed their way of explaining things in a simple and elegant manner. I am truly very fortunate to have the opportunity to work with them. I found their guidance to be extremely valuable.

I owe my deepest thanks to **M.B. Subramanya**, research scholar, Biomedical Instrumentation Laboratory, Indian Institute of Technology Roorkee, Uttarakhand for providing the diffused liver ultrasound images.

I thank all those reviewers who helped me to improve the quality of my publication through their valuable suggestions.

I am thankful to Thapar University-Patiala, Punjab, for providing constant patronage and support, I am thankful to all who have contributed directly or indirectly to this work.

Lastly, I would like to thank my parents for their years of unyielding love and encourage. They have always wanted the best for me and I admire their determination and sacrifice.

(Harish Kothari, 801451007)

List of Abbreviations

AFV	Additive feature vector
ARFV	Additive ratio features vector
ASM	Angular second moment
CAC	Computer-aided classification
CAD	Computer aided diagnosis
CFV	Combined features vector
CON	Contrast
COR	Correlation
CP	Cluster prominence
CRC	Colorectal cancer
CT	Computed tomography
CRFV	Combined ratio features vector
DCT	Discrete Cosine Transform
DE	Difference entropy
DM	Diagonal Moment
DROI	Diaphragm region of interest
DROI-M	Diaphragm region of interest-mean
DROI-R	Diaphragm region of interest-range
DV	Difference variance
ENT	Entropy
FLD	Fatty liver diseases
FOS	First order statistics
FS	Fuzzy sugeno
FV	Feature vector
GA	Genetic algorithm

GA-*k*NN	Genetic algorithm-*k* nearest neighbor
GLC	Gray level co-occurrence
GLCM	Gray level co-occurrence matrix
GLCM-M	Gray level co-occurrence matrix-mean
GLCM-R	Gray level co-occurrence matrix-range
GLRL	Gray level run matrix
HEM	Hemangioma
HCC	Hepatocellular carcinoma
ICA	Individual class accuracy
IDM	Inverse difference moment
IFC1	Information measures of correlation 1
IFC2	Information measures of correlation 2
IROI	Inside region of interest
IROI-M	Inside region of interest-mean
IROI-R	Inside region of interest-range
***k*-NN**	*k*-nearest neighbor
LHCC	Large hepatocellular carcinoma
LROI	Liver region of interest
LROI-M	Liver region of interest-mean
LROI-R	Liver region of interest-range
LTEM	Law's texture energy measure
MET	Metastatic carcinoma
MLP	Multilayer perceptron
NIH	National Institutes of Health
OCA	Overall classification accuracy
RF	Random forest
RT	Random transform

RBAs	ROI based approaches
SA	Sum average
SC	Sum correlation
SE	Sum entropy
SFM	Statistical features matrix
SGLCM	Spatial gray-level dependence matrices
SHCC	Small Hepatocellular carcinoma
SOM	Self organizing maps
SROI	Surrounding region of interest
SROI-M	Surrounding region of interest-mean
SROI-R	Surrounding region of interest-range
SV	Sum variance
SVM	Support vector machine
US	Ultrasound
VAR	Variance
WPT	Wavelet packet transform

List of Figures

List of Tables

Abstract

The study has been conducted on a comprehensive image database of 41 B-Mode US images, including 14 mild, 14 moderate and 13 severe fatty liver images and 42 B mode, focal liver US images, including (*1*) atypical and typical cases of Cyst, HEM and MET lesions, (*2*) small and large HCC lesions. Fatty liver images have been originally acquired from the Department of Radio-diagnosis, Himalayan Institute of Hospital and Trust (HIHT), Dehradun, India and focal liver images have been acquired from Department of Radiotherapy Postgraduate Institute of Medical Education and Research (PGMIER), Chandigarh, India.

The brief description of experiments carried out to developed a proposed CAC system is given in Fig 1 and Fig 2.

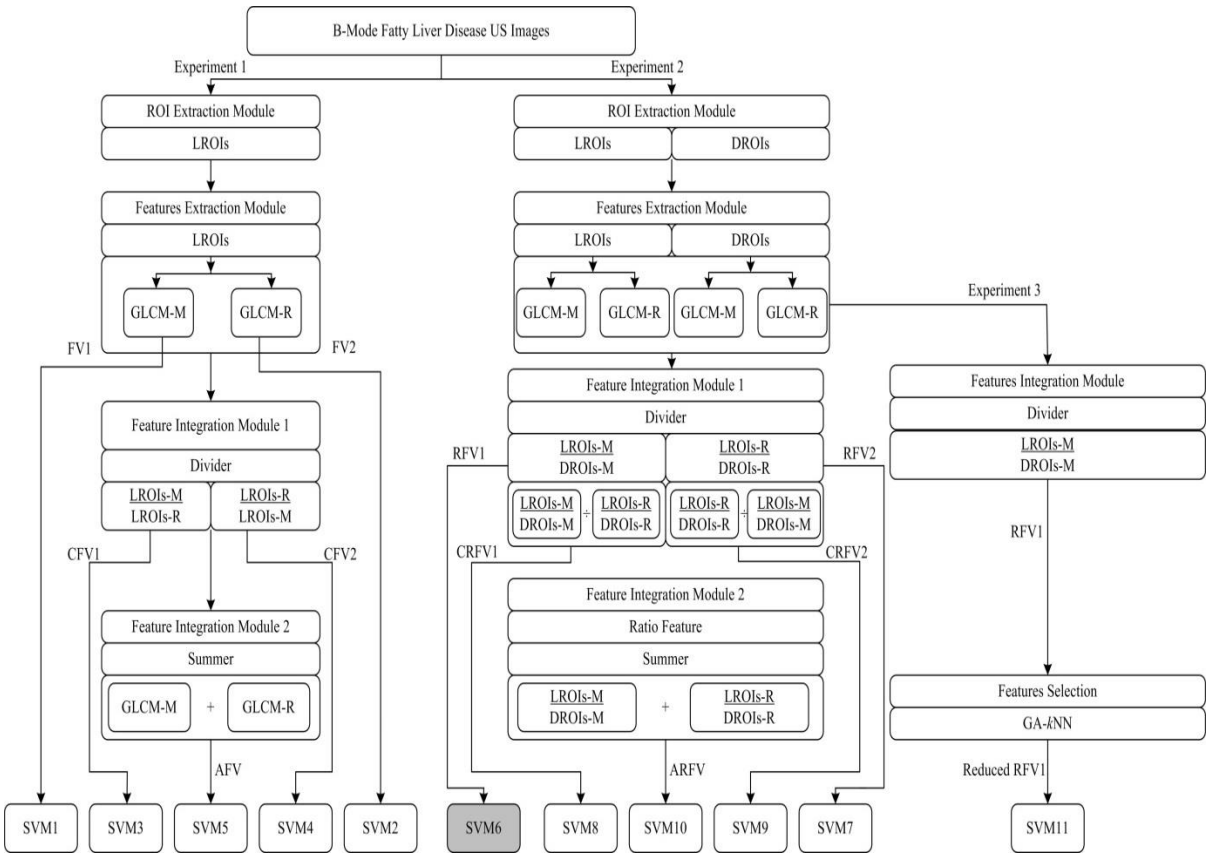

Fig 1 Experimental work flow for the design of SVM based CAC system for grading of fatty liver disease
Note:GLCM-M: Grey level co-occurrence matrix mean, GLCM-R: Grey level co-occurrence matrix range, LROI-M: Liver region of interest mean, , DROI-M: Diaphragm region of interest mean, LROI-R: Liver region of interest range, , DROI-R: Diaphragm region of interest range, FV1 :GLCM mean features, FV2 :GLCM range features , CFV1: GLCM mean upon range ratio features CFV2: GLCM range upon mean ratio features, AFV: GLCM mean + GLCM range additive features, RFV1: GLCM mean ratio features,RFV2: GLCM range ratio features CRFV1: (GLCM mean ratio) upon (GLCM range ratio) ratio features,CRFV2: (GLCM range ratio) upon (GLCM mean ratio) ratio features, ARFV: GLCM mean ratio + GLCM range ratio additive features, Reduced RFV1: Reduced ratio feature vector.

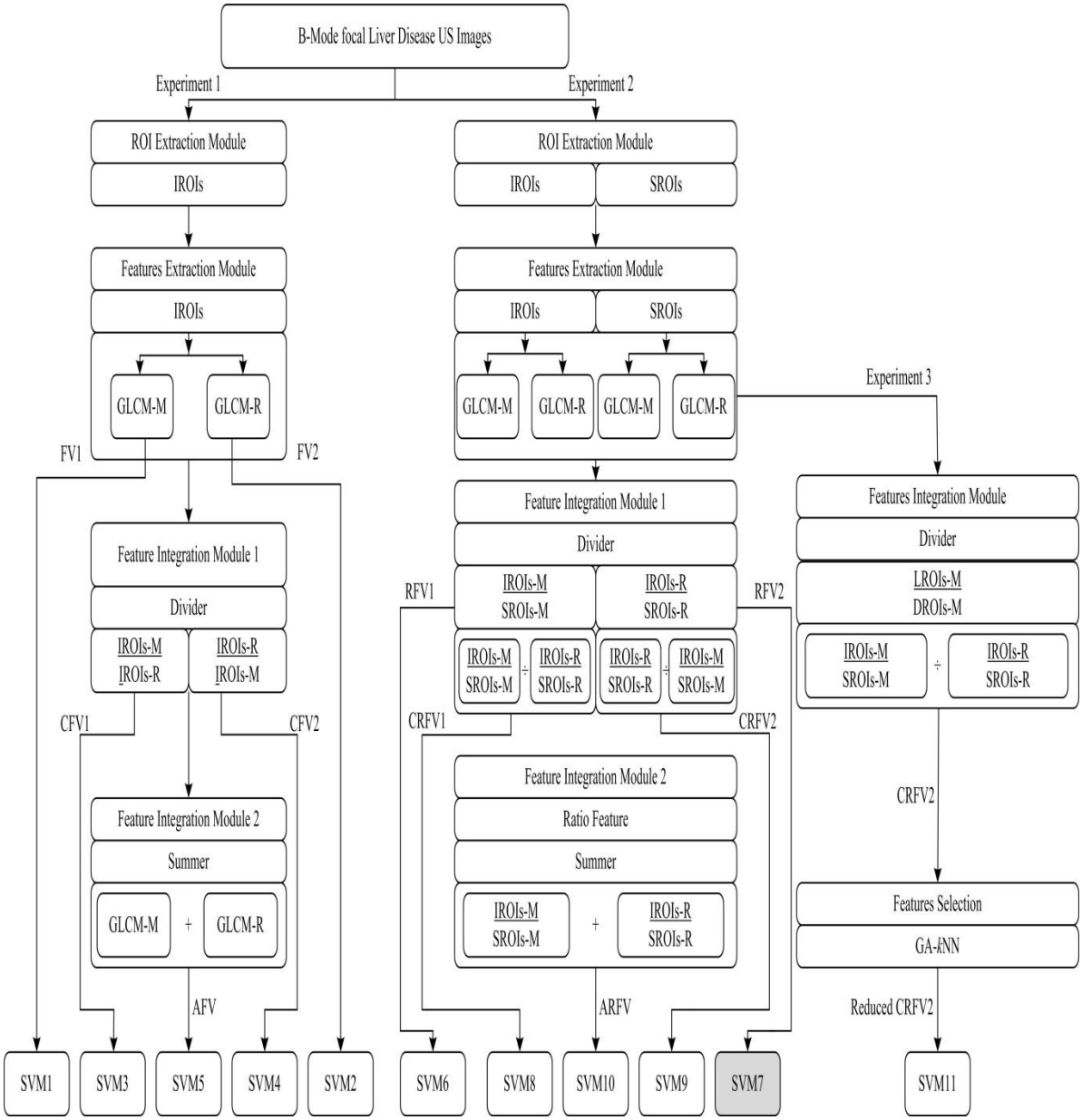

Fig 2 Experimental work flow for the design of SVM based CAC system for classification of focal liver lesions
Note: GLCM-M: Grey level co-occurrence matrix mean, GLCM-R: Grey level co-occurrence matrix range, IROI-M: Inside region of interest mean, , SROI-M: Surrounding region of interest mean, IROI-R: Inside region of interest range, , SROI-R: Surrounding region of interest range, FV1 :GLCM mean features, FV2 :GLCM range features , CFV1: GLCM mean upon range ratio features CFV2: GLCM range upon mean ratio features, AFV: GLCM mean + GLCM range additive features, RFV1: GLCM mean ratio features,RFV2: GLCM range ratio features CRFV1: (GLCM mean ratio) upon (GLCM range ratio) ratio features,CRFV2: (GLCM range ratio) upon (GLCM mean ratio) ratio features, ARFV: GLCM mean ratio + GLCM range ratio additive features, Reduced CRFV2: Reduced combined ratio feature vector.

The proposed interactive system for grading of fatty liver disease and classification of focal liver lesions using B-Mode US images consist of four modules as shown in Fig 3.The brief description of these modules is given below.

Module 1: SVM based CAC system for grading of fatty liver disease(without feature selection).

In module 1, the efficacy of second order statistical features has been exhaustively evaluated for classification of different grades of fatty liver disease, i.e., mild, moderate and severe fatty liver. The image database used in the present work consists of a total of 41 ultrasound images, including 14 mild, 14 moderate and 13 severe fatty liver images. Two types of regions of interest are used in our work LROIs and DROIs. The LROIs are multiple ROIs extracted from the liver parenchyma at the same depth from each image. The DROI is single ROI extracted from the diaphragm region of each image. The various combinations of second order statistical Gray level co-occurrence matrix based features i.e., (*a*) GLCM mean features, (*b*) GLCM range features (*c*) GLCM mean upon range ratio features (*d*) GLCM range upon mean ratio features (*e*) GLCM mean + GLCM range additive features, (*f*) GLCM mean ratio features, (*g*) GLCM mean ratio features (*h*) GLCM range ratio features (*i*) (GLCM mean ratio) upon (GLCM range ratio) ratio features (*j*) (GLCM range ratio) upon (GLCM mean ratio) ratio features and (*k*) GLCM mean ratio + GLCM range ratio additive features have been extracted. The proposed CAD system for fatty liver using SVM is shown in Fig 3.

Module 2: SVM based CAC system for grading of fatty liver disease (with feature selection).

The module 2 classifies the US images of fatty liver diseases into mild, moderate and severe fatty liver respectively. Feature selection technique (GA-*k*NN) has been used in this module to increase the classification accuracy of fatty liver diseases. It is observed that the maximum classification accuracy for fatty liver is 66.6 % and the individual class accuracy values of 68.8 %, 60.0 % and 73.2 % have been achieved using GLCM mean ratio features.

Module 3: SVM based CAC system for classification of focal liver lesions (without feature selection).

In module 3, second order statistical features has been comprehensively evaluated for classification of different grades of focal liver disease such as such, as cyst, hemangioma (HEM), hepatocellular carcinoma (HCC) and metastatic carcinoma (MET). The image index used in the present work consists of a total of 42 B mode US images, including (*1*) atypical and typical cases of cyst, HEM and MET lesions, (*2*) small and large HCC. Two types of regions of interest (ROI) used in our work are IROIs and SROIs. The IROIs are single ROI extracted from a focal liver lesion part of each image, whereas the SROI is single ROI extracted from surrounding of the lesion of each image. In the present work, texture features and texture ratio features are measured from regions outside and inside the lesions. The various combinations of second order statistical Gray level co-occurrence matrix based features. i.e. (*a*) GLCM mean

features, (*b*) GLCM range features (*c*) GLCM mean upon range ratio features (*d*) GLCM range upon mean ratio features (*e*) GLCM mean + GLCM range additive features, (*f*) GLCM mean ratio features, (*g*) GLCM mean ratio features (*h*) GLCM range ratio features (*i*) (GLCM mean ratio) upon (GLCM range ratio) ratio features (*j*) (GLCM range ratio) upon (GLCM mean ratio) ratio features and (*k*) GLCM mean ratio + GLCM range ratio additive features have been extracted. A proposed CAD system for focal liver using SVM is shown in Fig 3.

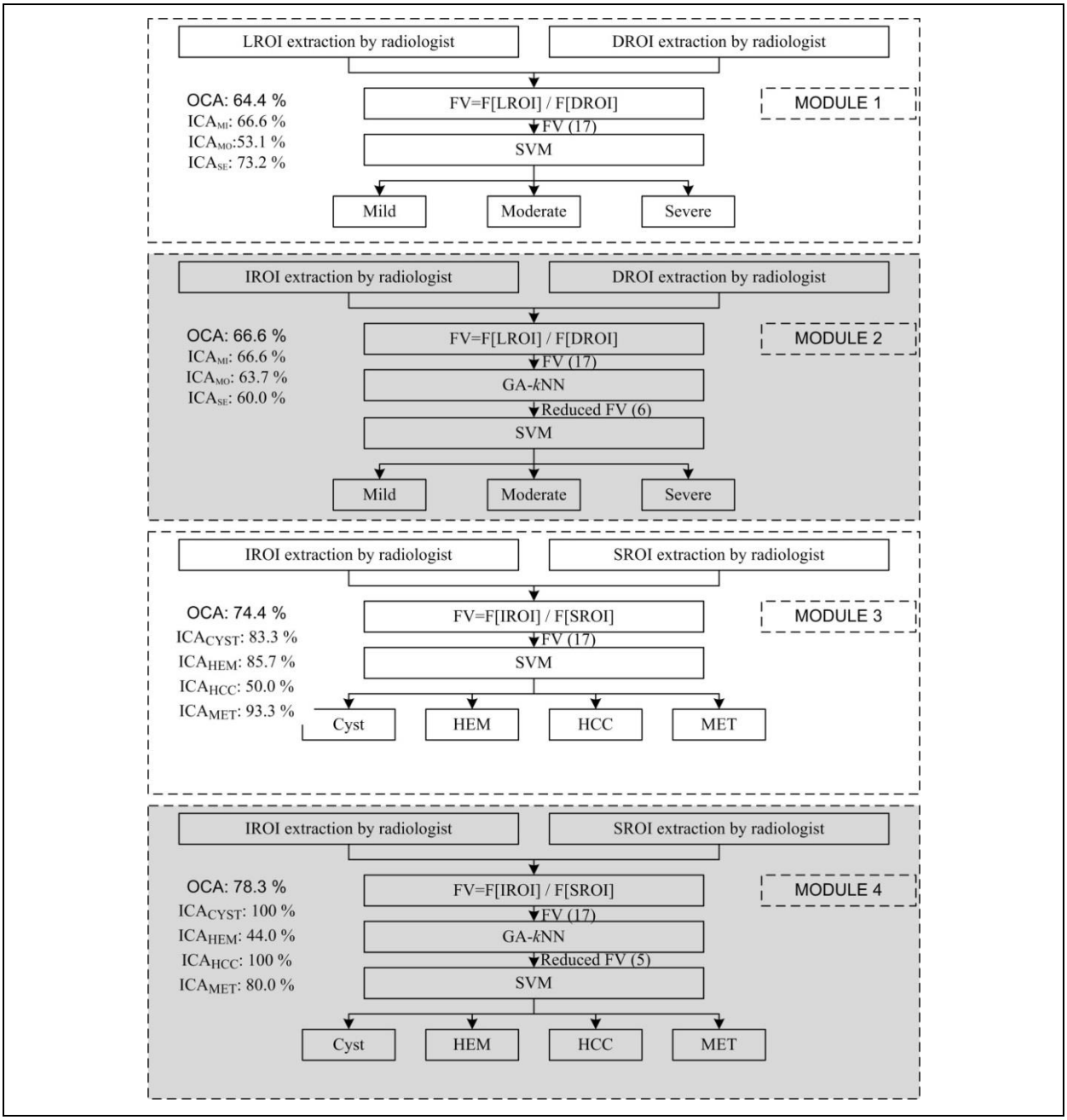

Fig 3 Block diagram of the proposed interactive system for grading of fatty liver disease and classification of focal liver lesions

Note: LROI: Liver region of interest, DROI: Diaphragm region of interest, IROI: Inside region of interest, SROI: Surrounding region of interest

Module 4: SVM based CAC system for classification of focal liver lesions (with feature selection).

The module 4 classifies the US images of focal liver lesions into cyst, HEM, HCC and MET focal liver respectively. In this module feature selection technique (GA-*k*NN) has been used to increase the classification accuracy of focal liver diseases. It is observed that the maximum classification accuracy for focal liver lesion is 78.3 % and the individual class accuracy values of 100 %, 44.0 %, 100 % and 80.0 % for Cyst, HEM, HCC and MET have been achieved using GLCM range ratio to GLCM mean ratio features.

A brief comparison of performance obtained by different implemented modules for diagnosis of fatty and focal liver diseases using B-Mode US images are depicted in Table 1.

Table 1 Classification performance of module 1, 2, 3 and 4.

CAC System Designs	*Classes*	*OCA*	*ICA*	*FV*	*l*
Module 1: SVM based CAC system for grading of fatty liver disease (without feature selection).	Mild Moderate Severe	64.4	66.6 53.1 73.2	RFV1	17
Module 2: SVM based CAC system for grading of fatty liver disease (with feature selection).	Mild Moderate Severe	66.6	68.8 60.0 73.2	Reduced RFV1	6
Module 3: SVM based CAC system for classification of focal liver lesions (without feature selection).	Cyst HEM HCC MET	74.4	83.3 85.7 50.0 93.3	CRFV2	17
Module 4: SVM based CAC system for classification of focal liver lesions (with feature selection).	Cyst HEM HCC MET	78.3	100 44.0 100 80	Reduced CRFV2	5

Note: HEM: Hemangioma, HCC: Hepatocellular carcinoma, MET: Metastatic carcinoma, OCA: Overall classification accuracy (%), ICA: Individual classification accuracy (%), RFV: Ratio feature vector, Reduced RFV1: Reduced ratio feature vector, CRFV2: Combined ratio feature vector, Reduced CRFV: Reduced combined ratio feature vector.

From Table 1, it can be observed that,

(*a*) *Module 3*: Ratio of GLCM mean statistics derived from LROI and DROI yield maximum classification accuracy value of 64.4 % at d = 10 and ICA values of 66.6 %, 53.1 % and 73.2 % for mild, moderate and severe image classes, respectively. After optimization using GA-*k*NN, classification accuracy increase to 66.6 % and ICA values of 68.8 %, 60.0 % and 73.2 % for **mild**, **moderate** and **severe** classes.

(*b*) *Module 4*: Ratio of GLCM range statistics and GLCM mean statistics derived from IROI and SROI yield maximum classification accuracy value of 74.4 % at $d = 1$ and ICA values of 83.3 %, 85.7 %, 50 % and 93.3 % for **Cyst**, **hemangioma (HEM)**, **hepatocellular carcinoma (HCC)** and **metastatic carcinoma (MET)** classes, respectively. After optimization using GA-*k*NN, overall classification accuracy increase to 78.37 % and ICA values of 100 %, 44.0 %, 100 % and 80.0 % for cyst, hemangioma (HEM), hepatocellular carcinoma (HCC) and metastatic carcinoma (MET) classes.

Contents

Chapter 1

Introduction

1.1 Motivation

Liver is a fundamental organ of the human body. Its main functions include bile secretion and detoxification of chemicals from the body that are useful for digestion. Other functions of the liver are regulation of glycogen storage, disintegration of red blood cells and production of hormones. Liver also plays a dominating role in the metabolism of the human body.

The adornment gland helps in emulsification of lipids and produce bile. Bile is produced by the liver just below it, in a little pouch. In the liver, large amount of biochemical reactions takes place which is responsible for the healthy metabolism of the human body. These reactions include the breakdown and synthesis of the large amount of molecules which are vital for normal and proper functioning of the human body. The diagram for anatomy of liver is shown in Fig 1.1.

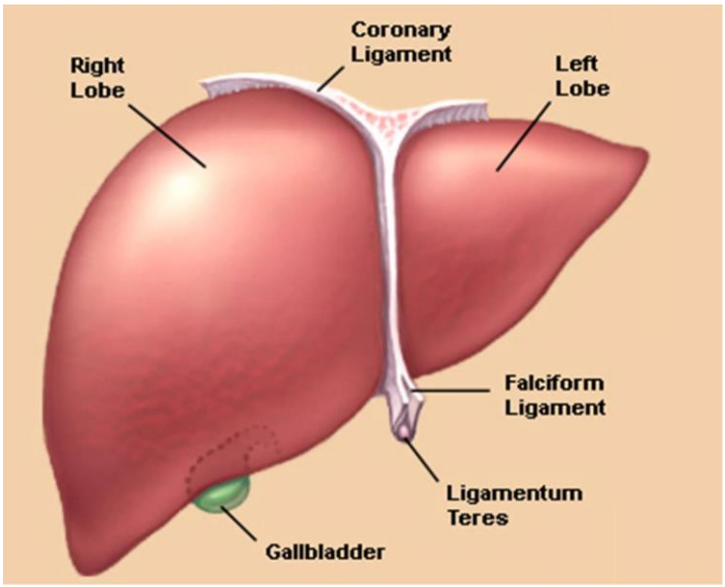

Fig 1.1 Anatomy of liver
Note: Image courtesy [1]

Liver is a cusp-shaped reddish brown organ with four unequal sized lobes, which weighs 1.45-1.66 kg normally. It is the heaviest and largest internal organ among all the glands in the human body. The liver is located just beneath the diaphragm in the uppermost right quadrant of the abdominal cavity. It is above the gallbladder towards the right of the stomach.

The hepatic artery and portal vein are the two large blood vessels which are associated with liver. Oxygen rich blood from the aorta is supplied through the hepatic artery, while the portal vein transmits nutrients which are rich in oxygen from the entire gastrointestinal tract.
Liver diseases are broadly classified in two categories, i.e., diffused liver diseases and focal liver diseases. The brief description of liver diseases and their types is discussed in the next section.

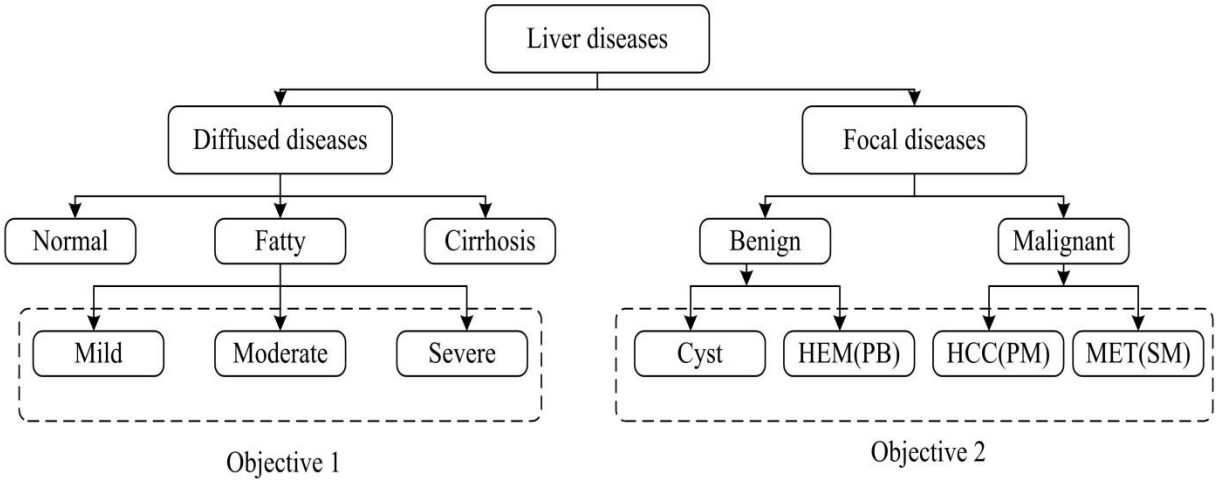

Fig 1.2 Brief description of types of liver diseases
Note: HEM: Hemangioma, HCC: Hepatocellular carcinoma, MET: Metastatic carcinoma, PB: Primary benign, PM: Primary malignant, SM: Secondary malignant.

1.2 Liver Diseases

The disease in the liver may either be genetic or arise through various other mechanisms such as high alcohol consumption, some infections, etc. The brief description of different types of liver diseases is shown in Fig 1.2.

The diseases are detected by different methods like blood tests, computed tomography (CT) scan and ultrasonography etc. The texture is a kind of visual features that is not influenced by color or intensity. Basically texture is in the form of information/data of the arrangement found in an image. So texture features have been extensively used in image processing.

Diagnostic sonography or ultrasonography is a real time, non-invasive imaging technique used to inspect the structure of internal body parts or disease influenced area of that body part if any [4-6]. Liver diseases are of two types

(*a*) Diffused liver diseases

(*b*) Focal liver lesions

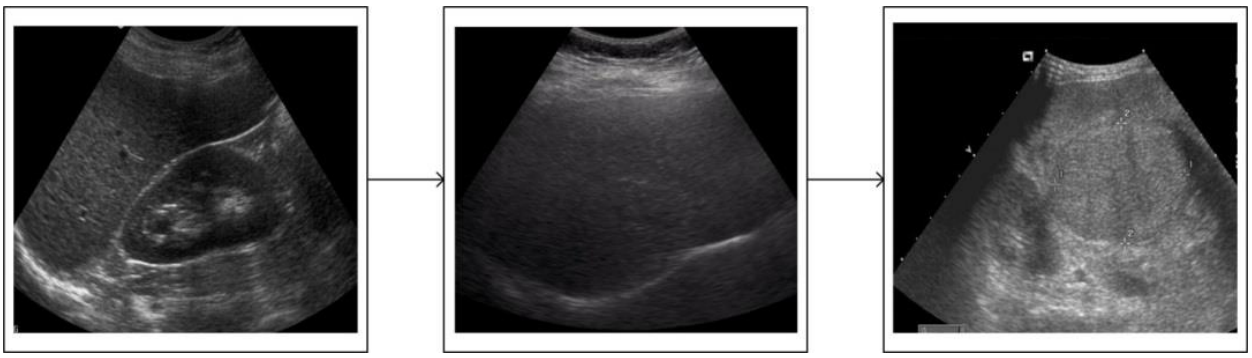

(*a*) Normal liver US image (*b*) Fatty liver US image (*c*) Cirrhotic liver US image

Fig 1.3 Progression of diffused liver disease images

1.2.1 Diffused Liver Diseases

Diffused liver diseases are the diseases which affect the entire parenchyma of the liver. There are three stages of the diffused liver disease: normal, fatty and cirrhosis as shown in Fig. 1.3.

1.2.1.1 Fatty Liver Disease

Fatty liver or steatosis is a state that is characterized by the aggregation of fats over the liver [7]. A person suffering from fatty liver disease [8] has 5-10 % weight increase in liver fat content [9-14]. The types of fatty liver disease are shown in Fig 1.4.

The spectrum of the fatty liver image varies from one state to another state, ranging from simple steatosis to cutaneous inflammation, fibrosis of the varying grades and then cirrhosis, which leads to the increased prospect of hepatocellular carcinoma [15, 16]. The advanced stage is the non-alcoholic steatohepatitis that is the 'inflammatory' component with respect to steatosis. It has a higher prospect of mortality and cardiovascular disease than simple steatosis [17]. The progression of non-alcoholic fatty liver disease generates metabolic syndrome, insulin resistance and obesity [18]. The metabolic syndromes increase four fold in subjects with a prevalence of non-alcoholic fatty liver disease in comparison to those without the disease [19]. The cardiovascular mortality risk approximately doubles conferring metabolic syndrome itself [20]. The metabolic syndrome criteria increase cardiovascular disease risk linking non-alcoholic fatty liver disease [21].

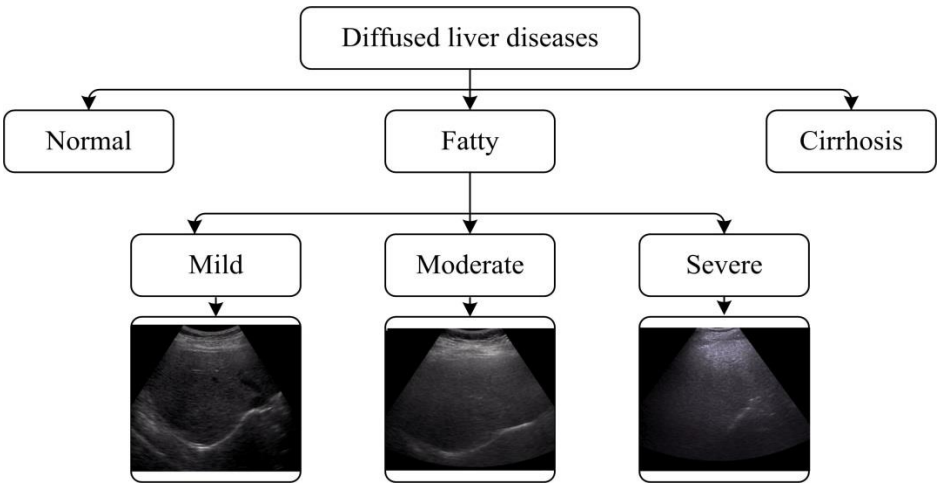

Fig 1.4 Brief description of types of diffused liver diseases

Diabetes, toxins, and hepatitis are the main causes of the lesion. Enlarged liver with diffused enlarged echogenicity is caused by severe fatty infiltration. According to the research [22] in America, 20 % of the population is suffering from the adequate volume of fat in their liver. Fatty liver disease appears mostly in people in the age class of 40 to 60. It is a reversible state, but if not treated in time, it can transform into a serious disease called cirrhosis.
Fatty liver has 3 stages: mild, moderate and severe [23] (as shown in Fig 1.5).

(*a*) *Mild:* Mild fatty liver is the earliest stage of fatty liver disease in which lesser amount of fat is deposited over the liver. In this stage the diaphragm is clearly visible in ultrasound image and appears brighter than the liver. It is a reversible case in which fatty liver can easily get back to its normal size by some remedies e.g. by taking proper medication and a healthy diet.

(*b*) *Moderate:* Moderate is the second state of the fatty liver disease in which diaphragm appears more hypoechoic in comparison to mild state as shown in Fig 1.5. This stage is also reversible if treated properly in time.

(*c*) *Severe:* Severe is the third and last reversible state of the fatty liver disease. In this stage, the liver has almost 11 % of its weight as fat. If not treated in time, it may change into cirrhosis, which completely damages the liver cells leading the liver to collapse. The sample image showing the classes of fatty liver disease is characterized in Fig. 1.5.

Fig 1.5 Sample ultrasound images of (*a*) mild (*b*) moderate (*c*) severe class

1.2.1.2 Cirrhosis

The liver does not function properly if cirrhosis [24, 25] state occurs. The functioning of liver slows down as tissues replace the healthy liver tissues. The processing of nutrients, drugs and hormones become slow as the movement of blood through the liver is blocked by scar tissues. Cirrhosis slows down the production of proteins and other substances secreted by the liver. The secretion of bile stops, due to the blockage of bile duct. Primary biliary cirrhosis disease blocks the bile ducts in adults. The Cirrhosis is ranked 12^{th} in death caused by disease as per the National Institutes of Health (NIH). The sample image of liver ultrasound (US) image with cirrhosis is shown in Fig 1.6.

Fig 1.6 Liver US image of cirrhosis

.

Detailed history and physical exams are required for diagnosis of cirrhosis. A complete medical history should be considered by the doctor. Yellow eyes (jaundice), reddened palms, pale skin, hand tremors, excess breast tissue (in men), an enlarged liver and decreased alertness signs are

the symptoms of cirrhotic liver which can be analyzed by taking the physical examination. Tests that can evaluate the liver are categorized as: ultrasound scan of the liver, MRI of the abdomen, CT scan of the abdomen, liver biopsy (definitive test for cirrhosis) and endoscopy.

Esophageal varices are the substitute to pass blood through the liver. High pressure can not be handled by these veins and they tend to bulge from the extra blood flow. Due to poor clotting and low platelet count, bleeding and bruising occurs. Other complications due to cirrhosis include liver cancer, kidney failure, enlarged spleen (splenomegaly), ascites and edema.

1.2.2 Focal Liver Lesions

Focal liver lesions affect only the small portion of the liver. There are four types of focal liver lesions: Cyst, hemangioma (HEM), hepatocellular Carcinoma (HCC) and metastatic Carcinoma (MET). The brief description of different types of focal liver lesions is shown in Fig 1.7. Focal liver lesion ranges from benign lesions to the tumorous malignant lesions in patients with non-specific abdominal complaints.

For effective treatment of tumors, initial estimation of factors is necessary which are responsible for predisposing the tumors. After cirrhosis [34-36], hepatocellular carcinoma is formed, thus a history of oral contraceptive for effective treatment of HEM is required. Imaging techniques and a cyto-histologic study are established as a definite diagnosis of focal liver lesions.

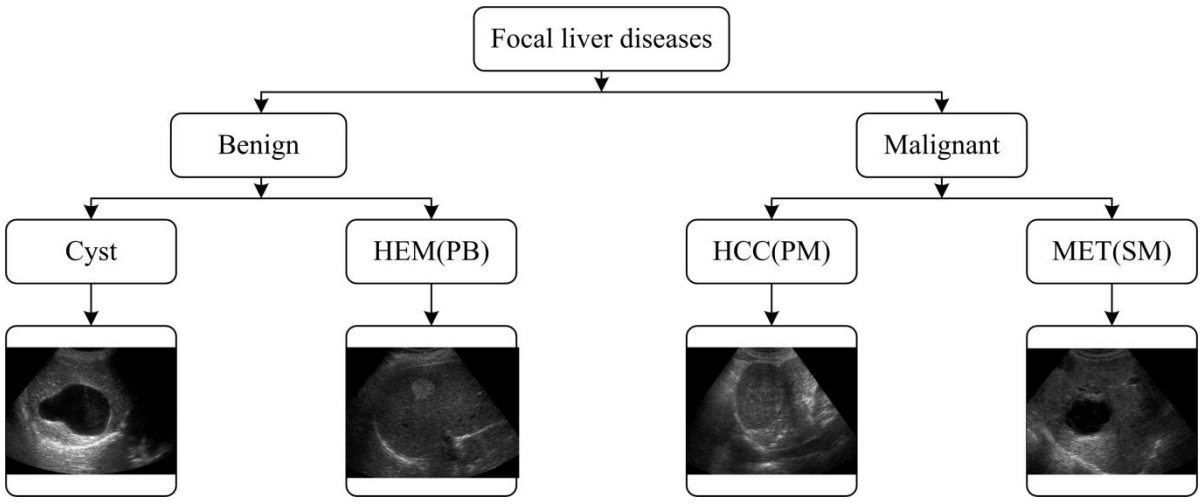

Fig 1.7 Brief description of types of focal liver lesions
Note: PB: Primary benign, PM: Primary malignant, SM: Secondary malignant

Solid lesion's (malignant or benign tumors) and liquid (cysts, abscesses, etc.) can be found through radiographies feature, which give the hint about the kind of lesion in the liver. Etiology

of solid tumor is easy to find by its vascularization [26]. Hepatocellular carcinoma, and metastases from hypernephroma or neuroendocrine tumors are generally tumors with arterial hyper vascularization, it may be benign or malignant. Instead of radionuclide tests, abdominal magnetic resonance imaging (MRI) and computed tomography (CT) with ferric (ferumoxides) or vascular (gadolinium) contrast techniques are used. Focal liver lesions [37-45] typical case US images are shown in Fig 1.8.

Because of the large variation of the texture of focal liver lesion, the radiologist has to face difficulty in the atypical diagnosis of particular classes of FHLs [26-31], focal liver lesions atypical case images are shown in Fig 1.9. Due to the non-invasive, non-ionizing, real time and low-cost nature, B-mode ultrasound is the best choice for diagnosis of lesions [26-27]. In resemblance with B-mode ultrasound some other expensive and more time consuming techniques like enhanced contrast spiral computed tomography are often used [26-33]. Therefore, for classification, of B-mode ultrasound images, an adequate CAC (computer-aided classification) is required.

Two types of focal liver diseases are benign and malignant focal liver diseases.

1.2.2.1 Benign Focal Liver Lesions

Benign indicate a condition, tumor or expansion which is not cancerous. This means that it does not infect the nearby parts of the body.

In a typical case, a benign tumor spreads slowly and is not harmful. Despite, this is not constantly the case. A benign tumor may spread big enough or be found in adjacent blood vessels, the nerves, and brain. As it develops, it can cause problems without growing in another part of the body. Sometimes, these issues can be serious. There are two types of benign focal liver diseases discussed below.

1.2.2.1.1 Cyst

Only 2-7 % of the people get affected by inveterate lesion called cyst .There is no transmission of bile ducts in the case of cyst, it has an epithelium description with cuboidal serous essence [46, 47]. It is an anechoic lesion which can be detected by ultrasonography [48-57] as a non-variable-enhanced mass that exhibits posterior acoustic enhancement [25].

1.2.2.1.2 Hemangioma (HEM)

More the 60 % of cases detected from diagnosis of HEM are typical HEMs. Typically, HEM [37, 38] occurs as a uniform encircle apparatchik echoic lesion. This tumor consists of broad vessels lined with sophisticated endothelial cells within a fibrous stroma. It is a mostly single small lesion of up to 20 cm in diameter, which is more commonly found in women. In maximum cases, a patient is found with unspecific abdominal complaints or no symptoms [31]. It does not infect other parts, but may spread in the presence of estrogenic therapies or pregnancy. Its US image may appear a hyper echogenic along with well-defined lesion that may be higher heterogeneous in case of intra-tumor thrombosis.

1.2.2.2 Malignant Focal Liver Lesions

Malignancy is the case of a medical situation in which cancer becomes moderately worse. Malignant is most familiar as a depiction of cancer. In case of malignant tumor contradiction with a non-cancerous benign tumor is that a malignancy is not self-limited in its expansion, it is able to enter into neighboring tissues, and may be able to grow in distant tissues. In comparison, tumors that stay limited and do not grow are called benign. Benign tumors may spread quite large and can harm, but they do not usually grow through the lymph vessels or bloodstream to other parts of the body.

1.2.2.2.1 Metastatic Carcinoma (MET)

Metastatic carcinoma is of various sizes and occurs singly or as multiple deposits . Liver metastases are the most typical malignant tumors in the liver, since 35-40 % of tumors develop this kind of dissemination. Most typical metastases emerge in the lung, the gastrointestinal portion (stomach, colon, gallbladder, pancreas), and ovary. The existence of metastatic liver disease commonly entails a poor prognosis. Two main exceptions constitute colorectal cancer (CRC) metastases when susceptible of the surgical section [41]. In elected patients with colorectal cancer (less than 4 nodules), resection grant survivals of 40 % at 5 years. For non-resectable neuroendocrine cancer, hepatic embolization may be helpful in the management of carcinoid syndrome.

1.2.2.2.2 Hepatocellular Carcinoma (HCC)

It is a case of primary malignant FHL, the fatty liver problem is the primary cause of HCC. Around 84 % patients, who has cirrhosis problem suffered from HCC liver lesion [35,42]. It is a primary task for the radiologist to find out the cirrhotic liver so that the development of HCC can be detected from B-mode US images [35,40,42,45]. There is no typical case in HCC that is presumed by radiologists. So that the appearance of ultrasound images of HCCs has a wide variety within small HCCs (SHCCs) and large HCCs (LHCCs). The SHCCs sonographic appearance varies from hypo-echoic to hyper-echoic. The ultrasound images of SHCC and LHCC is shown in Fig 1.10. While large HCC frequently exhibits the mixed echogenicity [26, 28,35,42]. For designing classifiers, radiologist suggests that it must consist of both SHCCs and LHCCs representative and a comprehensive data set. The LHCCs have lesion size varying from 2.1-5.6 cm while SHCCs have lesion size of 1.5-1.9 cm.

Diagnosis may be based upon non-invasive or histological criteria alone for cirrhotic patients [46]. Ultrasonography usually acknowledges a hypo-echogenic and hyper-vascular lesion by applying contrast media. CT scan displays a hypo dense lesion in baseline state that takes up contrast, during the arterial state and then becomes hypo vascular vs. the liver parenchyma in entrance and later phases [25]. MRI acknowledges a lesion that is hyper intense in T2 and hypo intense in T1, with a behavior identical to that, seen in CT in progressive studies [41, 47].

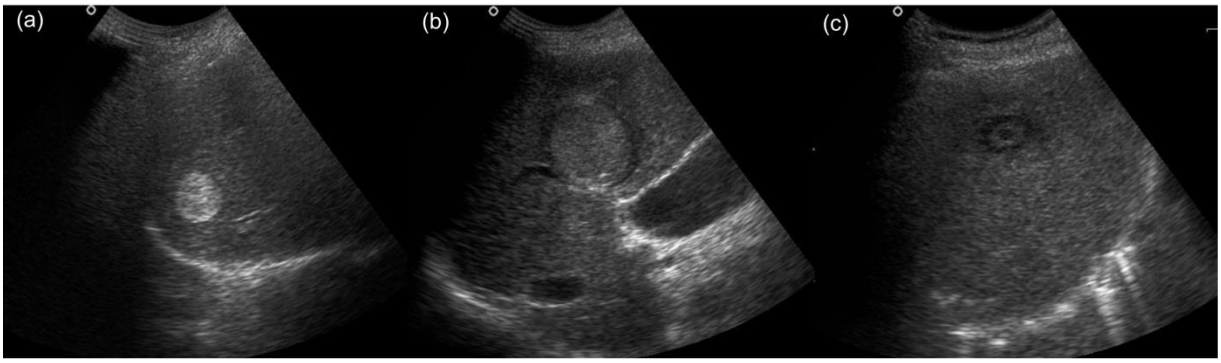

Fig 1.8 Liver US images showing typical case (*a*) Cyst (*b*) HEM (*c*) MET

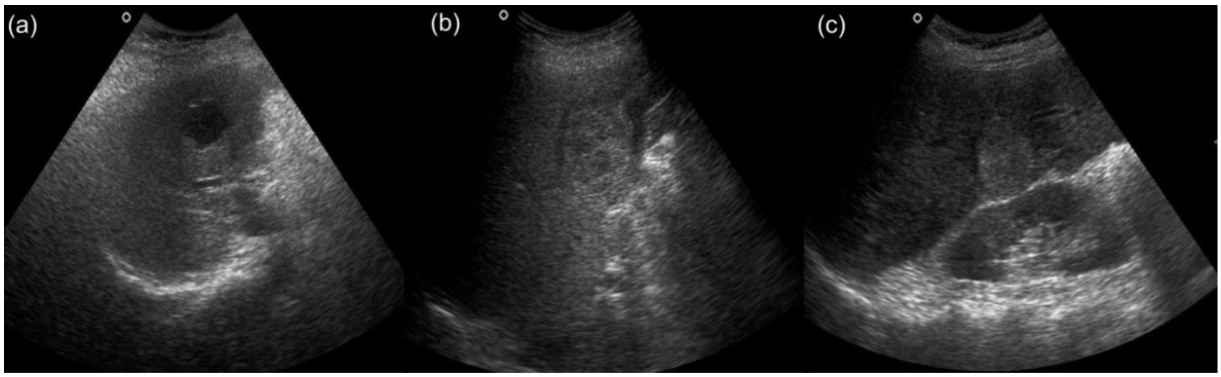

Fig 1.9 Liver US images showing atypical case (*a*) Cyst (*b*) HEM (*c*) MET

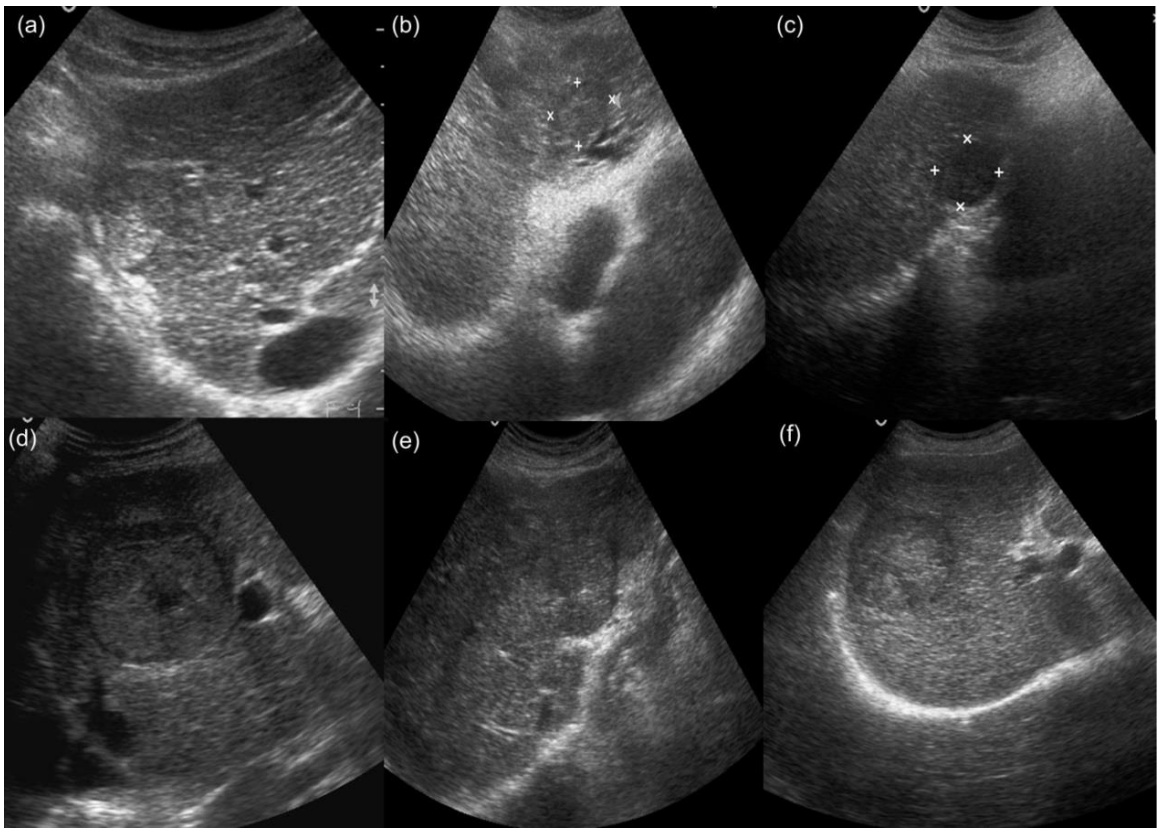

Fig 1.10 Liver US images showing small HCC (case (*a*), (*b*) and (*c*)) and large HCC (case (*d*), (*e*) and (*f*))

1.3 Ultrasound Imaging

Medical ultrasound or ultrasonography is based on the application of ultrasound [34]. It is a diagnostic imaging technique, which is used to view inside body structures, such as joints, tendons, muscles, vessels and internal organs. Because of the easy availability and affordability

ultrasound proves to be a good option for diagnosis. The sample ultrasound image of a normal liver is shown in Fig 1.11.

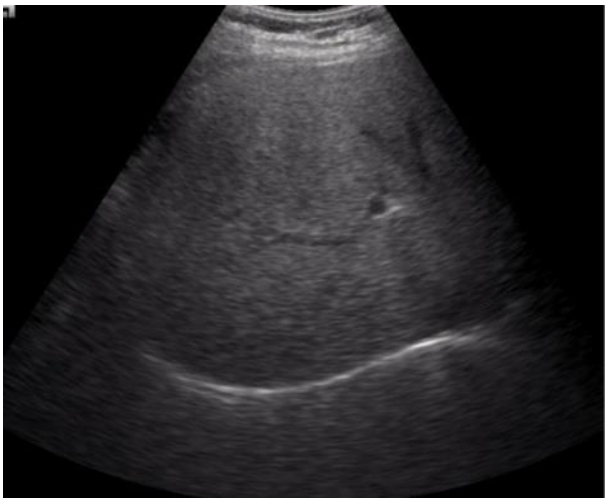

Fig 1.11 Normal liver US image

1.4 Computerized Tomography

Computerized tomography (CT) uses several X-ray images to take data of internal organs in the human body and convert this data into pictures on a monitor. Although CT offers high speed of acquisition, better spatial resolution and more precise contrast enhancement, it has low sensitivity and it needs a high radiation dose to detect the lesions which are smaller than 1cm. Fig 1.12 shows the CT image of the liver.

Fig 1.12 Sample CT image of liver
Note: Image courtesy [2]

1.5 Magnetic Resonance Imaging (MRI)

Detailed images of the tissues and organs of the body are created using a radio waves and magnetic field, this technique is called Magnetic Resonance Imaging. The Liver MRI image is shown in Fig 1.13.

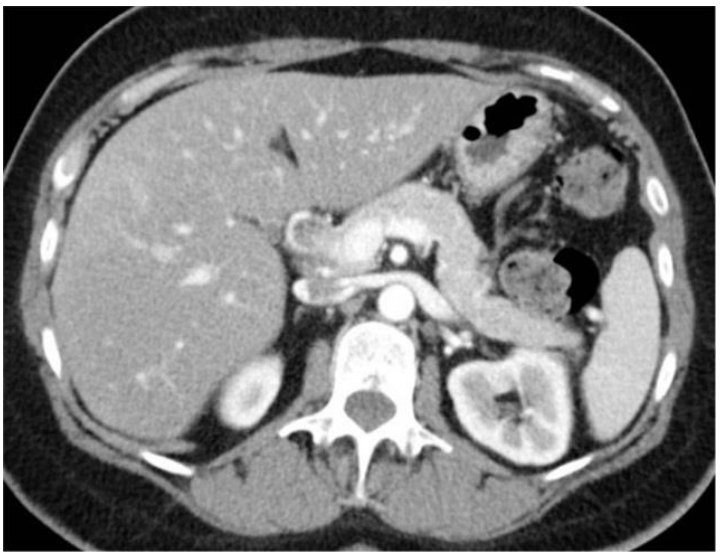

Fig 1.13 Sample MRI image of liver
Note: Image courtesy [3]

The imaging modalities are used to determine how well the liver is working. Ultrasound or diagnostic sonography is a real time, non-invasive imaging technique used to examine internal body parts [4, 5].

1.6 Objectives of the Present Study

The main objective of the research work presented is to enhance the potential of ultrasound imaging by designing efficient CAC systems for grading of fatty liver disease and classification of focal liver lesions with thorough image database. The various research objectives are depicted here:

(*i*) *Objective 1: The formulation of ROI extraction protocols and data bifurcation protocols.*

For efficient CAC system, the classifier used employs an image database consisting of relevant information and representative images from each subclass. The establishment of ROI extraction protocols for extracting ROIs from fatty and focal liver ultrasonic images and their bifurcation into testing and training data sets is the first objective of the proposed work.

(ii) Objective 2: To design a SVM based CAC system for the grading of fatty liver disease (without feature selection).

The statistical method is used to evaluate the potential of features extracted from fatty liver ultrasound images to classify into mild, moderate and severe fatty liver class using support vector machine (SVM) classifier.

(iii) Objective 3: To design a SVM based CAC system for the grading of fatty liver disease (with feature selection).

Feature selection method GA-*k*NN has been used to optimize the feature set by removing the redundant feature vector. These optimized feature set is used to classify the fatty liver ultrasound images into mild, moderate and severe fatty liver class using Support Vector Machine (SVM) classifier.

(iv) Objective 4: To design a SVM based CAC system for the classification of focal liver lesions (without feature selection).

The statistical method is applied to evaluate the potential of features extracted from focal liver ultrasound images to classify focal liver ultrasound images into Cyst, HEM, HCC and MET focal liver classes using the SVM classifier.

(v) Objective 5: To design a SVM based CAC system for the classification of focal liver lesions (without feature selection).

Feature selection method GA-*k*NN is used to optimize the feature set by removing the redundant feature vector. These optimized feature set is used to classify the focal liver ultrasound images into mild, moderate and severe fatty liver class using the SVM classifier.

1.7 Organization of Thesis

The structure of the dissertation is described below:

(*i*) Chapter 1 titled **"*Introduction*"** contains the information about the classification and analysis of B-Mode ultrasound images of fatty and focal liver disease. Different facts have been focused in this chapter like why liver? Types of liver diseases? Why liver diseases considered seriously? Why B-mode ultrasound? Why the CAC system is efficient for grading of fatty liver

disease and classification of focal liver lesions? What are the objectives of current research work? The basic motivation provided by this chapter is to design an efficient CAC system for grading of fatty liver disease and classification of focal liver lesions can upgrade the diagnostic property of B-mode US imaging method.

(*ii*) Chapter 2 titled **"*Literature Review*"** involves the literature survey, which explains the various works that have been carried out in the grading of fatty liver disease and focal liver lesions using B-mode liver US images.

(*iii*) Chapter 3 titled **"*Methodology*"** explain the complete database used in the present work. Various protocols followed in this chapter, i.e., estimation of liver US images, ROIs selection, and ROIs size for bifurcation of the dataset into training and testing data.

(*iv*) Chapter 4 titled **"*SVM based CAC system for grading of fatty liver disease*"** gives a precise information on different observation carried out to design an SVM based CAC system for classification of fatty liver disease into mild, moderate and severe fatty liver classes respectively.

(*v*) Chapter 5 titled **"*SVM based CAC system for classification of focal liver lesions*"** gives a precise information of different observation carried out to design an SVM based CAC system for classification of focal liver disease into Cyst, HEM, HCC and MET focal liver classes respectively.

(*vi*) Chapter 6 titled **"*Conclusion and Future Scope*"** conclude the work, which gives the brief summary of CAC system design for grading of fatty liver disease and classification of focal liver lesions. This chapter gives the idea of the future scope of this work.

Chapter 2

Literature Review

2.1 Introduction

Fatty liver or steatosis is a condition characterized by the accumulation of fats over the liver [2]. A person with increased liver fat content is said to have fatty liver disease as some fat molecules build-up inside the liver cells. Further, focal lesions occur in a small region of the liver. However, these focal lesions can be diagnosed by imaging techniques. These focal lesions are classified as typical and atypical focal hepatic lesion (FHLs). For prolong analysis of focal liver diseases among atypical FHLs, generally experienced radiologist(s) anticipate in the process of classification depending upon the textural information present in the region inside and outside of the lesion. In this chapter, the earlier studies done in this field are discussed.

2.2 CAC System Designs for Grading of Fatty Liver Disease

In the present study, the ROI based approach is used for the grading of fatty liver US images [58-60, 62]. The concise overview for classification of fatty liver ultrasound images on studies conducted is given in Fig 2.1.

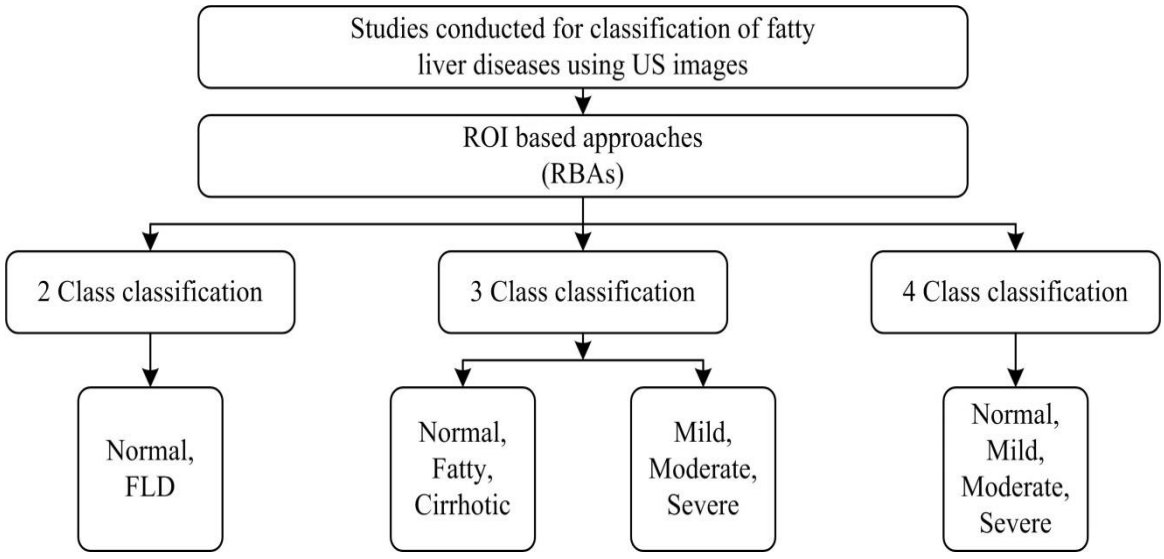

Fig 2.1 Brief description of studies conducted for grading of fatty liver disease

2.2.1 CAC System Designs using ROI based Approaches (RBAs)

M. B. Subramanya *et al*. [61] used the statistical features like gray level co-occurrence matrix (GLCM) for classification of mild, moderate and severe fatty liver classes and normal liver tissue. The CAD system developed consisted of 53 B-mode ultrasound images. The two types of regions of interest (ROIs), 293 in number with a size of 32 × 32 were marked which consisted of liver region of interest (LROIs) and diaphragm region of interest (DROIs). The multiple LROIs were extracted from the liver parenchyma at the same depth and the DROI was single ROI extracted from the diaphragm region of each image. The ratio feature consisted of the GLCM mean of LROIs and DROIs. Similarly, GLCM range features, inverse ratio features, additive ratio features were extracted. These features acted as inputs to the SVM classifier for classifying above mentioned diseases. However, it was noticed that the addition of Law's ratio features boosted the performance and gave maximum classification accuracy of 84.9 %.

U. R. Acharya *et al*. [9] classified fatty liver diseased ultrasound images. The total number of LROIs and DROIs extracted were 100 in number. In this work, discrete cosine transform (DCT) and random transform (RT) techniques were developed. 2D-DCT was implied on the random transformed image to obtain DCT coefficients. 2D-DCT frequency coefficient obtained was in a form of a 1D array. These were further subjected to Locality Sensitive Discriminant Analysis (LSDA) to reduce the number of features. The classification was performed using *k*-NN, PNN, Fuzzy Sugeno (FS) and SVM classifier. It was noticed that maximum classification accuracy of 98.1 % was achieved by FS.

M. K. Yasser *et al*. [63] presented computerized tissue based classification technique to diagnose the liver ultrasound images. Tissue characterization parameters were extracted for the feature extraction module. Further, obtained parameters were processed to obtain the minimum number of parameters. Learning data of over 120 distinct pathologies-investigated cases were obtained from preprocessing step. The feature set of data was divided into independent testing and training sets. Further classification was done using neural classifiers and maximum classification accuracy of 94.5 % was achieved.

W. C. Yeh *et al*. [64] performed classification by extracting wavelet transform and GLCM to classify the normal and fatty liver classes. The data set consisted of 19 B-mode ultrasound images. The research was based on predicting the steatosis grade. The samples taken were subdivided into four classes numbered from 0 to 3. Class 0 represented no change in liver shape due to fatty liver steatosis. Class 1 represented the case in which the affected area was less than

33 %. Similarly, class 2 was assigned if affected hepatocytes lied between 33 - 66 % and class 3 was consigned when it was greater than 66 %. These 4 classes were combined to form 2 new classes, namely class 0 and combined class ranging from 1-3. The grading consisted of steatosis & non- steatosis and other grades were considered in class-4. Further, classification was done using SVM and it was found that liver steatosis at high frequency could be more accurately characterized with the classification accuracy of 94.3 %.

Table 2.1 Summary of studies for grading of fatty liver disease

Author(s)	Classes considered	ROI size	No of ROIs	Classifier
U.R.Acharya *et al*. [9]	NOR/FLD	Variable ROI size	100	SVM
Y.M.Kadah *et al.* [58]	NOR/FATTY/CIRRHOTIC	60 × 60	120	NN
M.B.Subramanya *et al*.[61]	NOR/MILD/MODERATE/SEV	32 × 32	293	SVM
M.K.Yasser *et al*. [63]	NOR/FATTY/CIRRHOTIC	60 × 60	120	*k*-NN
W.C.Yeh *et al*. [64]	NOR/FATTY	−	19	SVM
S.Mukherjee *et al*. [65]	NOR/FATTY	60 × 60	88	SVM
R.Ricardo *et al*. [66]	NOR/FLD	−	20	Bayes
A.Anderia *et al*. [67]	NOR/FLD	50 × 50	262	SVM
M.Singh *et al*. [68]	NOR/FATTY	30 × 30	30	SVM
G. Li *et al.* [69]	NOR/FATTY	64 × 64	93	SVM
J.W.Jeong *et al.* [70]	NOR/FATTY	40 × 40	54	ANN
F.Minhas *et al.* [71]	NOR/FLD	50 × 50	88	SVM
U.R.Acharya *et al*. [72]	NOR/FLD	−	100	PNN
M.M.Dan *et al*. [73]	NOR/FLD	−	120	RF
U.R.Acharya *et al.* [74]	NOR/FLD	−	100	FS
Present study	MILD/MOD/SEV	32 × 32	180	SVM

Note: NOR: Normal, MOD: Moderate, SEV: Severe, FLD: Fatty liver diseases, SVM: Support vector machine, *k*NN: k-nearest neighbor, PNN: Probabilistic neural network, RF: Random forest, FS: Fuzzy Sugeno, NN: Neural network.

S. Mukherjee *et al*. [65] performed experiments on fatty liver ultrasound images. The degree of discrepancy was predicted between normal and fatty liver. US of 88 normal and fatty livers were considered. The GLCM, GLRL and Law's features were calculated. It was noticed that the accuracy of 96.2 % was obtained using the SVM classifier.

R. Ricardo *et al*. [66] classified liver ultrasound images of steatosis using automatic classification algorithm. Feature selection was based on visual inspection of ultrasound image. Two output images were obtained. The first output image consisted of information of anatomic and echogenic parameters and the other one had speckled. The RF signals were used to compute the ultrasound images where the dynamic range compression was performed and classification accuracy using Bayes classifier was obtained.

A. Anderia *et al*. [67] collected the dataset of 262 liver ultrasound images. The ROI of 50 × 50 size was extracted from each image. The system consisted of 3 modules, i.e. feature extraction, feature selection and classification. The feature extraction module consisted of 241 features. However, in classification stage, three classifiers namely ANN, SVM and *k*-NN were developed. It was observed that SVM transformed much better providing an accuracy of 97.5 %.

M. Singh *et al*. [68] characterized liver disease by developing a novel method based on quantative emmetricas technique for classifying normal and fatty ultrasound images. This method was inspired from the radiologists' visual criterion through echogenicity and texture of the liver ultrasound images. The metric was referred as a single parameter. This parameter was based on the homogeneity and the roughness of the surface. Five models of different texture were used to increase the feature space, namely spatial gray-level dependence matrices (SGLCM), statistical feature matrix (SFM), Law's texture energy measure (LTEM), Fourier power spectrum (FPS) and Fractal features. In this work Fisher's linear discriminative analysis was used for better feature selection. The classifiers were developed and accuracy of 92.7 % was obtained.

G. Li *et al*. [69] developed computerized tissue based classification technique for classifying liver ultrasound images. In this study ROI of size 64 × 64 pixels were taken and after feature reduction, learning data of over 93 distinct pathologies-investigated cases were obtained from preprocessing step. The feature set of data was divided into independent testing and training sets. Then, these features were classified using neural classifiers. The accuracy of 89.7 % was obtained.

X. Wang et *al.* [75] inspected ultrasonic image texture features of fatty and normal livers. The features extracted were GLCM and GLRL. The classifier model used ANN. Accuracy of 84 % and 97.1 % was obtained in the case of fatty and normal liver ultrasound images respectively.

F. Minhas *et al*. [71] classified B-scan ultrasound images of Fatty liver disease (FLD) using a novel approach named as texture analysis of liver parenchyma. In this work, ROI of size

50 × 50 pixels was automatically selected for the proposed system. 88 ROIs were segmented and WPT & other statistical features were calculated. An accuracy of 95 % was obtained using a multi-class linear Support vector machine (SVM).

M. M. Dan *et al*. [73] found the severity of ultrasound images of steatosis disease by designing computer aided systems. 120 ultrasound images of liver steatosis were collected. The dataset comprised 10 normal, 70 mild, 33 moderate and 7 severe steatosis. Liver steatosis images were graded into four stages. Training set consisted of 80 % images while testing sets consisted of only 20 % images for classification purpose. Support vector machine (SVM) and random forests (RF) were used for automatic evaluation of liver steatosis. It was observed that RF gave maximum classification accuracy of 96.9 %.

It was observed from the literature survey that an ROI of small size generally, 10 × 10 was considered which lacks complete information about the disease tissue [76-77]. Further the large size increases the computation complexity.

In the proposed work, different texture features including ratios of various parameters are calculated. The ROIs marked consisted of both the liver and diaphragm regions. Three classes, namely mild, moderate and severe classes are classified. The proposed system is described in the next section.

2.3 CAC System Designs for Classification of Focal Liver Lesions

The ROI based approach is used for the classification of focal liver US images. The concise overview for classification of focal liver ultrasound images on studies conducted is given in Fig 2.2.

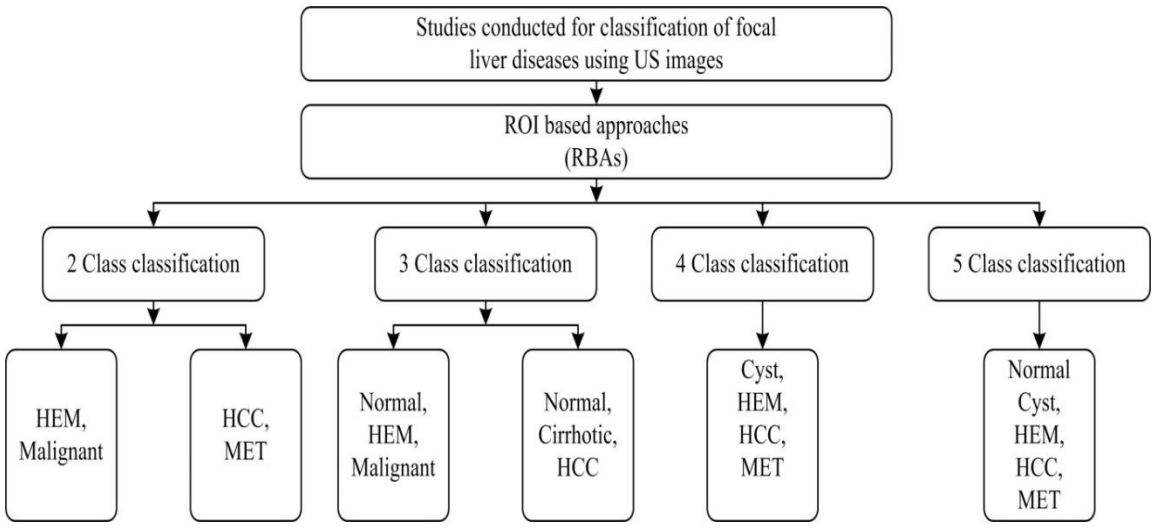

Fig 2.2 Brief description of studies conducted for classification of focal liver lesions

2.3.1 CAC System Designs using ROI based Approaches (RBAs)

D. Mittal *et al.* [54] used statistical features based on the second order statistics, i.e. gray level co-occurrence matrix (GLCM), first order statistics (FOS), for differentiation of Cyst, HEM, HCC and MET classes of the liver. 111 ultrasound images of focal liver disease consisted of 65 typical and 46 atypical images of 88 subjects were collected and 800 ROIs were extracted from the lesion region. This was done after preprocessing which included the enhancement of images. Further, 208 features were extracted. The neural network was used to classify the 5 liver classes. The classified data had 432 out of 500 correctly classified samples. In this study, two modules were developed, namely features extraction module and features classification module. It was noticed from experimentation that atypical cases gave less accuracy as compared to typical cases. It was further noticed that HEM consisted of 90 % atypical cases.

H. Sujana *et al.* [49] used GLRLM and FOS statistical features with NN (neural network) classifier to discriminate between normal, benign and malignant classes of the liver. It was noticed that 92.0 % accuracy was achieved.

S. Poonguzhali *et al*. [50] used autocorrelation, Law's, GLCM, and edge frequency based texture features for analysis of NOR, Cyst, HEM and MET liver classes. The accuracy obtained was 79.0 %.

In these studies [49, 50] malignant lesions were examined as a single class; despite, diagnosis of malignant lesion as MET or HCC was clinically significant for effective management and treatment of liver malignancies [51,52,53]. Moreover, manually feature selection technique was used for extracting better features.

J. Virmani *et al*. [61] classified the primary and secondary malignant focal liver lesions (HCCs and METs) from B-mode ultrasound images using the SVM classifier. In this study, 51 real ultrasound images were used with 54 malignant lesions, HCCs (small HCCs and 14 large HCCs) and MET. Both typical and atypical cases were considered. Further, 120 ROIs from inside and 54 ROI from the surroundings of the lesion were obtained. The size of the ROI used to be 32 × 32 pixels for the classification of five classes. A total of 112 features were extracted in the study (56 ratio and 56 without ratio). The feature selection was done by developing a genetic algorithm.

J. Jeon *et al*. [70] classified the Cyst, hemangioma (HEM) and Malignant focal liver diseases from B-mode ultrasound images using the SVM classifier. In this study, 150 real ultrasound

images with 50 cyst lesions, 50 HEM lesions and 50 malignant lesions were taken. 150 multiple ROIs were segregated from inside and outside the lesion. The features extracted were fed into SVM classifier. It was observed that the improved classification results were obtained in classifying hemangioma and malignant classes. The accuracy of hemangioma was 93 % and for malignant class was 89 %.

Table 2.2 Summary of studies for classification of focal liver lesions

Author(s)	Classes considered	ROI size	No of ROIs	Classifier
H.Yoshida *et al.* [44]	HEM/Malignant	64 × 64 pixels	193	Neural Network
H.Sujana *et al.* [49]	NOR/HEM/Malignant	10 × 10 pixels	113	Neural Network
S.Poonguzhali *et al.*[50]	NOR/Cyst/HEM/Malignant	10 × 10 pixels	120	Neural Network
J.Virmani *et al.* [53]	NOR/Cirrhotic/HCC	32 × 32 pixels	180	SVM
D.Mittal *et al.* [54]	NOR/Cyst/HEM/HCC/MET	25 × 25 pixels	800	Neural Network
J.Virmani *et al.* [61]	HCC/MET	32 × 32 pixels	174	SVM
J.Jeon *et al.* [77]	Cyst/HEM/Malignant	Variable ROI size	150	SVM
J.Virmani *et al.* [78]	NOR/Cyst/HEM/HCC/MET	32 × 32 pixels	491	BPNN
D.Mittal [79]	NOR/Cyst/HEM/HCC/MET	25 × 25 pixels	800	SVM
Present work	Cyst/HEM/HCC/MET	Size of lesion	168	SVM

Note: NOR: Normal, HEM: Hemangioma, HCC: Hepatocellular carcinoma, MET: Metastatic carcinoma, BPNN: Back propagation neural networks.

In another study, J. Virmani *et al*. [53] developed a CAC system for the classification of four focal liver classes (cyst, HEM, HCC and MET) and normal B-mode ultrasound images using a neural network classifier. In this study, 108 real ultrasound images were used, HCCs (10 small HCCs and 40 large HCCs and MET has typical and atypical cases were considered. Further, 300 ROI from inside (IROI) and 111 ROI from the surroundings (SROI) of the lesion were obtained. The size of the ROIs selected was 32 × 32 pixels, for the classification of five classes. A total of 208 features were extracted in the study (104 ratio features and 104 without ratio). These features were dimensionally reduced using principal component analysis (PCA). High classification accuracy of 87.2 % was achieved by the neural network.

H. Yoshida *et al*. [44] classified the HEM, HCC and Malignant focal liver diseases from B-mode ultrasound images using a neural network classifier and developed a system which was capable of differentiating the focal liver echo texture patterns. In this work, 44 ultrasound

images, including 17 HEM, 11 HCC and 16 metastasis cases were analyzed. Further, 193 ROIs consisting of 50 hemangiomas, 87 hepatocellular carcinomas and 56 metastases were used. The ROI of size 25 × 25 pixels was used for the classification of three classes. The first step was to divide the liver ultrasound images into 2 classes benign and malignant, further, multiple texture features were calculated using wavelet packets. These malignant classes were further classified as HCC and MET using neural network.

D. Mittal [45] performed an enhancement technique for focal liver lesions. Results were analyzed before and after enhancement techniques for ultrasound images. This technique increased the accuracy to detect focal liver lesions. Accuracy calculated through this technique was 72.4 %.

P. Bharti *et al.* [46] described liver abnormality appearance in ultrasound images and specified the practical issues experienced while categorizing diffuse liver diseases addressed by software techniques. Computer aided diagnosis along with classifiers and features relevant to the disease were discussed.

From the above studies, it was noticed that in these studies [49, 50] malignant lesions were examined as a single class, despite the diagnosis of malignant lesion as MET or HCC [51,52,53]. However, these classes shall be classified separately as they have significant clinical value. In the present work, the importance of texture analysis of the region neighboring of the lesions is discussed. A CAC system for classification of focal liver lesions is designed and SVM classifier is used to classify B-mode ultrasound images.

2.4 Concluding Remarks

Many researches were carried out in the past for classification of fatty and focal liver images, however, the results were not satisfactory.

(a) Fatty liver diseases: As per the best of the author's learning, a single study is noted in the literature for classifying three fatty liver classes. The experiment is done for grading of fatty liver disease for classifying three fatty liver image classes, i.e. mild, moderate and severe fatty liver. 208 texture features were extracted by using GLCM. The classification accuracy of 66.6 % is obtained using the CAC system. Therefore, in the present work, second order statistical features are comprehensively evaluated for grading of fatty liver disease such as mild, moderate and severe classes, respectively. The image index used in the present work consists of 41 ultrasound image data set and classification is performed by SVM classifier. The brief description of grading of fatty liver disease using US images is given in Fig 2.3.

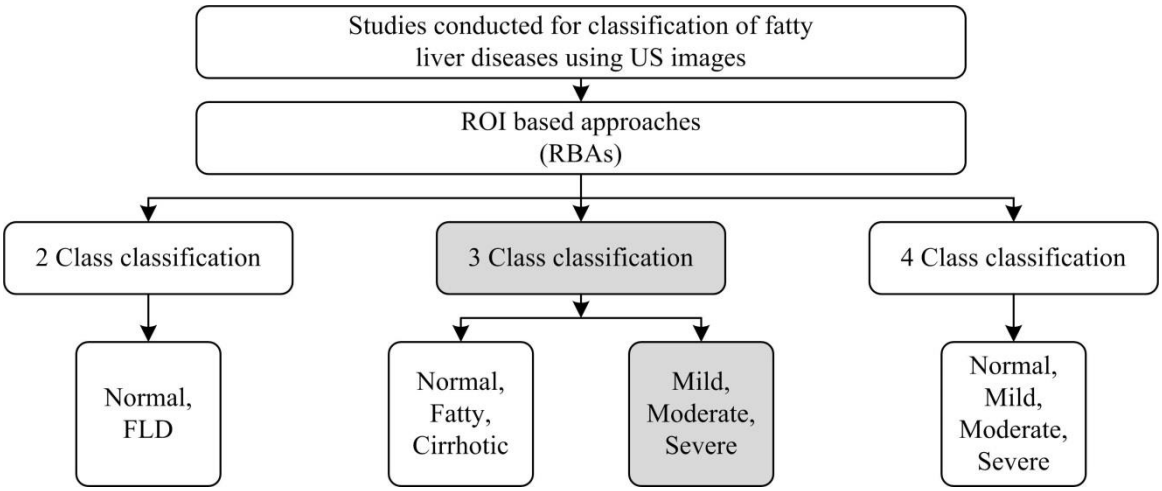

Fig 2.3 Brief description of grading of fatty liver disease
Note: The present work done is shown in the shaded region.

(b) Focal liver lesions: As per the best of the author's learning, three studies have been noted in the literature in which the classification of four liver image classes, i.e. Cyst, HEM, HCC and MET liver [62] was proposed. A large feature vector consisting of 208 texture features were extracted by using GLCM features. The CAC system designed giving better classification accuracy of 78.4 % as compared to other CAC system design by others [78]. In the present work, second order statistical features are comprehensively evaluated for classification of focal liver lesions such as Cyst, HCC, HEM and MET classes respectively. While performing such an experiment, it should be kept in mind that the pixel size less than 800 pixels should not be taken for evaluation statistics as much of the information is lost [69, 53, 57–60]. Therefore, in the proposed study, the author is used the ROI which covers the entire lesion for computing texture parameters. Different features (with and without ratio) are measured from regions inside and surrounding of the lesions.

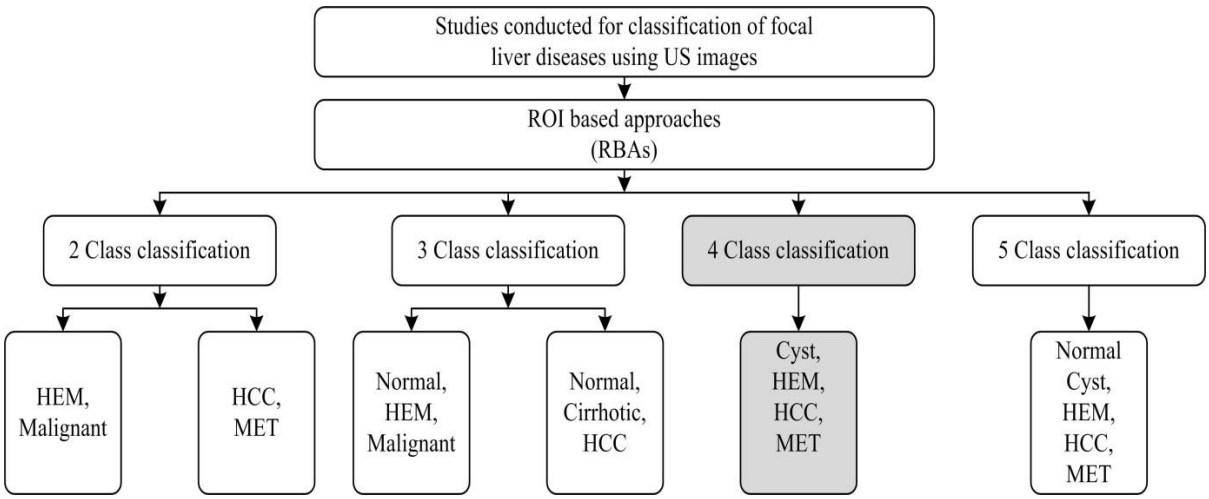

Fig 2.4 Brief description of classification of focal liver lesions
Note: The present work done is shown in the shaded region.

In next chapter methodology for grading of fatty liver disease and classification of focal liver lesions is discussed.

Chapter 3

Methodology

3.1 Introduction

Fatty liver or steatosis [74-81] is a state characterized by the aggregation of fats over the liver [7]. If a person has fatty liver tissue, his liver fat content increases by weight [82-93]. Focal liver diseases [94, 95] are the diseases which affect a small portion of the liver. The four classes of focal liver disease considered are Cyst, hepatocellular carcinoma (HCC), hemangioma (HEM), and metastatic carcinoma (MET). The present work is carried out with a view, grading of fatty liver disease [75-77] into mild, moderate and severe classes and classification of focal liver lesions into cyst, HEM, HCC and MET classes.

3.2 Proposed Interactive System for Grading of Fatty Liver Disease and Classification of Focal Liver Lesions

For grading of fatty liver disease and classification of focal liver lesions, an interactive system is proposed as shown in Fig 3.1.

3.2.1 Module 1: SVM based CAC system for grading of fatty liver disease (without feature selection)

This module classifies fatty liver US images into three classes, namely mild, moderate and severe fatty liver classes respectively. The visibility of the diaphragm is lower as we move from mild to severe fatty liver state. Therefore, ROIs are extracted from the liver parenchyma region as well as from the diaphragm region.

SVM classifier is used to classify the fatty liver ultrasound images into mild, moderate and severe fatty liver in (*Module 1*).

3.2.2 Module 2: SVM based CAC system for grading of fatty liver disease (with feature selection)

In this module, feature selection method GA-*k*NN is used to optimize the feature set by removing the redundant features. The optimized feature set is used to classify the fatty liver US images into mild, moderate and severe fatty liver classes using support vector machine (SVM) classifier.

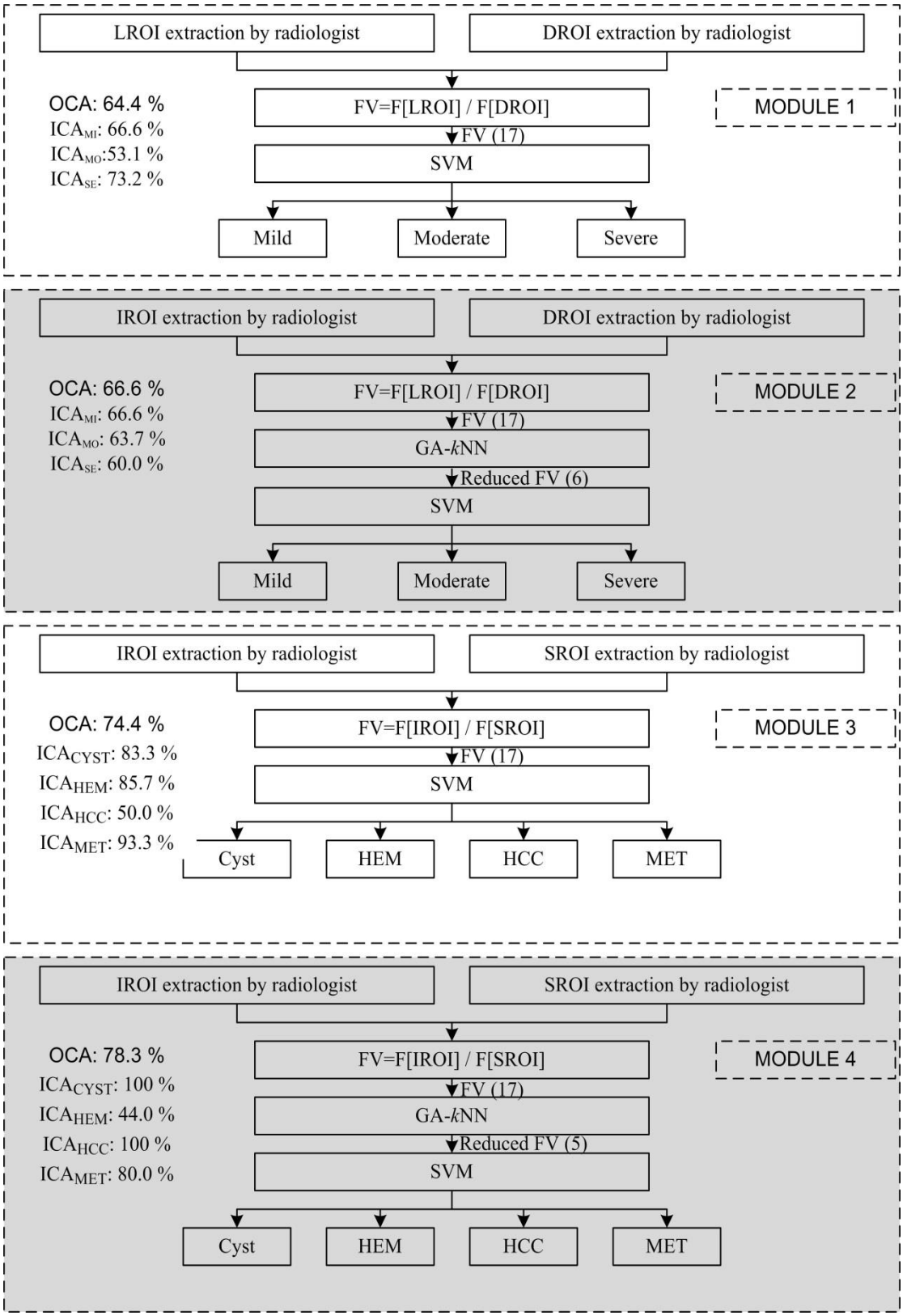

Fig 3.1 Block diagram of the proposed interactive system for grading of fatty liver disease and classification of focal liver lesions

Note: LROI: Liver region of interest, DROI: Diaphragm region of interest, IROI: Inside region of interest, SROI: Surrounding region of interest, Reduced FV: Reduced feature vector.

3.2.3 Module 3: SVM based CAC system for classification of focal liver lesions (without feature selection)

This module classifies focal liver ultrasound images into four classes, namely Cyst, HEM, HCC and MET focal liver classes respectively. The HCC focal liver lesion occurs after cirrhosis. Therefore, ROIs are extracted from the lesion region (IROI) as well as from the surrounding region (SROI).

SVM classifier is used to classify the focal liver US images into Cyst, HEM, HCC and MET focal liver in (*Module 3*).

3.2.4 Module 4: SVM based CAC system for classification of focal liver lesions (with feature selection)

This module classifies focal liver ultrasound images into four classes, namely cyst, HEM, HCC and MET focal liver classes respectively. Feature selection method GA-*k*NN is used to optimized the feature set by removing the redundant features. This optimized feature set is used to classify the focal liver ultrasound images into Cyst, HEM, HCC and MET focal liver classes using the SVM classifier.

3.3 Image Assessment Protocol

The ROI marked should be free from artifacts and sonographic appearance of liver diseases, i.e., fatty and focal liver diseases into different classes should be confirmed by the experienced radiologist based on their proficiency.

3.4 Dataset Description

(a) Fatty liver: In the present work, 41 B-mode ultrasound images containing 14 mild, 14 moderate and 13 severe fatty liver images, collected from Biomedical Instrumentation Laboratory, IIT-Roorkee, Uttarakhand, India, have been used. Images are of size 800 × 600 pixels, with a horizontal and vertical resolution of 96 dpi. The details of the dataset used are shown in Fig. 3.2.

(*b*) *Focal liver:* In the present work, 84 images containing 12 Cyst, 28 HEM, 14 HCC and 30 MET focal liver images have been used. Images are of size 800 × 600 pixels, with a vertical and horizontal resolution of 96 dpi. The detail of the dataset used is shown in Fig. 3.3.

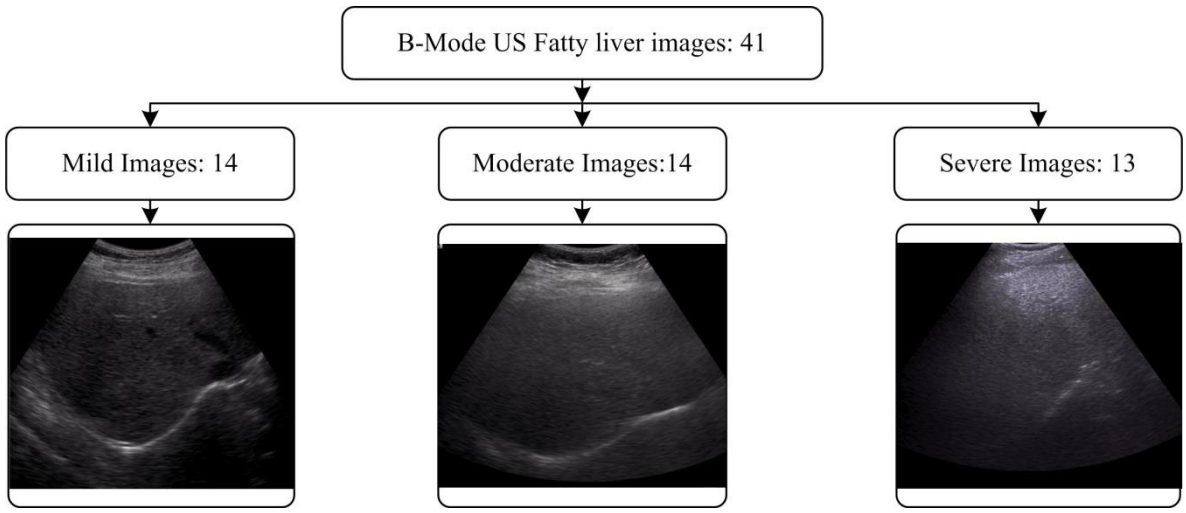

Fig 3.2 Data set description for grading of fatty liver disease

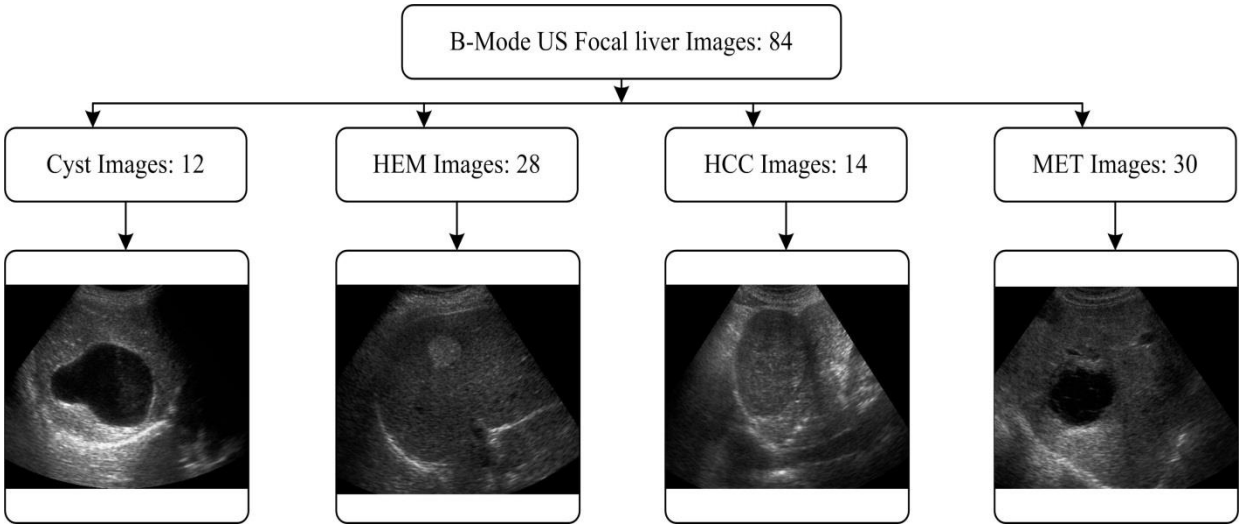

Fig 3.3 Data set description for classification of focal liver lesions

3.4.1 Data collection protocols

Protocols followed for data collection

(i) Ultrasound scanner, Siemens ACUSON X300 is used.

(ii) Extraction of ultrasound images from (right and left) hepatic ducts and blood vessels is not considered.

(iii) The ultrasound images of only liver diseases and no other liver disorder is considered.

3.4.2 ROI Extraction Protocols

The protocols followed for extraction of ROIs and selection of ROI size for design of different modules is explain in this section.

3.4.2.1 Selection of ROIs

The following protocols were followed for cropping the ROIs from the image dataset.

(i) Module 1: **SVM based CAC system for grading of fatty liver disease (without feature selection)**

Fatty liver disease is a diffused disease which affects the entire parenchyma of the liver. In the present study, two types of features are studied for analysis, i.e. Texture feature measure from liver ROI (LROIs) and texture ratio features measured by taking ratio of the texture feature measure from LROI and texture feature measure from corresponding diaphragm ROI (DROI).

A total of 60 LROIs and 14 DROIs are cropped from mild liver, 60 LROIs and 14 DROIs have been cropped from moderate liver and 60 LROIs and 13 DROIs are cropped from severe liver class. The LROI and DROI is not extracted from (right and left) hepatic ducts and blood vessels.

(ii) Module 2: **SVM based CAC system for grading of fatty liver disease (with feature selection)**

A total of 60 LROIs and 14 DROIs are cropped from mild liver, 60 LROIs and 14 DROIs are cropped from moderate liver and 60 LROIs and 13 DROIs are cropped from severe liver class.

(iii) Module 3: **SVM based CAC system for classification of focal liver lesions (without feature selection)**

Focal liver lesions affect the small region of the liver. In ROI extraction module, ROIs are extracted from two parts of the liver, one from inside the lesion inside ROI (IROI) and another from outside the lesion surrounding ROI (SROI). In the present study, analysis of type of texture feature is done, i.e. Texture features measure from IROIs and texture ratio features measured by taking the ratio of the texture feature measure from IROI and texture feature measure from corresponding SROI. The IROI and SROI are not extracted from (right and left) hepatic ducts and blood vessels. A total of 7 IROIs and 7 SROIs are cropped from cyst liver, 15 IROIs and 15 SROIs are cropped from HEM, 6 IROIs and 6 SROIs are cropped from HCC and 14 IROIs and 14 SROIs are cropped from MET liver class.

(iv) Module 4: **SVM based CAC system for classification of focal liver lesions (with feature selection)**

A total of 7 IROIs and 7 SROIs are cropped from cyst liver, 15 IROIs and 15 SROIs are cropped from HEM, 6 IROIs and 6 SROIs are cropped from HCC and 14 IROIs and 14 SROIs are cropped from MET liver class.

3.4.2.2 Selection of ROIs size

The general size varies in the literature from 10 × 10 pixels to 25 × 25 pixels. It is noticed from literature that Sujana et al. [49] has taken ROI size of 10 × 10 whereas in other studies [48, 50], ROI size of 25 × 25 is preferred. However, the pixels lesser than 800 will not give the reliable evaluation statistics. In this study the ROI sizes taken for different modules are discussed below:

(i) Module 1: **SVM based CAC system for grading of fatty liver disease (without feature selection)**

In ROI extraction module, from each ultrasound image, a total of 180 Liver ROIs (LROIs) and 41 Diaphragm ROIs (DROIs) of size 32 × 32 pixels are extracted from the liver parenchyma and diaphragm respectively [70, 71].

(ii) Module 2: **SVM based CAC system for grading of fatty liver disease (with feature selection)**

In ROI extraction module, from each ultrasound image, a total of 180 Liver ROIs (LROIs) and 41 Diaphragm ROIs (DROIs) of size 32 × 32 pixels are extracted from the liver parenchyma and from diaphragm respectively.

(iii) Module 3: **SVM based CAC system for classification of focal liver lesions (without feature selection)**

From each ultrasound image, a total of 84 inside ROIs (IROIs) of a size which cover maximum region of lesion and 84 surrounding ROIs (SROIs) of size 32 × 32 pixels are extracted from the lesion part of the liver and surrounding respectively [81, 82].

(iv) Module 4: **SVM based CAC system for classification of focal liver lesions (with feature selection)**

From each US image, a total of 84 inside ROIs (IROIs) of the size covering maximum region of the lesion and 84 surrounding ROIs (SROIs) of size 32 × 32 pixels are extracted from the lesion part of the liver and surrounding respectively.

3.4.4 Dataset Bifurcation Protocol

The overall distribution of a dataset into training and testing data is explained in this section.

(i) Module 1: **SVM based CAC system for grading of fatty liver disease (without feature selection)**

(*a*) For mild fatty liver, out of 74 ROIs, 36 ROIs are used for training data and 38 ROIs are used for testing data. (*b*) For moderate fatty liver, out of 74 ROIs, 38 ROIs are used for training data and 36 ROIs are used for testing data. (*c*) For severe fatty liver, out of 73 ROIs, 38 ROIs are used for training data and 35 ROIs are used for testing data.

(ii) Module 2: **SVM based CAC system for grading of fatty liver disease (with feature selection)**

(*a*) For mild fatty liver, out of 74 ROIs, 36 ROIs are used for training data and 38 ROIs are used for testing data. (*b*) For moderate fatty liver, out of 74 ROIs, 38 ROIs are used for training data and 36 ROIs are used for testing data. (*c*) For severe fatty liver, out of 73 ROIs, 38 ROIs are used for training data and 35 ROIs are used for testing data.

(iii) Module 3: **SVM based CAC system for classification of focal liver lesions (without feature selection)**

(*a*) For cyst focal liver, out of 24 ROIs, 12 ROIs are used for training data and 12 ROIs are used for testing data. (*b*) For HEM focal liver, out of 56 ROIs, 28 ROIs are used for training data and 28 ROIs are used for testing data. (*c*) For HCC focal liver, out of 28 ROIs, 14 ROIs are used for training data and 14 ROIs are used for testing data. (*d*) For MET focal liver, out of 60 ROIs, 30 ROIs are used for training data and 30 ROIs are used for testing data.

(iv) Module 4: **SVM based CAC system for classification of focal liver lesions (with feature selection)**

(*a*) For cyst focal liver, out of 24 ROIs, 12 ROIs are used for training data and 12 ROIs are used for testing data. (*b*) For HEM focal liver, out of 56 ROIs, 28 ROIs are used for training data and 28 ROIs are used for testing data. (*c*) For HCC focal liver, out of 28 ROIs, 14 ROIs are used for training data and 14 ROIs are used for testing data. (*d*) For MET focal liver, out of 60 ROIs, 30 ROIs are used for training data and 30 ROIs are used for testing data.

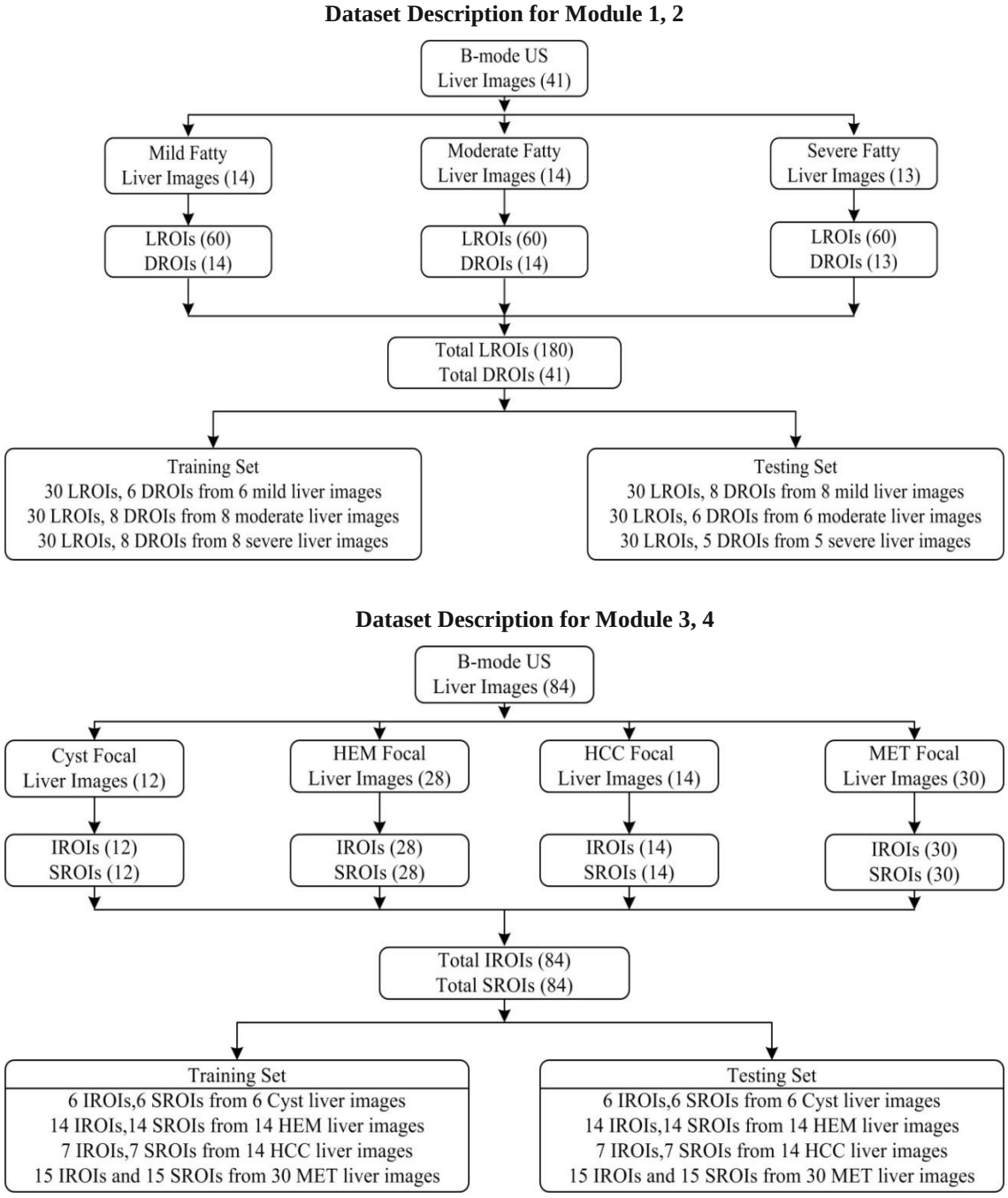

Fig 3.4 Dataset description for grading of fatty liver disease and classification of focal liver lesions and its division into training and testing sets
Note: LROI: Liver region of interest, DROI: Diaphragm region of interest, IROI: Inside region of interest, SROI: Surrounding region of interest.

3.5 Brief Description of Experiments carried out in Present work

The workflow diagram for generalized interactive system employed in present work is shown in Fig 3.5.

3.5.1 *Module 1:* SVM based CAC system for grading of fatty liver disease (without feature selection)

This module classifies fatty liver ultrasound images into three classes, namely mild, moderate and severe fatty liver classes respectively. The second order statistical method GLCM is used to classify the different classes using interpixel distance '*d*' from 1 to 10.

Two types of features have been studied for analysis, i.e. Texture features measure from liver ROI (LROIs) and texture ratio features measure by taking the ratio of the texture feature measure from LROI and texture feature measure from corresponding diaphragm ROI (DROI). For classification of different classes SVM classifier is used.

3.5.2 *Module 2:* SVM based CAC system for grading of fatty liver disease (with feature selection)

This module classifies fatty liver ultrasound images into three classes, namely mild, moderate and severe fatty liver classes respectively The second order statistical method GLCM is used to classify the different classes using interpixel distance '*d*' from 1 to 10. In this module, using GA-*k*NN the best features from module 1 are optimized and are then classified using the SVM classifier.

3.5.3 *Module 3:* SVM based CAC system for classification of focal liver lesions (without feature selection)

This module classifies focal liver ultrasound images into four classes, namely Cyst, HEM, HCC and MET focal liver classes respectively. The second order statistical method GLCM is used to classify the different classes using interpixel distance '*d*' from 1 to 10.

Two types of features have been studied for analysis, i.e. Texture features measure from IROIs and texture ratio features measured by taking the ratio of the texture feature measure from IROI and texture feature measure from corresponding surrounding ROI (SROI). For classification of different classes SVM classifier is used.

3.5.4 *Module 4:* SVM based CAC system for classification of focal liver lesions (with feature selection)

This module classifies focal liver ultrasound images into four classes, namely Cyst, HEM, HCC and MET focal liver classes respectively. The second order statistical method GLCM is used to classify the different classes using interpixel distance '*d*' from 1 to 10. In this module, GA-*k*NN is used for optimization of the best features and then classifies using the SVM classifier.

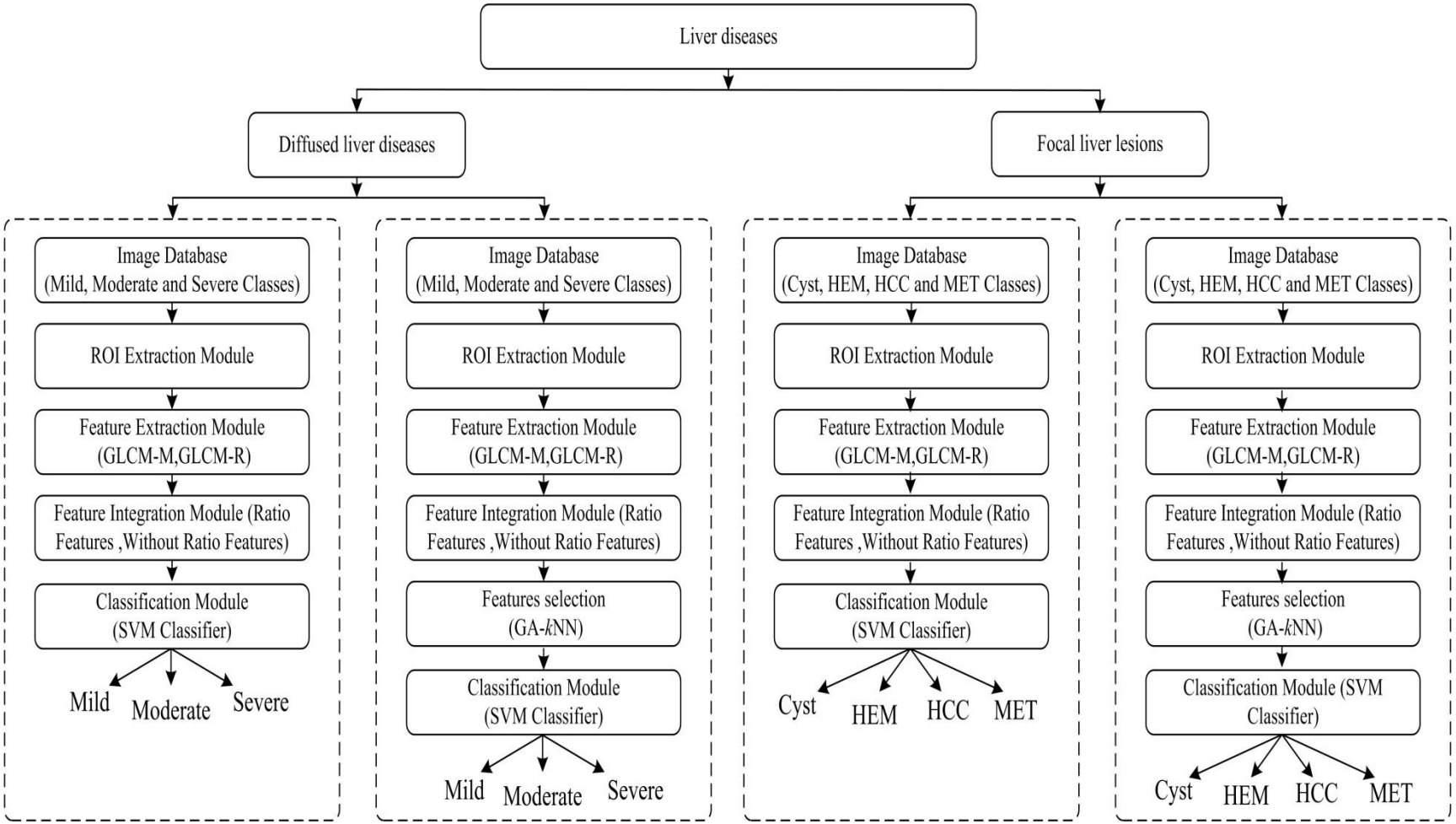

Fig 3.5 Workflow diagram for design of interactive system for diagnosis of liver diseases.
Note: GLCM-M: Grey level co-occurrence matrix mean, GLCM-R: Grey level co-occurrence matrix range, ROI: Region of interest, HEM: Hemangioma, HCC: Hepatocellular carcinoma, MET: Metastatic carcinoma, GA: Genetic algorithm, SVM: Support vector machine.

Concluding Remarks

This chapter covers the techniques for designing an efficient CAC system for grading of fatty liver disease and classification of focal liver lesions into their subclasses. The generalized block diagram for grading of fatty liver disease and classification of focal liver lesions is shown in Fig 3.6 and Fig 3.7.

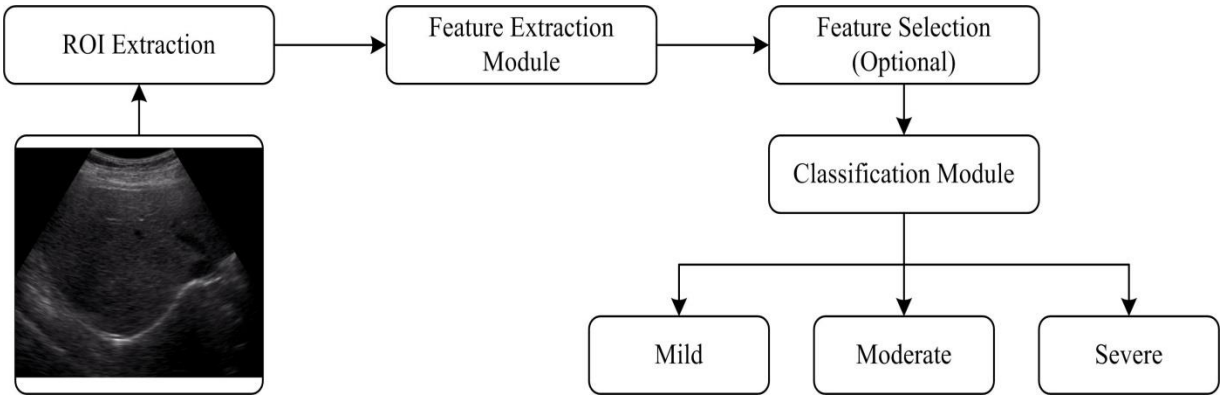

Fig 3.6 Block diagram for grading of fatty liver disease

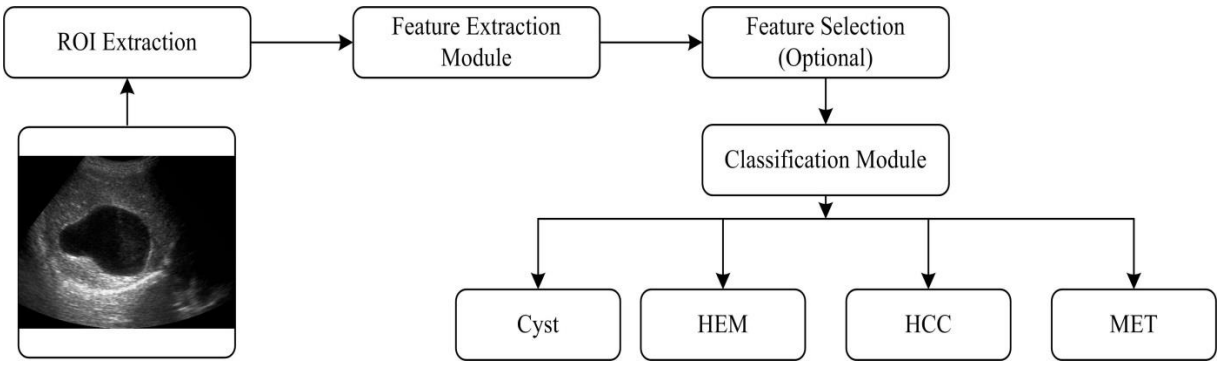

Fig 3.7 Block diagram for classification of focal liver lesions

The feature classification methodology developed is discussed in successive chapters.

Chapter 4

SVM based CAC System for Grading of Fatty Liver Disease

4.1 Introduction

The liver is a fundamental organ of the human body. Its main functions include: bile secretion and detoxification of chemicals from the body useful for digestion. Other functions of the liver are regulation of glycogen storage, disintegration of red blood cells and production of hormones. Liver also plays a dominating role in the metabolism of the human body

The imaging modalities are used to determine how well the liver is working. Ultrasonography or diagnostic sonography is a real time non-invasive imaging technique used to examine internal body parts, their structure or disease affected area of that body part if any [4,5]. As ultrasound is a noninvasive medical test and captures real time images, it gives the structure of internal organs and their activities. However, there are certain limitations in ultrasound imaging.

The CT offers high speed of acquisition, better spatial resolution and more precise contrast enhancement. It has low sensitivity and it needs a high radiation dose to detect the lesions which are smaller than 1cm. The detailed images of the tissues and organs of the body are created using a radio waves and magnetic field, this technique is called Magnetic Resonance Imaging. MRI is the best imaging technique as it provides high lesion-to-liver contrast.

Fatty liver problem occurs on the entire parenchyma of the liver. In the present work, a CAC system is designed for the classification of fatty liver ultrasound images into mild, moderate and severe fatty liver classes. The visibility of the diaphragm is lower as one moves from mild to severe fatty liver state. Therefore, ROIs are extracted from the liver parenchyma region as well as from the diaphragm region.

The sample images of mild, moderate and severe fatty liver classes with ROIs marked are shown in Fig 4.1. For classification of different classes SVM classifier is used. An efficient SVM based CAC system is designed for the grading of fatty liver disease.

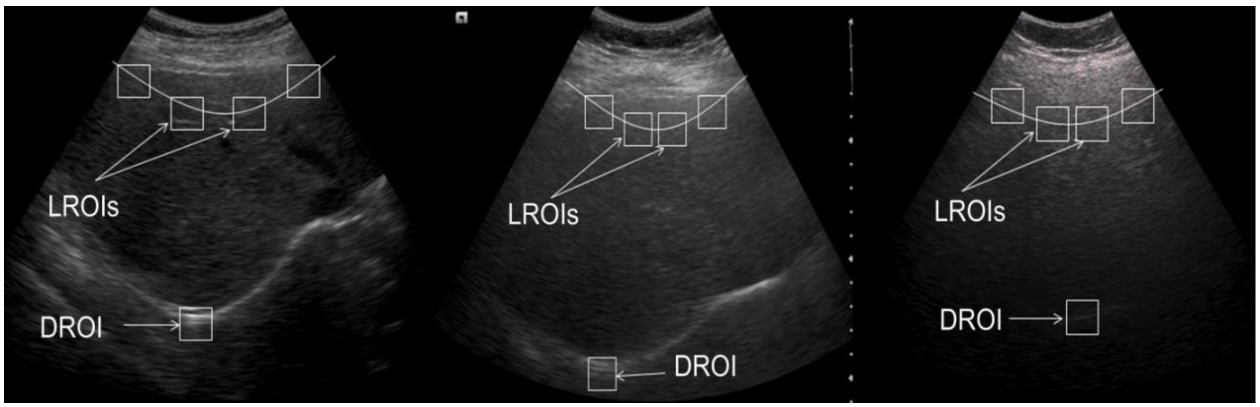

Fig 4.1 Sample images of mild, moderate and severe fatty liver with ROIs marked.
Note: ROI are extracted from the liver parenchyma (LROI) as well from the diaphragm region (DROI) at the same depth.

4.2 Dataset Description and its Bifurcation for Design of SVM based CAC System for Grading of Fatty Liver Disease

In the present work, 41 B-mode ultrasound images containing 14 mild, 14 moderate and 13 severe fatty liver images are used. A total of 180 Liver ROIs (LROIs) and 41 Diaphragm ROIs (DROIs) of size 32 × 32 pixels are extracted from the liver parenchyma and diaphragm respectively. The dataset description and its bifurcation into training and testing dataset for grading of fatty liver disease is depicted in Fig 4.2.

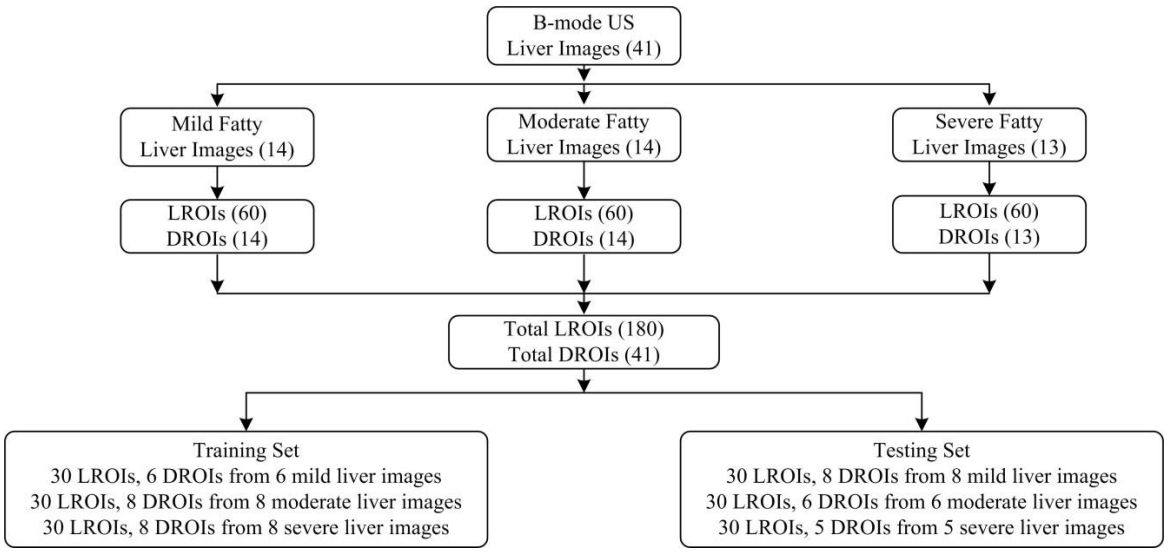

Fig 4.2 Dataset description and its bifurcation for grading of fatty liver

(*a*) For mild fatty liver out of 74 ROIs, 36 ROIs are used for training data and 38 ROIs are used for testing data. (*b*) For moderate fatty liver, out of 74 ROIs, 38 ROIs are used for training data and 36 ROIs are used for testing data. (*c*) For severe fatty liver, out of 73 ROIs, 38 ROIs are used for training data and 35 ROIs are used for testing data.

4.3 Experimental Workflow for the Design of SVM based CAC System for Grading of Fatty Liver Disease

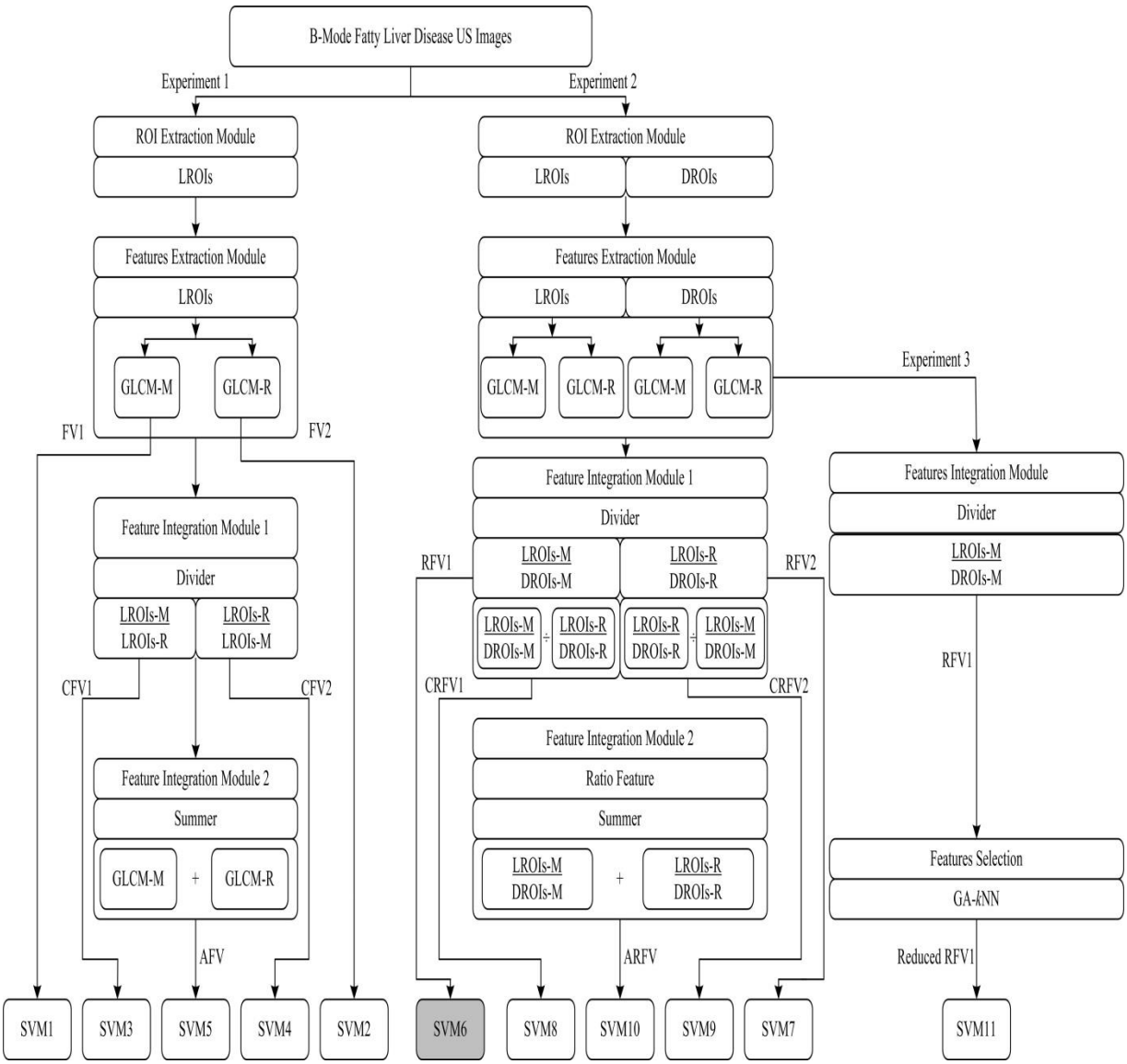

Fig 4.3 Experimental work flow for the design of SVM based CAC system for grading of fatty liver disease

Note:GLCM-M: Grey level co-occurrence matrix mean, GLCM-R: Grey level co-occurrence matrix range, LROI-M: Liver region of interest mean, , DROI-M: Diaphragm region of interest mean, LROI-R: Liver region of interest range, , DROI-R: Diaphragm region of interest range, FV1 :GLCM mean features, FV2 :GLCM range features , CFV1: GLCM mean upon range ratio features CFV2: GLCM range upon mean ratio features, AFV: GLCM mean + GLCM range additive features, RFV1: GLCM mean ratio features,RFV2: GLCM range ratio features CRFV1: (GLCM mean ratio) upon (GLCM range ratio) ratio features,CRFV2: (GLCM range ratio) upon (GLCM mean ratio) ratio features, ARFV: GLCM mean ratio + GLCM range ratio additive features..

The experimental workflow for the proposed computer aided classification (CAC) system design for fatty liver diseases is shown in Fig. 4.3. The present work is carried out for evaluating the efficiency of the proposed CAC system with a view to classify the fatty liver diseases into the mild, moderate and severe classes.

The ROI is an important aspect kept in mind while designing a CAC system. The pixels lesser than 800 will not give the reliable evaluation statistics as much of the information is lost. Second order statistical method GLCM is used for feature extraction. Further, SVM classifier is used for classification.

Different experiments carried out for the grading of fatty liver disease is given below:

4.3.1 Experiment 1: Design of SVM based CAC System for Grading of Fatty Liver Disease (without ratio)

In this experiment ROIs are extracted from the liver parenchyma at the same depth for mild, moderate and severe class. In this experiment GLCM is used for feature extraction. The classification of liver ultrasound images into mild, moderate and severe classes is carried out using the SVM classifier. Experimental workflow diagram for carrying out experiment 1 is given in Fig 4.4

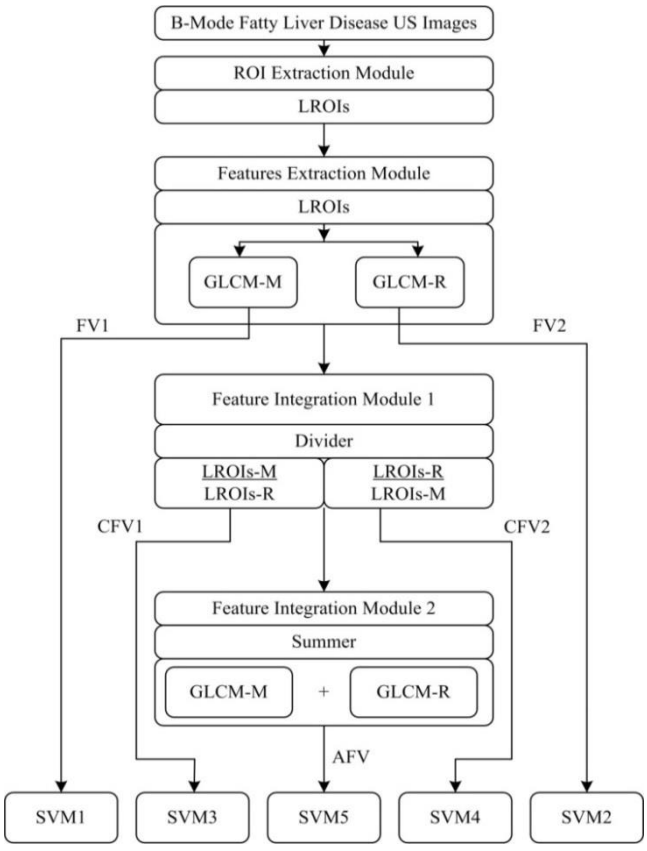

Fig 4.4 Experiment 1: Work flow for the design of SVM based CAC system for grading of fatty liver disease without ratio (only from LROI)

Note: GLCM-M: gray level co-occurrence matrix means, GLCM-R: gray level co-occurrence matrix range, LROI-M: Liver region of interest mean, DROI-M: Diaphragm region of interest mean, LROI-R: Liver region of interest range, DROI-R: Diaphragm region of interest range, FV1: GLCM main features, FV2: GLCM range features, CFV1: GLCM mean upon range ratio features CFV2: GLCM range upon mean ratio features, AFV: GLCM mean + GLCM range additive features,

Different feature vectors used in the design of SVM based CAC system for dgrading of fatty liver disease are given in Table 4.1.

Table 4.1 Different feature vectors used in the design of SVM based CAC system for grading of fatty liver disease (without ratio)

FV(s)	Depiction	*l*
FV1	GLCM mean feature vector	17
FV2	GLCM range feature vector	17
CFV1	GLCM mean and GLCM range ratio feature vector	17
CFV2	GLCM range and GLCM mean ratio feature vector	17
AFV	GLCM mean and GLCM range additive feature vector	17
ARFV	GLCM mean ratio and GLCM range ratio, additive feature vector	17

Note: FV: Feature vector, GLCM: gray level co-occurrence matrix, *l*: feature vector length.

The brief description of the experiment 1 carried out in the present work is given below:

(a) Feature extraction Module for the Design of SVM based CAC System for Grading of Fatty Liver Disease

First order statistics based texture features deal with the gray level distribution of an image. The first order statistics based features do not tell much about the information on the gray level pair of pixels and its relative location. The second order statistics features tell relation between two neighboring pixels in different offsets. The first pixel is called a reference pixel and the other is called a neighboring pixel. The gray level co-occurrence matrix (GLCM) is used to deal with the image attributes based on second order statistics. The GLCM features are calculated for grading of fatty liver disease are shown in Fig 4.1.

GLCM is a matrix where number of gray levels is equivalent to the number of rows and columns. The GLCM matrix of frequencies $P_{\theta,d}$ (I_1, I_2), shows the repetition or the occurrence of gray level pairs. In GLCM matrix, second order statistical probability values depend upon displacement '*d*' and particular angle 'θ' with gray level values of $I_1$and I_2. The second order statistical attributes are selected from GLCM matrix where pixels are treated as a pair and not individually. Basically occurrence matrix depends upon two important parameters:

1. The relative distance measured in between reference pixel and neighbor pixel, is represented as '*d*'.
2. The relative angle 'θ' determined in four directions.

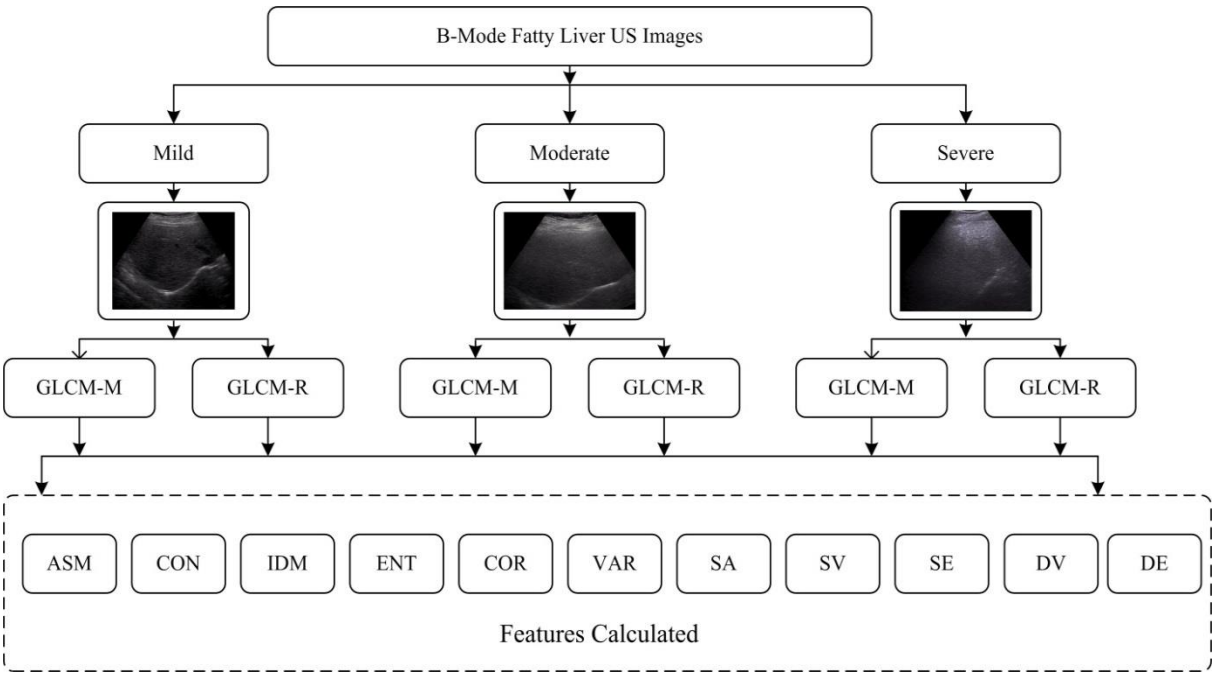

Fig 4.5 GLCM features calculated for grading of fatty liver disease
Note: GLCM-M: GLCM mean feature, GLCM-R: GLCM range feature, ASM: Angular second moment, CON: Contrast, IDM: Inverse difference moment, ENT: Entropy, COR: Correlation, VAR: Variance, SA: Sum average, SV: Sum variance, SE: Sum entropy, DV: Difference variance, DE: Difference entropy.

These four directions show horizontal, vertical, diagonal and anti-diagonal 0º, 45º, 90º and 135 º respectively, and can be represented by the equation (4.1) to equation (4.4).

$$P_{0^0,d}(I_1,I_2)=\left|\left\{\begin{array}{c}[(k,l),(m,n)]\in D\\ k-m=0,|l-n|=d\\ f(k,l)=I_1,\ f(m,n)=I_2\end{array}\right\}\right| \tag{4.1}$$

$$P_{45^0,d}(I_1,I_2)=\left|\left\{\begin{array}{c}[(k,l),(m,n)]\in D\\ (k-m=d,l-n=-d)\vee(k-m=-d,l-n=d)\\ f(k,l)=I_1,\ f(m,n)=I_2\end{array}\right\}\right| \tag{4.2}$$

$$P_{90^0,d}(I_1,I_2)=\left|\left\{\begin{array}{c}[(k,l),(m,n)]\in D\\ k-m=0,|l-n|=0\\ f(k,l)=I_1,\ f(m,n)=I_2\end{array}\right\}\right| \tag{4.3}$$

$$P_{135^0,d}(I_1, I_2) = \left| \left\{ \begin{array}{c} [(k,l),(m,n)] \in D \\ (k-m=d, l-n=d) \vee (k-m=-d, l-n=-d) \\ f(k,l)=I_1,\ f(m,n)=I_2 \end{array} \right\} \right| \tag{4.4}$$

where, these four sets refer to cardinality, $f(k, l)$ is the intensity at pixel position (k, l) in the image of order $(M \times N)$ and order of matrix D is $(M \times N) \times (M \times N)$. The features extracted from GLCM are: coarseness, smoothness and texture- related information that has high discriminatory power. Let Fig. 1 is a matrix of gray levels of an image and Fig. 2 is a co-occurrence matrix of this segment of the image.

1	1	5	6	8
2	3	5	7	1
4	5	7	1	2
8	5	1	2	5

Fig 4.6 (*a*) Gray scale value matrix

	1	2	3	4	5	6	7	8
1	1	2	0	0	1	0	0	0
2	0	0	1	0	1	0	0	0
3	0	0	0	0	1	0	0	0
4	0	0	0	0	1	0	0	0
5	1	0	0	0	0	1	2	0
6	0	0	0	0	0	0	0	1
7	2	0	0	0	0	0	0	0
8	0	0	0	0	1	0	0	0

Fig 4.6 (*b*) Co-occurrence matrix (GLCM)

The GLCM matrix has number of occurrences of a particular pixel pair in an image. These pixel pairs are indicated as (i, j). The GLCM matrix indicates the horizontal repetition of a pixel with a value i adjacent to another pixel having value j. It is clear from Fig4.6 that the occurrences of pixel pairs (1, 1) are only one time and the repetition of pixel pair (1, 2) is two times. These repetitions are clearly defined by the GLCM matrix. The inter-pixel distance 'd' (which is generally defined by offset) and angle θ within a given neighborhood is used for calculated of the probability distribution between pixels.

The example of GLCM is shown in Fig 4.7.

Fig 4.7 (*a*) Test image

0	0	1	1
0	0	1	1
0	2	2	2
2	2	3	3

Fig 4.7 (*b*) Gray level co-occurrence matrix

The intermediate output of the above Figure is given below with GLCM consisting of 16 data cells.

Neighbor pixel value	0	1	2	3
0	0,0	0,1	0,2	0,3
1	1,0	1,1	1,2	1,3
2	2,0	2,1	2,2	2,3
3	3,0	3,1	3,2	3,3

Fig 4.8 (*a*) Intermediate output

The final filled matrix framework obtained is given in Fig 4.8 (*b*):

2	2	1	0
0	2	0	0
0	0	3	1
0	0	0	1

Fig 4.8 (*b*) Final fill framework of GLCM

Angular Second Moment (ASM)

$$ASM = \sum_{i=0}^{G-1}\sum_{j=0}^{G-1}\{P(i,j)\}^2 \tag{4.5}$$

Contrast (CON)

$$CON = \sum_{n=0}^{G-1}(n)^2 \sum_{i=1}^{G}\sum_{j=1}^{G}\{P(i,j)\}, |i-j| = n \tag{4.6}$$

Inverse Difference Moment (IDM)

$$IDM = \sum_{i=0}^{G-1}\sum_{j=0}^{G-1}\frac{1}{1+(i-j)^2}P(i,j) \tag{4.7}$$

Entropy (ENT)

$$ENT = -\sum_{i=0}^{G-1}\sum_{j=0}^{G-1}P(i,j)*\log\big(P(i,j)\big) \tag{4.8}$$

Correlation (COR)

$$COR = \sum_{i}\sum_{j}\frac{(i,j)P(i,j)-\mu_x\mu_y}{\sigma_x\sigma_y} \tag{4.9}$$

Sum of Squares Variance (VAR)

$$VAR = \sum_{i=0}^{G-1}\sum_{j=0}^{G-1}\big(i-\mu\big)^2\,P(i,j) \tag{4.10}$$

Sum Average (SA)

$$SA = \sum_{i=2}^{2N_g} i.P_{x+y}(i) \tag{4.11}$$

Sum Variance (SV)

$$SV = \sum_{i=2}^{2N_g}(i-f_4)^2.P_{x+y}(i) \tag{4.12}$$

Sum Entropy (SE)

$$SE = -\sum_{i=0}^{2N_g}P_{x+y}(i)\left\{\log\left(P_{x+y}(i)\right)\right\} \tag{4.13}$$

Difference Variance (DV)

$$DV = \text{variance of } P_{x-y} \tag{4.14}$$

Difference Entropy (DE)

$$DE = -\sum_{i=0}^{N_g-1} P_{x-y}(i)\left\{\log\left(P_{x-y}(i)\right)\right\} \tag{4.14}$$

Cluster Shade (CS)

$$\text{CS} = \sum_{i,j=1}^{N-1} P_{ij}(i - M_x + 1 - M_y)^3 \tag{4.15}$$

Cluster Prominence (CP)

$$\text{CP} = \sum_{i,j=1}^{N-1} P_{ij}(i - M_x + 1 - M_y)^4 \tag{4.16}$$

Information measures of correlation (IFC):

$$\text{IFC1} = \frac{[-\sum_i \sum_j P(i,j)\log(P(i,j))] - [-\sum_i \sum_j P(i,j)\log(P_x(i)P_y(j))]}{\max[[-\sum_i \sum_j P(i,j)\log(P(i,j))] - [-\sum_i \sum_j P(i,j)\log(P_x(i)P_y(j))]]} \tag{4.17}$$

$$\text{IFC2} = (1 - \exp[-2.0([-\sum_i \sum_j P_x(i)P_y(j)\log(P_x(i)P_y(j))] - [-\sum_i \sum_j P(i,j)\log(P_x(i)P_y(j))])^{\frac{1}{2}} \tag{4.18}$$

Sum correlation (SC)

$$SC = \frac{1}{N^2}\sum_{\substack{i,j=1 \\ i \neq j}}^{N} \Theta(\in - \| \vec{x}(i) - \vec{x}(j) \|), x(i) \in R^m \tag{4.19}$$

Diagonal Moment (DM)

$$DM = \frac{N_{ij}}{\sum_j N_{ij}} \tag{4.20}$$

In the present work, 2nd order statistics based Gray level co-occurrence matrix (GLCM) features are extracted from each ROI. Features namely GLCM-Mean (GLCM-M) and GLCM-Range (GLCM-R) are computed from LROIs for different values of inter-pixel distance '*d*' =1 to 10. A total of 17 features, namely the angular second moment, contrast, correlation, inverse difference moment, variance, sum average, sum variance, difference variance, sum entropy, entropy, difference entropy, information measures of correlation-1, information measures of correlation-2, cluster shade, cluster prominence, diagonal moment, sum correlation are computed from each (LROI and DROI) [72-74].

(b) Feature Integration Module for the Design of SVM based CAC System for Grading of Fatty Liver Disease

(i) Feature Integration Module 1: In feature integration module ratios of (LROIs-M / LROIs-R, LROIs-R / LROIs-M) have been calculated.

(ii) Feature Integration Module 2: In feature integration module 2 additive features have been calculated by adding ratio features [(LROIs-M / LROIs-R) + (LROIs-R/LROIs-M)].

(c) Feature Classification Module for the Design of SVM based CAC System for Grading of Fatty Liver Disease

In the present work, classification of three fatty liver classes, namely mild, moderate and severe is done. Further, SVM classifier is used for classification. The SVM classifier is a supervised classifier that uses decision planes to separate the class boundaries. It uses Gaussian radial basis function kernel to map the data points from the input space to higher dimensional feature space. The C and γ parameters of SVM are selected using a grid search by performing 10-fold cross validation on training data. The feature values are normalized between 0 and 1 by using a method of min-max normalization [96-113].

The results obtained after conducting experiment 1 are shown below:

In experiment 1, 5 different experiments are carried out using different feature vectors (FVs) measure using GLCM statistics by varying inter-pixel distance '*d*' from 1 to 10.

4.3.1.1 ***Experiment 1 (a):*** Evaluating the efficacy of GLCM-M feature vector FV1 using SVM classifier.

In this experiment GLCM-M features are extracted from each LROI by varying the inter-pixel distance '*d*' from 1 to 10 is reported in Table 4.2. The extracted features are passed to SVM classifier and the performance of the proposed CAC system is evaluated.

Table 4.2 Performance of FV1 computed for inter pixel distance *d* from 1 to 10 using SVM classifier

FV (*l*)	*d*	OCA	ICA_{MI}	ICA_{MO}	ICA_{SE}
FV1 (17)	1	20.0	33.3	9.9	16.5
	2	35.5	53.1	26.4	26.4
	3	35.5	53.1	19.8	33.3
	4	38.8	30.0	9.9	43.2
	5	36.6	36.9	53.1	19.8
	6	38.8	46.5	26.4	43.2
	7	41.1	53.1	30.0	39.9
	8	36.6	39.9	26.4	43.2
	9	36.6	53.1	30.0	26.4
	10	41.1	33.3	36.6	53.1

Note: *d*: Inter-pixel distance, OCA: Overall classification accuracy; ICA_{MI}: Individual classification accuracy of mild class, ICA_{MO}: Individual classification accuracy of moderate class, ICA_{SE}: Individual classification accuracy of severe class. OCA and ICA values are expressed in %age.

GLCM-M statistics derived from LROI yield maximum overall classification accuracy value of 41.1 % and ICA values of 53.1 %, 30 % and 39.9 % at d = 7. For '*d*' = 10, the overall classification accuracy of 41.1 % and ICA values of 33.3 %, 36.6 % and 53.1 % is achieved for the above mentioned three stages.

4.3.1.2 ***Experiment 1 (b):*** Evaluating the efficacy of GLCM-R feature vector FV2 using SVM classifier.

In this experiment GLCM-R features are extracted from each LROI by varying the inter-pixel distance '*d*' from 1 to 10 is reported in Table 4.3. The extracted features are passed to SVM classifier and the performance of the proposed CAC system is evaluated.

Table 4.3 Performance of FV2 computed for inter pixel distance *d* from 1 to 10 using SVM classifier.

FV (*l*)	*d*	OCA	ICA_{MI}	ICA_{MO}	ICA_{SE}
FV2 (17)	1	25.5	33.3	23.1	19.8
	2	30.0	49.8	16.5	23.1
	3	25.5	33.3	13.2	30.0
	4	33.3	46.5	16.5	36.6
	5	35.5	63.3	26.4	16.5
	6	33.3	49.8	26.4	23.1
	7	36.6	39.9	13.2	56.4
	8	33.3	49.8	6.6	43.2
	9	36.6	63.3	3.3	43.2
	10	26.6	33.3	16.5	30.0

Note: *d*: Inter-pixel distance, OCA: Overall classification accuracy; ICA_{MI}: Individual classification accuracy of mild class, ICA_{MO}: Individual classification accuracy of moderate class, ICA_{SE}: Individual classification accuracy of severe class. OCA and ICA values are expressed in % age.

GLCM-R statistics derived from LROI yield maximum overall classification accuracy (OCA) value of 36.6 % at '*d*' =7 and ICA values of 39.9 %, 13.2 % and 56.4 % for mild, moderate and severe classes, respectively.

4.3.1.3 ***Experiment 1 (c):*** Evaluating the efficacy of GLCM-M and GLCM-R ratio feature vector CFV1 using SVM classifier.

In this experiment ratio of GLCM-M and GLCM-R features are extracted from each LROI by varying the inter-pixel distance '*d*' from 1 to 10 is reported in Table 4.4. The extracted features are passed to SVM classifier and the performance of the proposed CAC system is evaluated.

Table 4.4 Performance of CFV1 computed for inter pixel distance *d* from 1 to 10 using SVM classifier.

FV (*l*)	***d***	**OCA**	**ICA_{MI}**	**ICA_{MO}**	**ICA_{SE}**
CFV1 (17)	1	44.4	76.5	13.2	43.2
	2	56.6	83.1	19.8	66.6
	3	47.7	60	19.8	63.3
	4	38.8	53.1	6.6	56.4
	5	41.1	56.4	3.3	63.3
	6	48.8	60.0	13.2	73.2
	7	48.8	73.2	23.1	49.8
	8	47.7	69.9	16.5	56.4
	9	44.4	56.4	16.5	60.0
	10	51.1	69.9	19.8	63.3

Note: *d*: Inter-pixel distance, OCA: Overall classification accuracy; ICA_{MI}: Individual classification accuracy of mild class, ICA_{MO}: Individual classification accuracy of moderate class, ICA_{SE}: Individual class accuracy of severe class. OCA and ICA values are expressed in % age.

The ratio of GLCM-M and GLCM-R statistics derived from LROI yield maximum OCA value of 56.6 % at '*d*' = 2 and ICA values of 83.1 %, 19.8 % and 66.6 % for mild, moderate and severe classes, respectively.

4.3.1.4 ***Experiment 1 (d):*** Evaluating the efficacy of GLCM-R and GLCM-M ratio feature vector CFV2 using SVM classifier.

In this experiment ratio of GLCM-R and GLCM-M features are extracted from each LROI by varying the inter-pixel distance '*d*' from 1 to 10 is reported in Table 4.5. The extracted features are passed to SVM classifier and the performance of the proposed CAC system is evaluated.

Table 4.5 Performance of CFV2 computed for inter pixel distance *d* from 1 to 10 using SVM classifier.

FV (*l*)	***d***	**OCA**	**ICA_{MI}**	**ICA_{MO}**	**ICA_{SE}**
CFV2 (17)	1	24.0	33.3	26.6	36.6
	2	26.6	50.0	10.0	13.3
	3	22.2	23.3	30.0	26.6
	4	23.3	43.3	10.0	23.3
	5	30.0	60.0	6.6	23.3
	6	28.8	30.0	20.0	33.3
	7	37.7	46.6	23.3	46.6
	8	28.8	40.0	23.3	33.3
	9	31.1	3.0	80.0	10.0
	10	30.0	0.0	60.0	30.0

Note: *d*: Inter-pixel distance, OCA: Overall classification accuracy; ICA_{MI}: Individual classification accuracy of mild class, ICA_{MO}: Individual classification accuracy of moderate class, ICA_{SE}: Individual class accuracy of severe class. OCA and ICA values are expressed in % age.

The ratio of GLCM-R statistics and GLCM-M statistics derived from IROI yield maximum OCA value of 37.7 % at '*d*' = 7 and ICA values of 46.6 %, 23.3 % and 46.6 % for mild, moderate and severe classes, respectively.

4.3.1.5 ***Experiment 1 (e):*** Evaluating the efficacy of GLCM-M and GLCM-R addition feature vector AFV using SVM classifier.

In this experiment addition of GLCM-M and GLCM-R features are extracted from each LROI by varying the inter-pixel distance '*d*' from 1 to 10 is reported in Table 4.6. The extracted features are passed to SVM classifier and the performance of the proposed CAC system is evaluated.

Table 4.6 Performance of AFV computed for inter pixel distance *d* from 1 to 10 using SVM classifier.

FV (*l*)	***d***	**OCA**	**ICA_{MI}**	**ICA_{MO}**	**ICA_{SE}**
AFV (17)	1	27.7	43.3	16.6	23.3
	2	30.0	56.6	13.0	20.0
	3	33.3	53.3	13.3	33.3
	4	30.0	43.3	16.6	30.0
	5	30.0	43.3	13.3	33.3
	6	33.3	53.3	13.3	40.0
	7	35.3	33.3	20.0	53.3
	8	33.3	46.6	3.3	50.0
	9	34.4	33.3	0.0	50.0
	10	24.4	33.3	6.6	33.3

Note: *d*: Inter-pixel distance, OCA: Overall classification accuracy; ICA_{MI}: Individual classification accuracy of mild class, ICA_{MO}: Individual classification accuracy of moderate class, ICA_{SE}: Individual class accuracy of severe class. OCA and ICA values are expressed in % age.

The ratio of GLCM-R statistics and GLCM-M statistics derived from LROI yield maximum classification accuracy value of 35.3 % at '*d*' = 7 and ICA values of 33.3 %, 20.0 % and 53.3 % for mild, moderate and severe classes, respectively.

From experiment 1, it is observed that for feature extracted using statistical method, maximum OCA value of 56.6 % is obtained with ratio of GLCM-M and GLCM-R feature vector (CFV1) computed at inter-pixel distance d = 1 along with ICA values of 79.8 %, 30.0 % and 60.0 % for mild, moderate and severe classes, respectively. The detailed result obtained from GLCM-M and GLCM-R statistics is given in Table 4.7.

Table 4.7 Description of FVs yielding the best classification accuracy values in experiments 1 (*a*) to 1 (*e*) using SVM classifier.

FV (*l*)	*d*	OCA	ICA_{MI}	ICA_{MO}	ICA_{SE}
FV1 (17)	7	41.1	53.1	30.0	39.9
FV2 (17)	9	36.6	63.3	3.3	43.2
CFV1 (17)	1	56.6	79.8	30.0	60.0
CFV2 (17)	7	35.3	33.3	20.0	53.3
AFV (17)	7	37.7	46.6	23.3	46.6

Note: *d*: Inter-pixel distance, OCA: Overall classification accuracy; ICA_{MI}: Individual classification accuracy of mild class, ICA_{MO}: Individual classification accuracy of moderate class, ICA_{SE}: Individual classification accuracy of severe class. OCA and ICA values are expressed in % age.

4.3.2 Experiment 2: Design of SVM based CAC System for Grading of Fatty Liver Disease (with ratio)

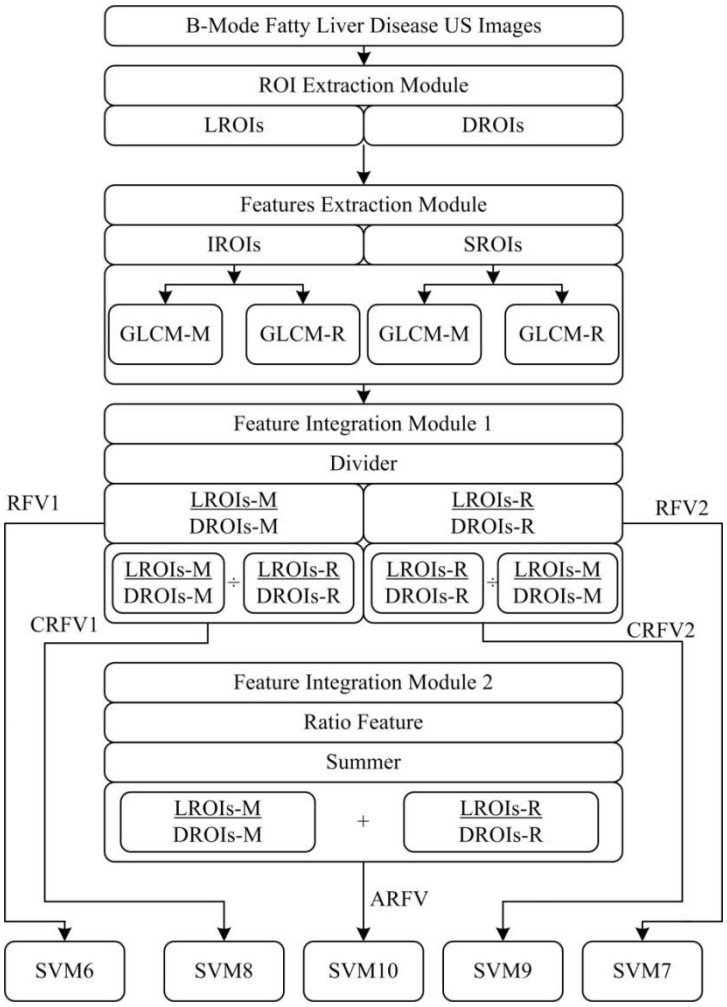

Fig 4.9 Experiment 2: Work flow for the design. of SVM based CAC system for grading of fatty liver disease with ratio (LROI and DROI)

Note: GLCM-M: Grey level co-occurrence matrix mean, GLCM-R: Grey level co-occurrence matrix range, LROI-M: Liver region of interest mean, , DROI-M: Diaphragm region of interest mean, LROI-R: Liver region of interest range, , DROI-R: Diaphragm region of interest range, RFV1: GLCM mean ratio features,RFV2: GLCM range ratio features CRFV1: (GLCM mean ratio) upon (GLCM range ratio) ratio features,CRFV2: (GLCM range ratio) upon (GLCM mean ratio) ratio features, ARFV: GLCM mean ratio + GLCM range ratio additive features..

In this experiment ROIs are extracted from liver parenchyma as well as from the diaphragm region for mild, moderate and severe class. In this experiment GLCM is used for feature extraction. The classification of liver US images into mild, moderate and severe classes is carried out using the SVM classifier. Experimental workflow diagram for carrying out experiment 2 is given in Fig 4.9

Different feature vectors used in design of SVM based CAC system for grading of fatty liver disease (with ratio) is given in Table 4.8.

Table 4.8 Different feature vectors used in design of SVM based CAC system for grading of fatty liver disease (with ratio).

FV(s)	Depiction	*l*
RFV1	GLCM mean ratio feature vector	17
RFV2	GLCM range ratio feature vector	17
CRFV1	GLCM mean ratio and GLCM range ratio, ratio feature vector	17
CRFV2	GLCM range ratio and GLCM mean ratio, ratio feature vector	17
ARFV	GLCM mean ratio and GLCM range ratio, additive feature vector	17

Note: FV: Feature vector, GLCM: Grey level co-occurrence matrix, *l*: feature vector length.

The brief description of experiment 2 carried out in the present work is given below:

(a) Feature extraction Module for the Design of SVM based CAC System for Grading of Fatty Liver Disease

First order statistics based texture features deal with the gray level distribution of an image. The first order statistics based features do not tell much about the information on the gray level pair of pixels and its relative location. The second order statistics features tell relation between two neighboring pixels in different offsets. The first pixel is called a reference pixel and other is called a neighboring pixel. The gray level co-occurrence matrix (GLCM) is used to deal with the image attributes based on second order statistics.

In the present work, 2^{nd} order statistics based Gray level co-occurrence matrix (GLCM) features have been extracted from each ROI. Features namely GLCM-Mean (GLCM-M) and GLCM-Range (GLCM-R) have been computed from LROIs, DROIs for different values of inter-pixel distance '*d*' = 1 to 10. These feature sets of (LROIs and DROIs) are combined in three ways in the present work: (*a*) Ratio features, (*b*) Inverse ratio features and (*c*) additive ratio features. A total of 17 features, namely the angular second moment , contrast, correlation, inverse difference moment, variance, sum average, sum variance, difference variance, sum entropy, entropy, difference entropy, information measures of correlation-1, information measures of

correlation-2, Cluster Shade, Cluster Prominence, Diagonal Moment, Sum Correlation have been computed from each (LROI and DROI) [72-74].

(b) Feature Integration Module for the Design of SVM based CAC System for Grading of Fatty Liver Disease

(*i*) *Feature Integration Module 1:* In feature integration module ratios of (LROIs-M / DROIs-M ratio with LROIs-R / DROIs-R, LROIs-R / DROIs-R ratio with LROIs-M / DROIs-M) have been calculated.

(*ii*) *Feature Integration Module 2:* In feature integration module 2 additive features have been calculated by adding ratio features [(LROIs-M / DROIs-M ratio with LROIs-R / DROIs-R) + (LROIs-R / DROIs-R ratio with LROIs-M / DROIs-M)].

(c) Feature Classification Module for the Design of SVM based CAC System for Grading of Fatty Liver Disease

For classification of different grades of fatty liver SVM classifier is used. The results obtained are given below:

In the experiment 2, 5 different experiments are carried out using different feature vectors (FVs) measure using GLCM statistics by varying inter-pixel distance '*d*' from 1 to 10.

4.3.2.1 ***Experiment 2 (a):*** Evaluating the efficacy of GLCM mean ratio feature vector RFV1 using SVM classifier.

In this experiment ratio of GLCM-M features are extracted from each LROIs and DROIs by varying the inter-pixel distance '*d*' from 1 to 10 is reported in Table 4.9. The extracted features are passed to SVM classifier and the performance of the proposed CAC system is evaluated.

Table 4.9 Performance of RFV1 computed for inter pixel distance *d* from 1 to 10 using SVM classifier.

FV (*l*)	*d*	OCA	ICA_{MI}	ICA_{MO}	ICA_{SE}
RFV1 (17)	1	41.1	60.0	43.2	19.8
	2	48.8	60.0	43.2	43.2
	3	54.4	76.5	23.1	63.3
	4	53.3	73.2	33.3	53.1
	5	53.3	76.5	43.2	39.9
	6	57.7	79.8	39.9	53.1
	7	41.1	53.1	30.0	39.9
	8	41.1	66.6	19.8	36.6
	9	44.4	53.1	19.8	60.0
	10	64.4	66.6	53.1	73.2

Note: *d*: Inter-pixel distance, OCA: Overall classification accuracy; ICA_{MI}: Individual classification accuracy of mild class, ICA_{MO}: Individual classification accuracy of moderate class, ICA_{SE}: Individual classification accuracy of severe class. OCA and ICA values are expressed in % age.

The ratio of GLCM-M statistics derived from LROI and DROI yield maximum classification accuracy value of 64.4 % at '*d*' = 10 and ICA values of 66.6 %, 53.1 % and 73.2 % for mild, moderate and severe classes, respectively.

4.3.2.2 ***Experiment 2 (b):*** Evaluating the efficacy of GLCM-R ratio feature vector RFV2 using SVM classifier.

In this experiment ratio of GLCM-R features are extracted from each LROIs and DROIs by varying the inter-pixel distance '*d*' from 1 to 10 is reported in Table 4.10. The extracted features are passed to SVM classifier and the performance of the proposed CAC system is evaluated.

Table 4.10 Performance of RFV2 computed for inter pixel distance *d* from 1 to 10 using SVM classifier.

FV (*l*)	***d***	**OCA**	**ICA_{MI}**	**ICA_{MO}**	**ICA_{SE}**
RFV2 (17)	1	56.6	73.2	19.8	76.5
	2	48.8	69.9	69.9	36.6
	3	47.7	49.8	30.0	63.3
	4	43.3	63.3	30.0	36.6
	5	46.6	46.5	63.3	30.0
	6	45.5	60.0	43.2	33.3
	7	43.3	46.5	39.9	43.2
	8	41.11	46.5	39.9	36.6
	9	47.7	53.1	49.8	39.9
	10	56.6	79.8	30.0	60.0

Note: *d*: Inter-pixel distance, OCA: Overall classification accuracy; ICA_{MI}: Individual classification accuracy of mild class, ICA_{MO}: Individual classification accuracy of moderate class, ICA_{SE}: Individual classification accuracy of severe class. OCA and ICA values are expressed in % age.

The ratio of GLCM-R statistics derived from LROI and DROI yield maximum OCA value of 56.6 % at '*d*' = 1 and ICA values of 73.2 %, 19.8 % and 76.5 %. For *d* = 10, the OCA value of 56.6 % and ICA values of 79.8 %, 30 % and 60 % for mild, moderate and severe classes, respectively.

4.3.2.3 ***Experiment 2 (c):*** Evaluating the efficacy of GLCM-M and GLCM-R, ratio feature vector CRFV1 using SVM classifier.

In this experiment ratio of GLCM-M and GLCM-R features are extracted from each LROIs and DROIs by varying the inter-pixel distance '*d*' from 1 to 10 is reported in Table 4.11. The extracted features are passed to SVM classifier and the performance of the proposed CAC system is evaluated.

Table 4.11 Performance of CRFV1 computed for inter pixel distance *d* from 1 to 10 using SVM classifier.

FV (*l*)	*d*	OCA	ICA_{MI}	ICA_{MO}	ICA_{SE}
CRFV1 (17)	1	54.4	83.1	9.9	69.9
	2	52.2	79.8	3.3	73.2
	3	52.2	73.2	19.8	63.3
	4	56.6	79.8	30.0	60.0
	5	63.3	86.4	23.1	79.8
	6	56.6	83.1	30.0	56.4
	7	50.0	73.2	16.5	60.0
	8	46.6	56.4	26.4	56.4
	9	51.1	66.6	23.1	63.3
	10	47.7	66.6	26.4	49.8

Note: *d*: Inter-pixel distance, OCA: Overall classification accuracy; ICA_{MI}: Individual classification accuracy of mild class, ICA_{MO}: Individual classification accuracy of moderate class, ICA_{SE}: Individual classification accuracy of severe class. OCA and ICA values are expressed in % age.

Ratio of GLCM-M statistics and GLCM-R statistics derived from LROI and DROI yield maximum OCA value of 63.3 % at '*d*' = 5 and ICA values of 86.4 %, 23.1 % and 79.8 % for mild, moderate and severe classes, respectively.

4.3.2.4 ***Experiment 2 (d):*** Evaluating the efficacy of GLCM-R and GLCM-R ratio, ratio feature vector CRFV2 using SVM classifier.

In this experiment ratio of GLCM-R and GLCM-M features are extracted from each LROIs and DROIs by varying the inter-pixel distance '*d*' from 1 to 10 is reported in Table 4.12. The extracted features are passed to SVM classifier and the performance of the proposed CAC system is evaluated.

Table 4.12 Performance of CRFV2 computed for inter pixel distance *d* from 1 to 10 using SVM classifier.

FV (*l*)	*d*	OCA	ICA_{MI}	ICA_{MO}	ICA_{SE}
CRFV2 (17)	1	53.3	76.5	16.5	66.9
	2	51.1	79.8	6.6	66.6
	3	53.3	73.2	23.1	63.3
	4	57.7	56.4	43.2	73.2
	5	45.5	39.9	23.1	73.2
	6	54.4	66.6	26.4	69.9
	7	52.2	66.6	30.0	60.0
	8	45.5	79.8	36.6	19.8
	9	50.0	73.2	33.3	43.2
	10	45.5	73.2	26.4	36.6

Note: *d*: Inter-pixel distance, OCA: Overall classification accuracy; ICA_{MI}: Individual classification accuracy of mild class, ICA_{MO}: Individual classification accuracy of moderate class, ICA_{SE}: Individual classification accuracy of severe class. OCA and ICA values are expressed in % age.

The inverse ratio of GLCM-M and GLCM-R statistics derived from LROI and DROI yield maximum OCA value of 54.4 % at '*d*' = 6 and ICA values of 66.6 %, 26.4 % and 69.9 % for mild, moderate and severe classes, respectively.

4.3.2.5 ***Experiment 2 (e):*** Evaluating the efficacy of GLCM-M and GLCM-R additive, ratio feature vector ARFV using SVM classifier.

In this experiment addition of GLCM-M and GLCM-R features are extracted from each LROIs and DROIs by varying the inter-pixel distance '*d*' from 1 to 10 is reported in Table 4.13. The extracted features are passed to SVM classifier and the performance of the proposed CAC system is evaluated.

Table 4.13 Performance of ARFV computed for inter-pixel distance *d* from 1 to 10 using SVM classifier.

	d	**OCA**	**ICA_{MI}**	**ICA_{MO}**	**ICA_{SE}**
ARFV (17)	1	53.3	86.4	6.6	66.6
	2	47.7	69.9	9.9	66.6
	3	43.3	49.8	16.5	63.3
	4	51.1	63.3	30.0	60.0
	5	45.5	53.1	19.8	63.3
	6	46.6	63.3	19.8	56.4
	7	40.0	60.0	9.9	49.8
	8	40.0	63.3	9.9	46.5
	9	43.3	56.4	19.8	53.1
	10	41.1	66.6	13.2	43.2

Note: *d*: Inter-pixel distance, OCA: Overall classification accuracy; ICA_{MI}: Individual classification accuracy of mild class, ICA_{MO}: Individual classification accuracy of moderate class, ICA_{SE}: Individual classification accuracy of severe class. OCA and ICA values are expressed in % age.

The addition of the ratio of GLCM mean and GLCM range statistics derived from LROI and DROI yield maximum OCA value of 53.1 % at d=1 and ICA values of 86.4 %, 6.6 % and 66.6 % for mild, moderate and severe classes, respectively.

From experiment 2, it is observed that for feature extracted using statistical method, maximum OCA value of 64.4 % is obtained with ratio of GLCM-M statistics derived from LROI and DROI (RFV1) computed at inter-pixel distance d = 10 along with ICA values of 66.6 %, 53.1 % and 73.2 % for mild, moderate and severe classes, respectively. The detailed result obtained from GLCM-M and GLCM-R statics is given in Table 4.14.

Table 4.14 Description of FVs yielding the best classification accuracy values in experiments 2 (*a*) to 2 (*e*) using SVM classifier.

FVs (*l*)	***d***	**OCA**	**ICA_{MI}**	**ICA_{MO}**	**ICA_{SE}**
RFV1 (17)	10	64.4	66.6	53.1	73.2
RFV2 (17)	1	56.6	79.8	30.0	60.0
CRFV1 (17)	6	63.3	86.4	23.1	79.8
CRFV2 (17)	4	57.7	56.4	43.2	73.2
ARFV (17)	1	53.3	86.4	6.6	66.6

Note: *d*: Inter-pixel distance, OCA: Overall classification accuracy; ICA_{MI}: Individual classification accuracy of mild class, ICA_{MO}: Individual classification accuracy of moderate class, ICA_{SE}: Individual classification accuracy of severe class. OCA and ICA values are expressed in % age.

4.3.3 SVM based CAC System for Grading of Fatty Liver Disease (with feature selection)

Optimization is a process which makes something as fully as perfect by finding the maximum value of function involved in it. Different types of optimization techniques have been used for feature selection in image processing. In this study, GA-*k*NN feature selection technique has been used [42,114,115]. A GA implementation step is shown in Fig 4.10.

The classification task in real time can be increased when irrelevant features present and the classification accuracy also reduces. In the present work, two steps are as follows:-

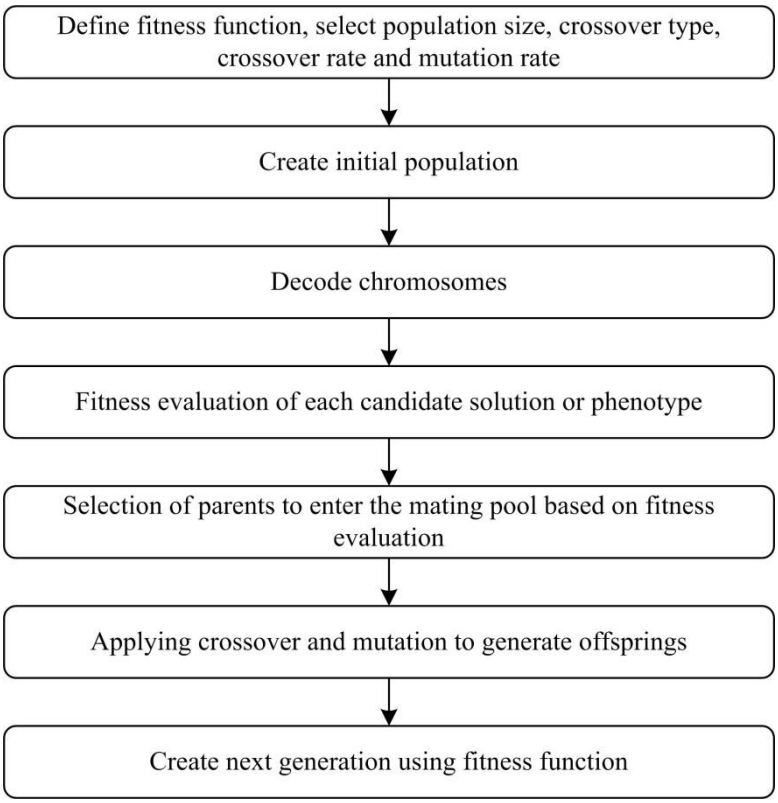

Fig 4.10 GA implementation steps

(*a*) Removal of (FVs) whose classification accuracy is less and find the FV, which has a maximum classification accuracy among them with the help of *k*-NN classifier.

(*b*) Here the binary genetic algorithm (GA) is applied for feature selection to find the subset of The FV and the fitness function for GA is maximum classification accuracy obtained by the *k*-NN.

In the present study population size = 20, mutation rate = 0.05, crossover rate= 0.7 is used.

The features selected after applying GA-*k*NN feature selection technique are angular second moment-mean, contrast-mean, sum of average-mean, sum of variance-mean, entropy-mean and difference entropy-mean.

The ratio of GLCM mean statistics derived from LROI and DROI yield maximum classification accuracy value of 64.4 % and ICA values of 66.6 %, 53.1 % and 73.2 % at '*d*' = 10 for mild, moderate and severe classes, respectively. After feature selection using GA-*k*NN, classification accuracy increase to 66.6 % and ICA values of 68.8 %, 60.0 % and 73.2 % for mild, moderate and severe image classes. Optimized fatty liver features are shown in Fig 4.3.

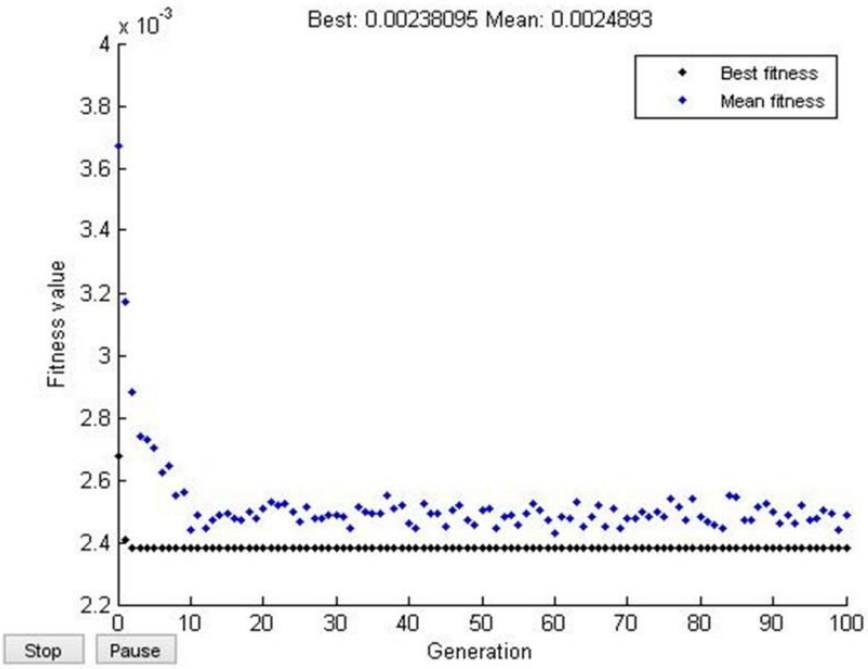

Fig 4.11: Optimized GLCM features for grading of fatty liver disease

4.3.3.1 *Experiment 3*: *Evaluating the efficacy of GLCM-M ratio, reduced feature vector (Reduced-RFV1) using SVM classifier*

In this experiment ratio of GLCM-M features are extracted from each LROIs and DROIs by taking the inter-pixel distance '*d*' = 10 is reported in Table 4.15. The extracted features are passed to SVM classifier and the performance of the proposed CAC system is evaluated.

From experiment 3, it is observed that for feature extracted using statistical method, maximum OCA value of 66.6 % is obtained with reduced ratio feature of GLCM-M statistics derived

from LROI and DROI (Reduced-RFV1) computed at inter-pixel distance d = 10 along with ICA values of 68.8 %, 60.0 % and 73.2 %.

Table 4.15 Performance of reduced RFV1 computed for inter pixel distance *d* = 10 using SVM classifier.

FV (*l*)	**CM**				**OCA**	**ICA_{MI}**	**ICA_{MO}**	**ICA_{SE}**
		MI	MO	SE				
Reduced RFV1 (6)	MI	18	12	0	66.6	68.8	60.0	73.2
	MO	4	18	8				
	SE	0	9	21				

Note: '*l*': Length of feature vector, CM: Confusion matrix, MI: Mild, MO: Moderate, SE: Severe, OCA: Overall classification accuracy, ICA: Individual classification accuracy, GA: Genetic algorithm, The ICA and OCA values in %.

A proposed CAC system for grading of fatty liver disease using GA-*k*NN is shown in Fig 4.12.

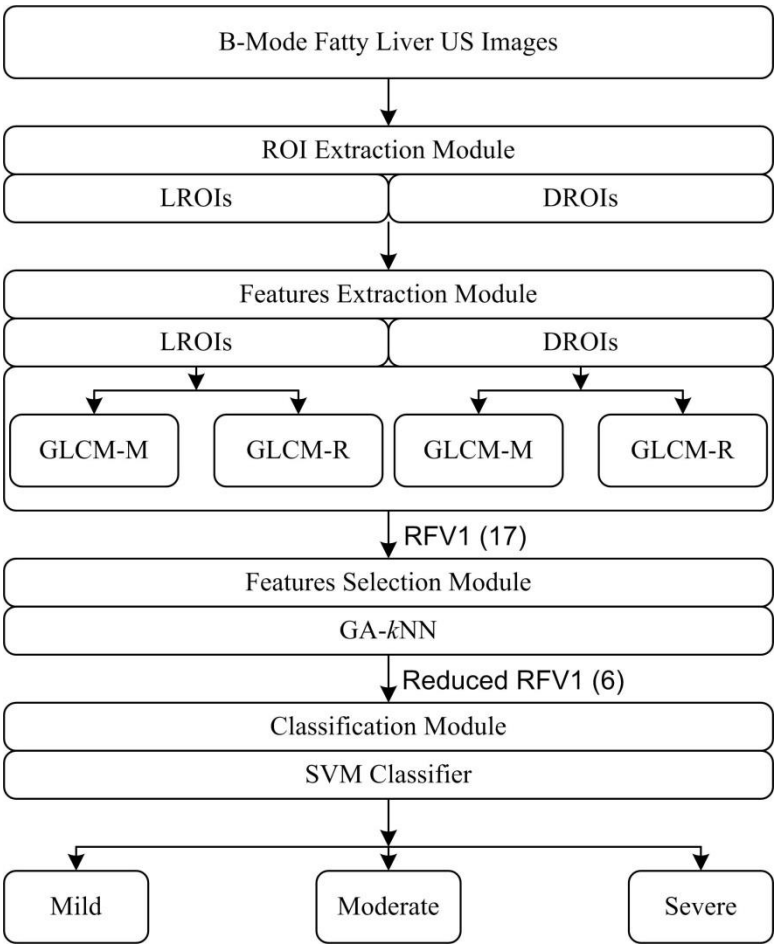

Fig 4.12 Proposed CAC system for grading of fatty liver disease using SVM classifier
Note: Reduced RFV: Reduced ratio feature vector

4.4 Concluding Remarks

In the present work, to classify the instances of the testing the dataset of fatty classes into one of the three classes named as: mild, moderate and severe, SVM classifier is used to classify the fatty liver diseases. The Reduced-RFV1 yielding the best overall maximum OCA value of 66.6 % at '*d*' = 10 and ICA values of 68.8 %, 60.0 % and 73.2 % for mild, moderate and severe liver classes of fatty liver disease.

Table 4.16 Classification performance of experiment 1, 2 and 3.

CAC System Designs	*FV*	*l*	*Classes*	*OCA*	*ICA*
Experiment 1	CFV1	17	Mild Moderate Severe	56.6	79.8 30.0 60.0
Experiment 2	RFV1	17	Mild Moderate Severe	64.4	66.6 53.1 73.2
Experiment 3	Reduced-RFV1	6	Mild Moderate Severe	66.6	68.8 60.0 73.2

Note: Reduced-RFV1: Reduced ratio feature vector, OCA: Overall classification accuracy (%), ICA: Individual classification accuracy (%)

The structure of features classification methods for the classification of focal liver lesions into Cyst, HEM, HCC and MET classes are explained in next chapter.

Chapter 5

SVM based CAC System for Classification of Focal Liver Lesions

5.1 Introduction

The liver is a fundamental organ of the human body. Its main functions include: bile secretion and detoxification of chemicals from the body useful for digestion. Other functions of the liver are regulation of glycogen storage, disintegration of red blood cells and production of hormones. Liver also plays a dominating role in the metabolism of the human body

The sample images of the Cyst, HEM, HCC and MET focal liver lesions with ROIs marked are shown in Fig 5.1. For classification of different classes SVM classifier is used. An efficient SVM based CAC system is designed for the classification of focal liver lesions.

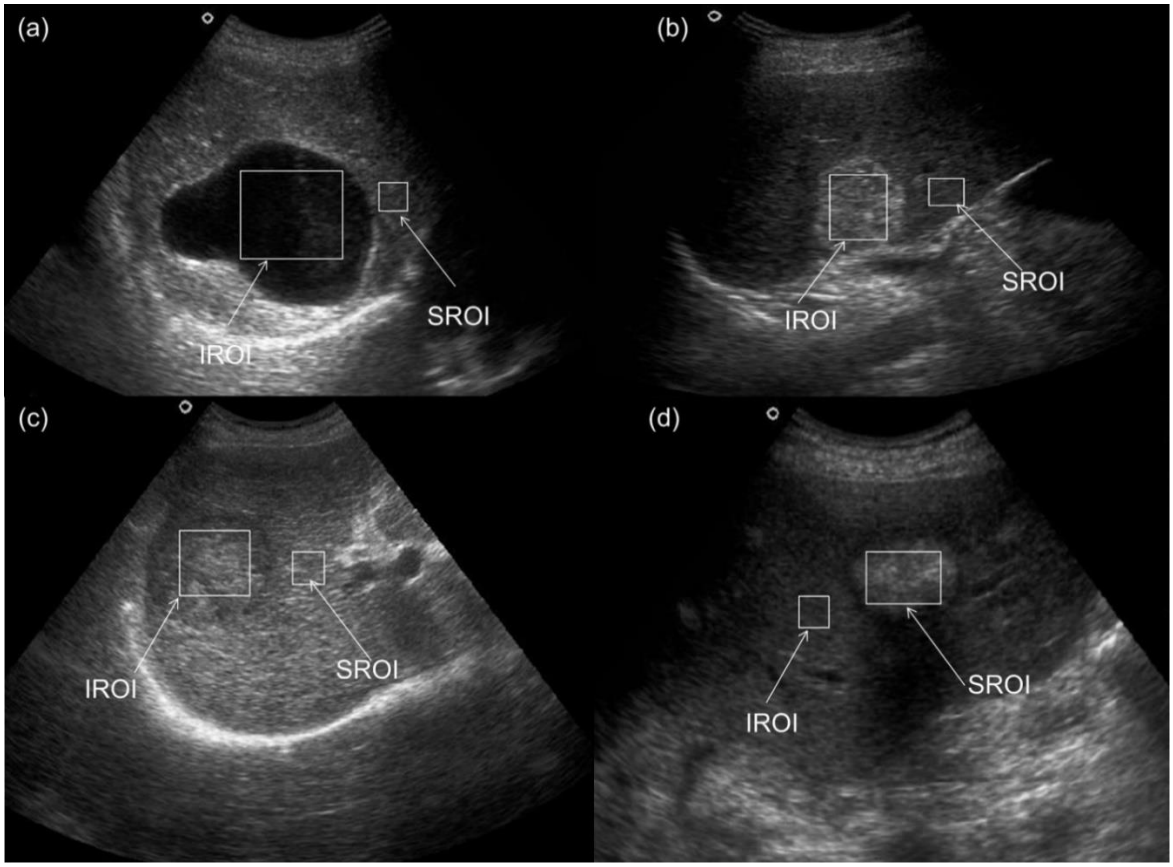

Fig 5.1 Sample US images of Cyst, HEM, HCC and MET liver with ROIs marked.

Focal liver lesions occurs only in the small region of the liver.In the proposed work, a CAC system is designed for the classification of focal liver US images into the Cyst, HEM, HCC

and MET classes. The HCC focal liver state occurs after the cirrhosis. Therefore, ROIs are extracted from region inside the lesion as well as from the surrounding of the lesion.

5.2 Dataset description and its Bifurcation for Design of SVM based CAC System for Classification of Focal Liver Lesions

In the present work, 84 B-mode US images containing 12 Cyst, 28 HEM, 14 HCC and 30 MET focal liver images have been used. A total of 84 Inside ROIs (IROIs) and 84 Surrounding ROIs (SROIs) of size equal to the size of the lesion are extracted from the liver lesion region and the surroundings of the lesion, respectively. The image dataset is depicted in Fig 5.2.

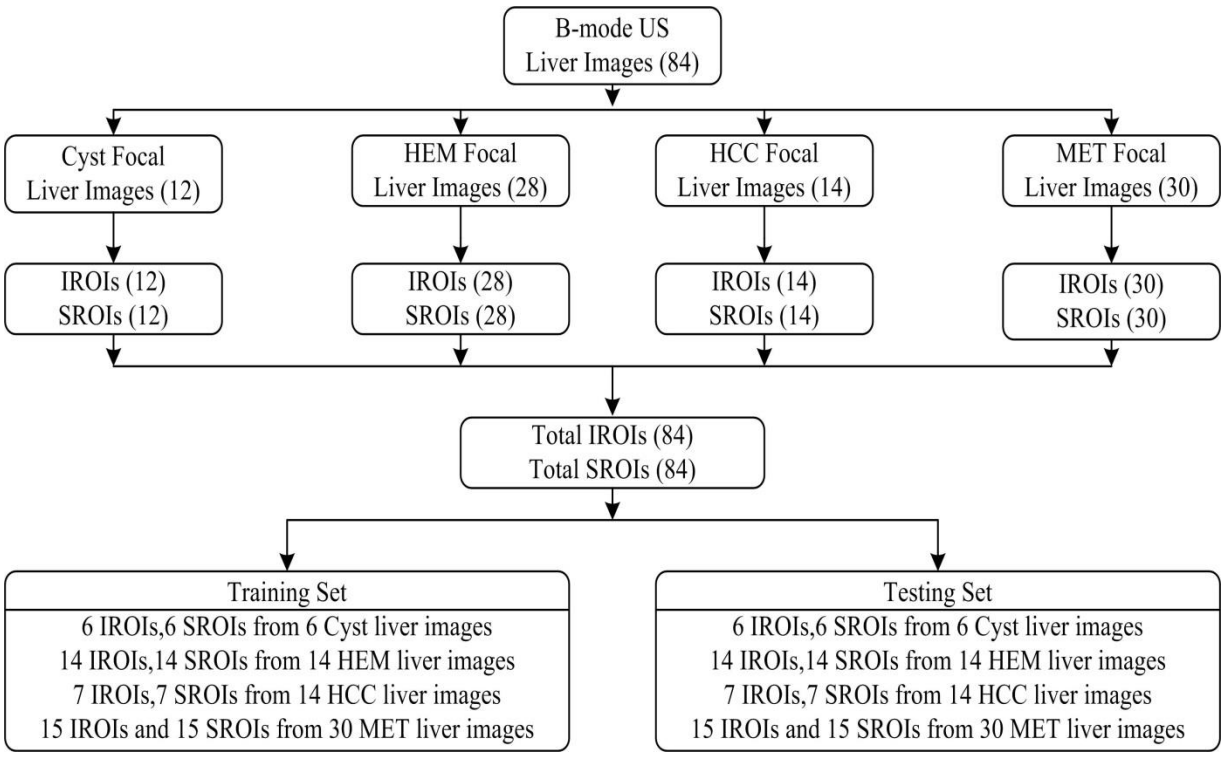

Fig 5.2 Data set description and its bifurcation for classification of focal liver lesions

(*a*) For Cyst focal liver, out of 24 ROIs, 12 ROIs are used for training data and 12 ROIs are used for testing data. (*b*) For HEM focal liver, out of 56 ROIs, 28 ROIs are used for training data and 28 ROIs are used for testing data. (*c*) For HCC focal liver, out of 28 ROIs, 14 ROIs are used for training data and 14 ROIs are used for testing data. (*d*) For MET focal liver, out of 60 ROIs, 30 ROIs are used for training data and 30 ROIs are used for testing data.

5.3 Experimental Workflow for the Design of SVM based CAC System for Classification of Focal Liver Lesions

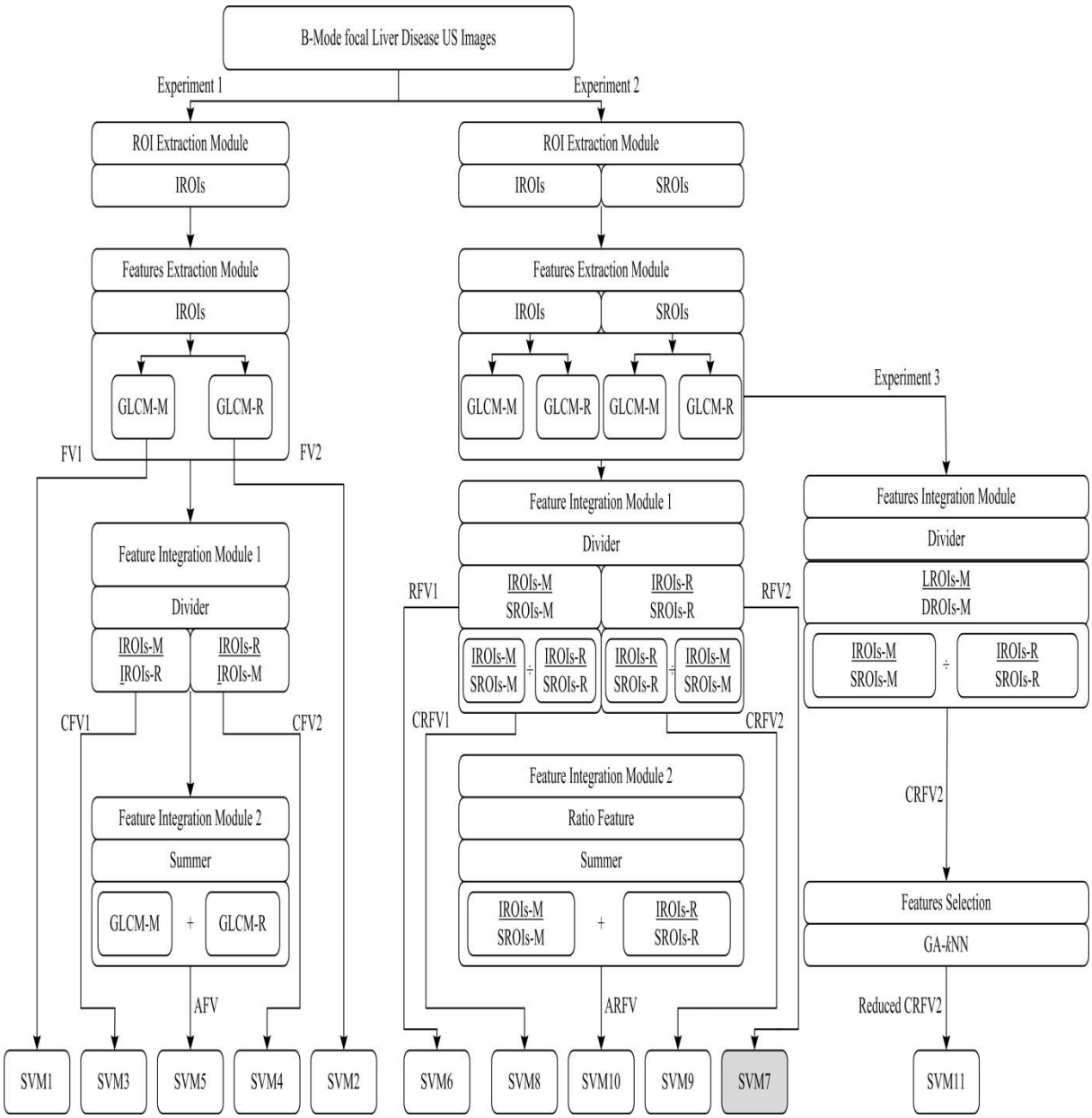

Fig 5.3 Experimental work flow for the design of SVM based CAC system for classification of focal liver lesions
Note: GLCM-M: Grey level co-occurrence matrix mean, GLCM-R: Grey level co-occurrence matrix range, IROI-M: Inside region of interest mean, , SROI-M: Surrounding region of interest mean, IROI-R: Inside region of interest range, , SROI-R: Surrounding region of interest range, FV1 :GLCM mean features, FV2 :GLCM range features , CFV1: GLCM mean upon range ratio features CFV2: GLCM range upon mean ratio features, AFV: GLCM mean + GLCM range additive features, RFV1: GLCM mean ratio features,RFV2: GLCM range ratio features CRFV1: (GLCM mean ratio) upon (GLCM range ratio) ratio features,CRFV2: (GLCM range ratio) upon (GLCM mean ratio) ratio features, ARFV: GLCM mean ratio + GLCM range ratio additive features.

The experimental workflow for the proposed computer aided classification (CAC) system design for fatty liver diseases is shown in Fig. 5.3. The present work is carried out for

evaluating the efficacy of the proposed CAC system with a view to classify the focal liver lesions into the Cyst, HEM, HCC and MET classes.

The ROI is the important aspect which is to be kept in mind while designing a CAC system. For doing such an experiment it should be kept in mind that the pixels lesser than the 800 will not give the reliable evaluation statistics as much of the information is lost.Second order statistical method GLCM is used for feature extraction. Further, SVM classifier is used for classification purpose.

The brief description of the experiments carried out for the classification of focal liver lesions is given below:

5.3.1 *Experiment 1: Design of SVM based CAC System for Classification of Focal Liver Lesions*

As discussed earlier, the ROIs are extracted from the focal liver lesion for Cyst, HEM, HCC and MET class. In this experiment GLCM is used for feature extraction. The classification of liver US images into Cyst, HEM, HCC and MET classes is carried out using the SVM classifier. Experimental workflow diagram for carrying out experiment 1 is given in Fig 5.4

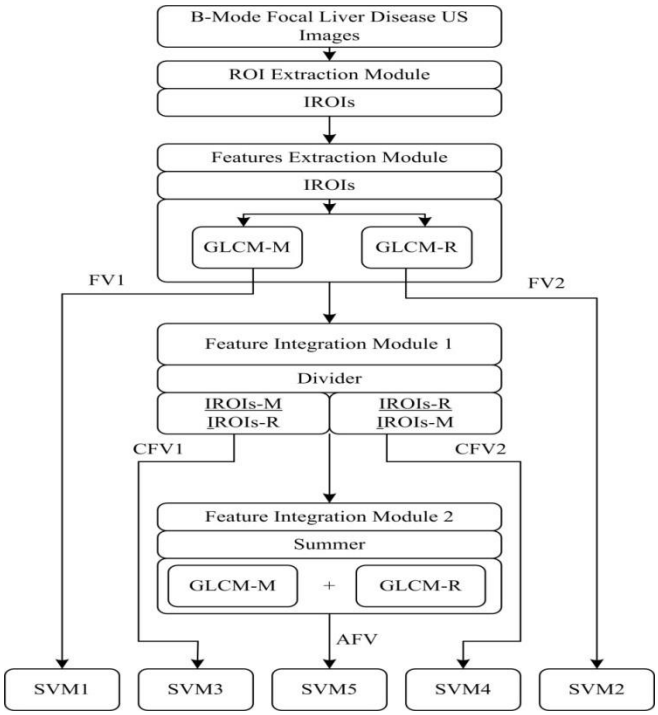

Fig 5.4 Experiment 1: Work flow for the design of SVM based CAC system for classification of focal liver lesions (without ratio)

Note:GLCM-M: Gray level co-occurrence matrix mean, GLCM-R: Gray level co-occurrence matrix range, IROI-M: Inside region of interest mean, SROI-M: Surrounding region of interest mean, IROI-R: Inside region of interest range, SROI-R: Surrounding region of interest range, FV1: GLCM mean features, FV2: GLCM range features , CFV1: GLCM mean upon range ratio features CFV2: GLCM range upon mean ratio features, AFV: GLCM mean + GLCM range additive features.

The brief description of the feature vectors used in the design of SVM based CAC system for classification of focal liver lesions is given in Table 5.1.

Table 5.1 Different feature vectors used in the design of SVM based CAC system for classification of focal liver lesions (without ratio)

FV(s)	**Depiction**	***l***
FV1	GLCM mean feature vector	17
FV2	GLCM range feature vector	17
CFV1	GLCM mean and GLCM range ratio feature vector	17
CFV2	GLCM range and GLCM mean ratio feature vector	17
AFV	GLCM mean and GLCM range additive feature vector	17
ARFV	GLCM mean ratio and GLCM range ratio, additive feature vector	17

Note: FV: Feature vector, GLCM: Gray level co-occurrence matrix, *l*: feature vector length.

The brief description of Experiment 1 is given below:

(a) Feature Extraction Module for the Design of SVM based CAC System for Classification of Focal Liver Lesions

First order statistics based texture features deal with the gray level distribution of an image. The first order statistics based features do not tell much about the information on the gray level pair of pixels and its relative location. The second order statistical features tells the relation between two neighboring pixels in different offsets. The first pixel is called a reference pixel and the other is called a neighbor pixel.The gray level co-occurrence matrix (GLCM) is used to deal with the image attributes based on second order statistics. The GLCM features are calculated for focal liver lesions is shown in Fig 5.5. A GLCM is a matrix where number of gray levels is equivalent to the number of rows and columns. The GLCM matrix has the number of occurrences of a particular pixel pair in an image.

In the present work, 2^{nd} order statistics based Gray level co-occurrence matrix (GLCM) features are extracted from each ROI. Features namely GLCM-Mean (GLCM-M) and GLCM-Range (GLCM-R) are computed from LROIs for different values of inter-pixel distance '*d*' = 1 to 10. A total of 17 features, namely angular second moment, contrast, correlation, inverse difference moment, variance, sum average, sum variance, difference variance, sum entropy, entropy, difference entropy, information measures of correlation-1, information measures of correlation-2, cluster shade, cluster prominence, diagonal moment, Sum correlation are computed from each IROI and SROI [83-85].

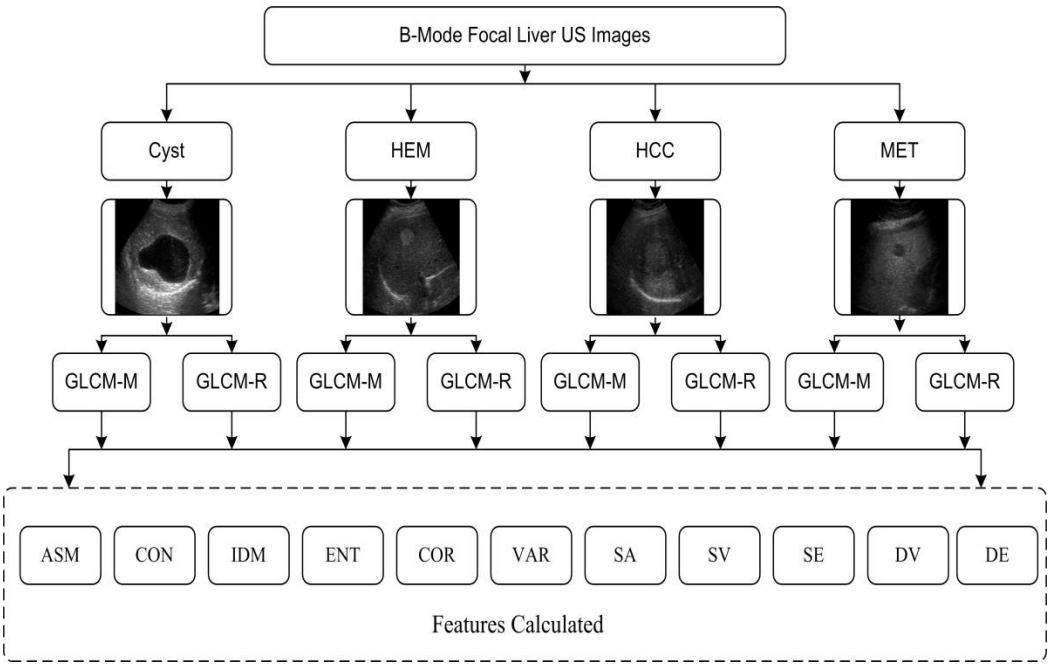

Fig 5.5 GLCM features calculated for classification of focal liver lesions

Note: GLCM-M: GLCM mean feature, GLCM-R: GLCM range feature,ASM: Angural second moment, CON: Contrast, IDM: Inverse difference moment, ENT: Entropy, COR: Correlation, VAR: Variance, SA: Sum average, SV: Sum variance, SE: Sum entropy, DV: Difference variance , DE: Difference entropy.

(b) Feature Integration Module for the Design of SVM based CAC System for Classification of Focal Liver Lesions

(i) Feature Integration Module 1: In feature integration module ratios of (IROIs-M / IROIs-R, IROIs-R / IROIs-M) are calculated.

(ii) Feature Integration Module 2: In feature integration module 2 additive features are calculated by adding ratio features [(IROIs-M / IROIs-R) + (IROIs-R/IROIs-M)].

(c) Feature Classification Module for the Design of SVM based CAC System for Classification of Focal Liver Lesions

In the present work, to classify the instances of the testing the data set of focal liver classes into one of the four classes named as: Cyst, HEM, HCC and MET, the SVM classifier is used for the classification of four classes [96-113].

The results obtained are given below:

In experiment 1, 5 different experiments have been carried out using different feature vectors (FVs) measure using GLCM statistics by varying inter-pixel distance '*d*' from 1 to 10.

5.3.1.1 ***Experiment 1 (a):*** Evaluating the efficacy of GLCM-M feature vector FV1 using SVM classifier.

In this experiment GLCM-M features are extracted from each LROI by varying the inter-pixel distance '*d*' from 1 to 10 is reported in Table 5.2. The extracted features are passed to SVM classifier and the performance of the proposed CAC system is evaluated.

Table 5.2 Performance of FV1 computed for inter pixel distance '*d'* from 1 to 10 using SVM classifier

FV (*l*)	***d***	**OCA**	**ICA_{CYST}**	**ICA_{HEM}**	**ICA_{HCC}**	**ICA_{MET}**
FV1 (17)	1	39.5	0.0	0.0	35.7	80.0
	2	46.5	83.3	0.0	57.1	46.6
	3	48.8	100	14.2	14.2	80.0
	4	55.8	83.3	14.2	42.8	80.0
	5	51.1	100	0.0	28.5	80.0
	6	46.5	83.3	14.2	42.8	56.6
	7	48.8	66.6	28.5	35.7	66.6
	8	51.1	100	14.2	57.1	46.6
	9	44.1	83.3	0.0	57.1	40.0
	10	53.4	100	14.2	57.1	53.3

Note:*d*: Inter-pixel distance, OCA: Overall classification accuracy; ICA_{CYST}: Individual classification accuracy of cyst class, ICA_{HEM}: Individual classification accuracy of HEM class, ICA_{HCC}: Individual classification accuracy of HCC class, ICA_{MET}: Individual classification accuracy of MET class. OCA and ICA values are expressed in %age.

GLCM mean statistics derived from IROI yield maximum OCA value of 55.8 % and ICA values of 83.3 %, 14.4 %, 42.8 % and 80 % at '*d*' = 4 for Cyst, HEM, HCC and MET classes respectively.

5.3.1.2 ***Experiment 1 (b):*** Evaluating the efficacy of GLCM-R feature vector FV2 using SVM classifier.

In this experiment GLCM-R features are extracted from each LROI by varying the inter-pixel distance '*d*' from 1 to 10 is reported in Table 5.3. The extracted features are passed to SVM classifier and the performance of the proposed CAC system is evaluated.

Table 5.3 Performance of FV2 computed for inter pixel distance '*d'* from 1 to 10 using SVM classifier.

FV (*l*)	***d***	**OCA**	**ICA_{CYST}**	**ICA_{HEM}**	**ICA_{HCC}**	**ICA_{MET}**
FV2 (17)	1	44.1	16.6	0.0	64.2	66.6
	2	48.8	50.0	0.0	64.2	40.0
	3	48.8	66.6	0.0	71.4	46.6
	4	48.8	66.6	0.0	64.2	53.3
	5	44.1	33.3	14.2	64.2	46.6
	6	37.2	0.0	0.0	7.1	100
	7	46.5	50.0	0.0	71.4	46.6
	8	46.5	16.6	0.0	60.0	66.6
	9	37.2	50.0	14.2	53.3	60.0
	10	48.8	66.6	0.0	64.2	53.3

Note:*d*: Inter-pixel distance, OCA: Overall classification accuracy; ICA_{CYST}: Individual classification accuracy of cyst class, ICA_{HEM}: Individual classification accuracy of HEM class, ICA_{HCC}: Individual classification accuracy of HCC class, ICA_{MET}: Individual classification accuracy of MET class. OCA and ICA values are expressed in %age.

GLCM range statistics derived from IROI yield maximum OCA value of 48.8 % and ICA values of 50 %, 0 %, 64.2 % and 40 %at '*d*' = 2. For '*d*' = 3 OCA value of 48.8 % and ICA values of 66.6 %, 0 %, 71.4 % and 46.6 %. For '*d*' = 10 OCA value of 48.8 % and ICA values of 66.6 %, 0.0 %, 64.2 % and 53.3 %. For '*d*' = 10 OCA value of 48.8 % and ICA values of 66.6 %, 0 %, 64.2 % and 53.3 % for Cyst, HEM, HCC and MET classes, respectively.

5.3.1.3 ***Experiment 1 (c):*** Evaluating the efficacy of GLCM-M and GLCM-R ratio feature vector CFV1 using SVM classifier.

In this experiment ratio of GLCM-M and GLCM-R features are extracted from each LROIby varying the inter-pixel distance '*d*' from 1 to 10 is reported in Table 5.4. The extracted features are passed to SVM classifier and the performance of the proposed CAC system is evaluated.

Table 5.4 Performance of AFV computed for inter pixel distance '*d'* from 1 to 10 using SVM classifier.

FV (*l*)	***d***	**OCA**	**ICA_{CYST}**	**ICA_{HEM}**	**ICA_{HCC}**	**ICA_{MET}**
AFV (17)	1	44.1	16.6	0.0	64.2	66.6
	2	48.8	83.3	0.0	42.8	66.6
	3	51.1	83.3	0.0	57.1	60.0
	4	48.8	66.6	0.0	64.2	53.3
	5	48.8	66.6	0.0	64.2	53.3
	6	44.1	33.3	14.2	64.2	46.6
	7	53.4	100	14.2	64.2	46.6
	8	41.8	66.6	0.0	57.1	40.0
	9	41.8	0.0	0.0	78.5	46.6
	10	46.5	66.6	0.0	57.1	53.3

Note: *d*: Inter-pixel distance, OCA: Overall classification accuracy; ICA_{CYST}: Individual classification accuracy of cyst class, ICA_{HEM}: Individual classification accuracy of HEM class, ICA_{HCC}: Individual classification accuracy of HCC class, ICA_{MET}: Individual classification accuracy of MET class. OCA and ICA values are expressed in %age.

The addition of GLCM-M statistics and GLCM-R statistics derived from IROI yield maximum classification accuracy value of 53.4 % and ICA values of 100 %, 14.2 %, 64.2% and 46.6 % at '*d'* = 7 for Cyst, HEM, HCC and MET classes, respectively.

5.3.1.4 ***Experiment 1 (d):*** Evaluating the efficacy of GLCM-R and GLCM-M ratio feature vector CFV2 using SVM classifier.

In this experiment ratio of GLCM-R and GLCM-M features are extracted from each LROIby varying the inter-pixel distance '*d*' from 1 to 10 is reported in Table 5.5. The extracted features are passed to SVM classifier and the performance of the proposed CAC system is evaluated.

Table 5.5 Performance of CFV1 computed for inter pixel distance '*d'* from 1 to 10 using SVM classifier

FV (*l*)	*d*	OCA	ICA_{CYST}	ICA_{HEM}	ICA_{HCC}	ICA_{MET}
CFV1 (17)	1	44.1	16.6	0.0	64.2	66.6
	2	46.5	83.3	0.0	14.2	86.6
	3	48.8	83.3	14.2	14.2	86.6
	4	46.5	83.3	0.0	28.5	73.3
	5	44.1	50.0	0.0	35.7	73.3
	6	46.5	66.6	0.0	57.1	53.3
	7	58.1	83.3	14.2	64.2	66.6
	8	44.1	50.0	0.0	71.4	40.0
	9	46.5	66.6	0.0	28.5	80.0
	10	48.8	50.0	0.0	57.1	66.6

Note: *d*: Inter-pixel distance, OCA: Overall classification accuracy; ICA_{CYST}: Individual classification accuracy of cyst class, ICA_{HEM}: Individual classification accuracy of HEM class, ICA_{HCC}: Individual classification accuracy of HCC class, ICA_{MET}: Individual classification accuracy of MET class. OCA and ICA values are expressed in %age.

The ratio of GLCM-M statistics and GLCM-R statistics derived from IROI yield maximum OCA value of 58.1 % and ICA values of 83.3 %, 14.2 %, 64.2 % and 66.6 % at '*d'* = 7 for Cyst, HEM, HCC and MET classes, respectively.

4.3.1.5 ***Experiment 1 (e):*** Evaluating the efficacy of GLCM-M and GLCM-R addition feature vector AFV using SVM classifier.

In this experiment addition of GLCM-M and GLCM-R features are extracted from each LROI by varying the inter-pixel distance '*d*' from 1 to 10 is reported in Table 5.6. The extracted features are passed to SVM classifier and the performance of the proposed CAC system is evaluated.

Table 5.6 Performance of CFV2 computed for inter pixel distance '*d'* from 1 to 10 using SVM classifier.

FV (*l*)	*d*	OCA	ICA_{CYST}	ICA_{HEM}	ICA_{HCC}	ICA_{MET}
CFV2 (17)	1	44.1	16.6	0.0	64.2	66.6
	2	48.8	83.3	0.0	71.4	40.0
	3	48.8	83.3	0.0	71.4	40.0
	4	51.1	83.3	0.0	71.4	40.0
	5	39.5	66.6	0.0	60.0	26.6
	6	46.5	66.6	0.0	28.5	80.0
	7	44.1	66.6	0.0	57.1	46.6
	8	48.8	66.6	0.0	64.2	53.33
	9	48.8	66.6	0.0	57.1	60.0
	10	34.8	16.6	0.0	42.8	53.3

Note: *d*: Inter-pixel distance, OCA: Overall classification accuracy; ICA_{CYST}: Individual classification accuracy of cyst class, ICA_{HEM}: Individual classification accuracy of HEM class, ICA_{HCC}: Individual classification accuracy of HCC class, ICA_{MET}: Individual classification accuracy of MET class. OCA and ICA values are expressed in %age.

The ratio of GLCM-R statistics and GLCM-M statistics derived from IROI yield maximum OCA value of 51.1 % and ICA values of 83.3 %, 0 %, 71.4 % and 40 % at '*d*' = 4 for Cyst, HEM, HCC and MET classes, respectively.

From experiment 1, it is observed that for feature extracted using statistical method, maximum OCA value of 58.1 % is obtained with GLCM-M feature vector (CFV1) computed at inter-pixel distance d = 4 along with ICA values of 83.3 %, 14.2 % and 42.8 % and 80.0 % for Cyst, HEM, HCC and MET classes, respectively. The detailed result obtained from GLCM-M and GLCM-R statistics is given in Table 5.7.

Table 5.7 Description of FVs yielding the best classification accuracy values in experiments 1 (*a*) to 1 (*e*) using SVM classifier.

FVs (*l*)	*d*	OCA	ICA_{CYST}	ICA_{HEM}	ICA_{HCC}	ICA_{MET}
FV1 (17)	4	55.8	83.3	14.2	42.8	80.0
FV2 (17)	2	48.8	50.0	0	64.2	40.0
CFV1 (17)	7	58.1	83.3	14.2	64.2	66.6
CFV2 (17)	4	51.1	83.3	0.0	71.4	40.0
AFV (17)	7	53.4	100	14.2	64.2	46.6

Note:*d*: Inter-pixel distance, OCA: Overall classification accuracy; ICA_{CYST}: Individual classification accuracy of cyst class, ICA_{HEM}: Individual classification accuracy of HEM class, ICA_{HCC}: Individual classification accuracy of HCC class, ICA_{MET}: Individual classification accuracy of MET class. OCA and ICA values are expressed in %age.

5.3.2 Experiment 2: Design of SVM based CAC System for Classification of Focal Liver Lesions (with Ratio)

In this experiment ROIs are extracted from focal liver lesion as well as from the surrounding of the lesion for Cyst, HEM, HCC and MET class. In this experiment GLCM is used for feature extraction. The classification of focal liver US images into Cyst, HEM, HCC and MET classes is carried out using the SVM classifier. Experimental workflow diagram for carrying out experiment 2 is given in Fig 5.6.

The brief description of feature vectors used in the design of SVM based CAC system for classification of focal liver lesions are given in Table 5.8.

Table 5.8 Different feature vectors used in the design of an SVM based CAC system for classification of focal liver lesions (with ratio)

FV(s)	Depiction	*l*
RFV1	GLCM mean ratio feature vector	17
RFV2	GLCM range ratio feature vector	17
CRFV1	GLCM mean ratio and GLCM range ratio, ratio feature vector	17
CRFV2	GLCM range ratio and GLCM mean ratio, ratio feature vector	17
ARFV	GLCM mean ratio and GLCM range ratio, additive feature vector	17

Note: FV: Feature vector, GLCM: Gray level co-occurrence matrix, *l*: feature vector length.

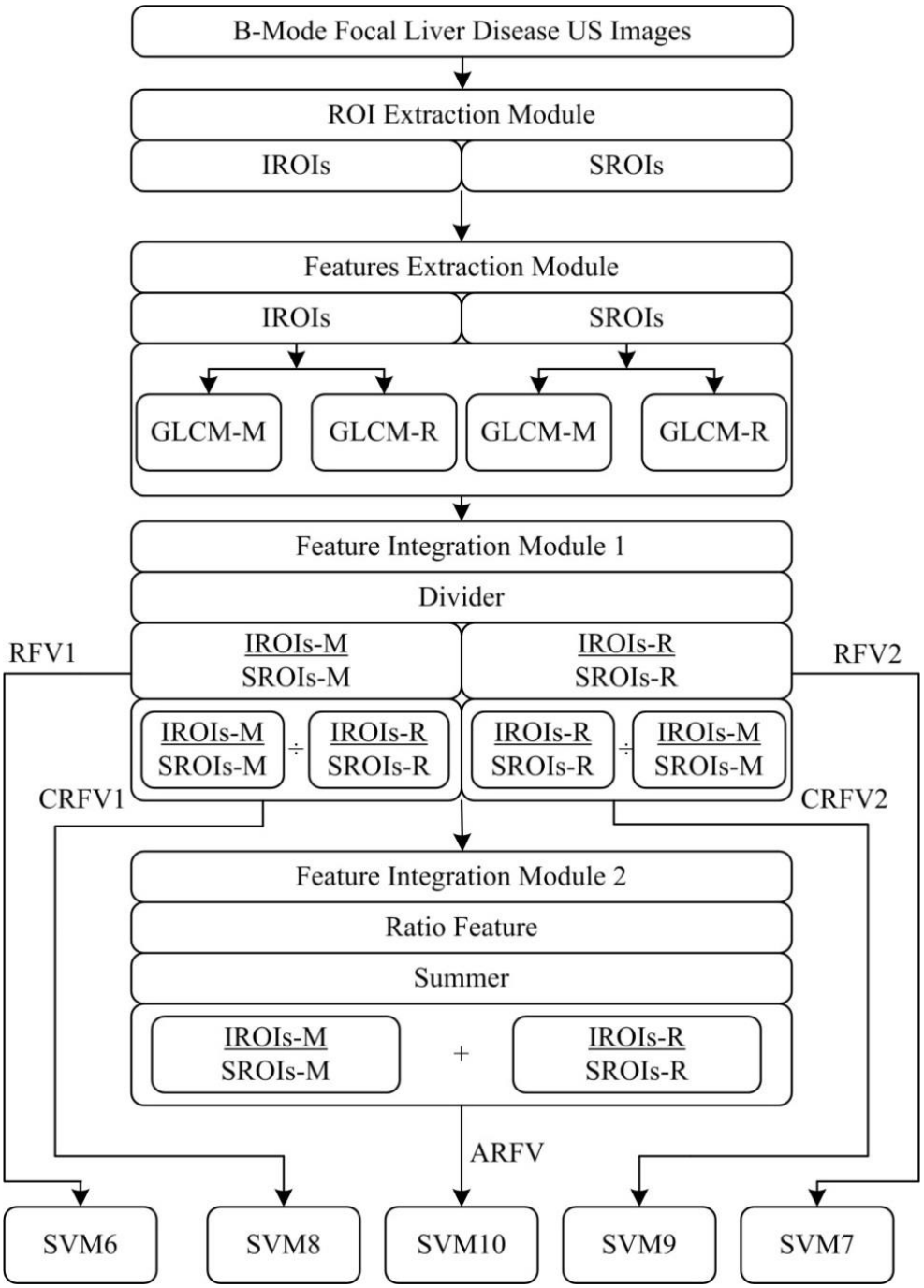

Fig 5.6 Experiment 2: Work flow for the design of SVM based CAC system for classification of focal liver lesions (with ratio).

Note: GLCM-M: Grey level co-occurrence matrix mean, GLCM-R: Grey level co-occurrence matrix range, IROI-M: Inside region of interest mean, SROI-M: Surrounding region of interest mean, IROI-R: Inside region of interest range, , SROI-R: Surrounding region of interest range,RFV1: GLCM mean ratio features,RFV2: GLCM range ratio features CRFV1: (GLCM mean ratio) upon (GLCM range ratio) ratio features,CRFV2: (GLCM range ratio) upon (GLCM mean ratio) ratio features, ARFV: GLCM mean ratio + GLCM range ratio additive features.

The brief description of experiment 2 is given below:

(a) Feature extraction Module for the Design of SVM based CAC System for Classification of Focal Liver Lesions

In the present work, 2nd order statistics based Gray level co-occurrence matrix (GLCM) features are extracted from each ROI. Features namely GLCM-Mean (GLCM-M) and GLCM-Range (GLCM-R) are computed from IROIs for different values of inter-pixel distance '*d*' = 1 to 10. A total of 17 features, namely angular second moment, contrast, correlation, inverse difference moment, variance, sum average, sum variance, difference variance, sum entropy, entropy, difference entropy, information measures of correlation-1, information measures of correlation-2, cluster shade, cluster prominence, diagonal moment, sum correlation are computed from each IROI and SROI.

(b) Feature Integration Module for the Design of SVM based CAC System for Classification of Focal Liver Lesions

(*i*) *Feature Integration Module 1:* In feature integration module ratios of (IROIs-M / SROIs-M ratio with IROIs-R / SROIs-R, IROIs-R / SROIs-R ratio with IROIs-M / SROIs-M) have been calculated.

(*ii*) *Feature Integration Module 2:* In feature integration module 2 additive features have been calculated by adding ratio features [(IROIs-M / SROIs-M ratio with IROIs-R / SROIs-R) + (IROIs-R / SROIs-R ratio with IROIs-M / SROIs-M)].

(c) Feature Classification Module for the Design of SVM based CAC System for Classification of Focal Liver Lesions

For classification of focal liver lesion SVM classifier is used.

The results obtained are given below:

In the experiment 2, 5 different experiments are carried out using different feature vectors (FVs) measure using GLCM statistics by varying inter-pixel distance '*d*' from 1 to 10.

5.3.2.1 ***Experiment 2 (a):*** Evaluating the efficacy of GLCM-M ratio feature vector RFV1 using SVM classifier.

In this experiment ratio of GLCM-M features are extracted from each IROIs and SROIs by varying the inter-pixel distance '*d*' from 1 to 10 is reported in Table 5.9. The extracted features are passed to SVM classifier and the performance of the proposed CAC system is evaluated.

Table 5.9 Performance of RFV1 computed for inter pixel distance '*d'* from 1 to 10 using SVM classifier.

FV (*l*)	*d*	OCA	ICA_{CYST}	ICA_{HEM}	ICA_{HCC}	ICA_{MET}
RFV1 (17)	1	62.7	0.0	57.1	64.2	93.3
	2	51.1	0.0	83.3	71.4	40.0
	3	58.1	66.6	16.6	57.1	80.0
	4	58.1	50.0	0.0	64.2	86.6
	5	48.8	66.6	28.5	42.8	60.0
	6	51.1	83.3	0.0	71.4	40.0
	7	51.1	33.3	0.0	50.0	86.6
	8	55.5	66.6	42.8	50.0	66.6
	9	46.5	66.6	0.0	28.5	80.0
	10	55.8	33.3	0.0	64.2	86.6

Note: *d*: Inter-pixel distance, OCA: Overall classification accuracy; ICA_{CYST}: Individual classification accuracy of cyst class, ICA_{HEM}: Individual classification accuracy of HEM class, ICA_{HCC}: Individual classification accuracy of HCC class, ICA_{MET}: Individual classification accuracy of MET class. OCA and ICA values are expressed in %age.

GLCM-M statistics derived from IROI and SROI yield maximum OCA value of 58.1 % and ICA values of 66.6 %, 16.6 %, 57.1 % and 80 % at '*d*' = 3. For d= 4 OCA value of 58.1 % and ICA values of 50 %, 0 %, 64.2 % and 86.6 % for Cyst, HEM, HCC and MET classes, respectively.

5.3.2.2 ***Experiment 2 (b):*** Evaluating the efficacy of GLCM-R ratio feature vector RFV2 using SVM classifier.

In this experiment ratio of GLCM-R features are extracted from each LROIs and DROIs by varying the inter-pixel distance '*d*' from 1 to 10 is reported in Table 5.10. The extracted features are passed to SVM classifier and the performance of the proposed CAC system is evaluated.

Table 5.10 Performance of RFV2 computed for inter pixel distance '*d'* from 1 to 10 using SVM classifier.

FV (*l*)	*d*	OCA	ICA_{CYST}	ICA_{HEM}	ICA_{HCC}	ICA_{MET}
RFV2 (17)	1	58.1	66.6	16.6	57.1	80.0
	2	46.5	66.6	42.8	57.1	33.3
	3	41.8	50	42.8	42.8	40.0
	4	48.8	66.6	28.5	42.8	60.0
	5	51.1	50.0	0.0	64.2	66.6
	6	44.1	0.0	14.2	35.7	86.6
	7	41.8	50.0	14.2	57.1	40.0
	8	46.5	16.6	14.2	78.5	46.6
	9	60.4	50.0	14.2	64.2	86.6
	10	41.8	20.0	14.2	64.2	46.6

Note: *d*: Inter-pixel distance, OCA: Overall classification accuracy; ICA_{CYST}: Individual classification accuracy of cyst class, ICA_{HEM}: Individual classification accuracy of HEM class, ICA_{HCC}: Individual classification accuracy of HCC class, ICA_{MET}: Individual classification accuracy of MET class. OCA and ICA values are expressed in %age.

GLCM-R statistics derived from IROI and SROI yield maximum overall classification accuracy value of 60.4 % and ICA values of 50 %, 14.2 %, 64.2 % and 86.6 % at '*d*' = 9 for Cyst, HEM, HCC and MET classes, respectively.

5.3.2.3 ***Experiment 2 (c):*** Evaluating the efficacy of GLCM-M and GLCM-R, ratio feature vector CRFV1 using SVM classifier.

In this experiment ratio of GLCM-M and GLCM-R features are extracted from each LROIs and DROIs by varying the inter-pixel distance '*d*' from 1 to 10 is reported in Table 5.11. The extracted features are passed to SVM classifier and the performance of the proposed CAC system is evaluated.

Table 5.11 Performance of CRFV1 computed for inter pixel distance '*d'* from 1 to 10 using SVM classifier.

FV (*l*)	***d***	**OCA**	**ICA_{CYST}**	**ICA_{HEM}**	**ICA_{HCC}**	**ICA_{MET}**
CRFV1 (17)	1	62.7	83.3	14.2	57.1	86.6
	2	46.5	66.6	42.8	57.1	33.3
	3	58.1	83.3	0.0	42.8	93.3
	4	53.4	66.6	0.0	42.8	86.6
	5	55.8	50.0	0.0	57.1	80.0
	6	58.1	83.3	14.2	57.1	73.3
	7	41.8	50.0	14.2	57.1	40.0
	8	48.8	16.6	0.0	50.0	86.6
	9	55.8	50.0	0.0	57.1	86.6
	10	60.4	83.3	14.2	57.1	80.0

Note: *d*: Inter-pixel distance, OCA: Overall classification accuracy; ICA_{CYST}: Individual classification accuracy of cyst class, ICA_{HEM}: Individual classification accuracy of HEM class, ICA_{HCC}: Individual classification accuracy of HCC class, ICA_{MET}: Individual classification accuracy of MET class. OCA and ICA values are expressed in %age.

The ratio of GLCM-M statistics and GLCM-R statistics derived from IROI and SROI yield maximum OCA value of 62.7 % and ICA values of 83.3 %, 14.2 %, 57.1 % and 86.6 % at d=1 for Cyst, HEM, HCC and METclasses, respectively.

5.3.2.4 ***Experiment 2 (d):*** Evaluating the efficacy of GLCM-R and GLCM-R ratio, ratio feature vector CRFV2 using SVM classifier.

In this experiment ratio of GLCM-R and GLCM-M features are extracted from each LROIs and DROIs by varying the inter-pixel distance '*d*' from 1 to 10 is reported in Table 5.12. The extracted features are passed to SVM classifier and the performance of the proposed CAC system is evaluated.

Table 5.12 Performance of CRFV2 computed for inter pixel distance *d* from 1 to 10 using SVM classifier.

FV (*l*)	*d*	OCA	ICA_{CYST}	ICA_{HEM}	ICA_{HCC}	ICA_{MET}
CRFV2 (17)	1	74.4	83.3	85.7	50.0	93.3
	2	46.5	66.6	42.8	57.1	33.3
	3	53.0	66.6	0.0	42.8	86.6
	4	48.8	66.6	0.0	42.8	73.3
	5	53.8	66.6	14.2	50.0	80.0
	6	55.8	50.0	0.0	57.1	86.6
	7	65.1	83.3	42.8	64.2	73.3
	8	53.4	50.0	14.2	71.4	60.0
	9	48.8	16.6	0.0	50.0	86.6
	10	53.4	16.6	14.2	64.2	80

Note: *d*: Inter-pixel distance, OCA: Overall classification accuracy; ICA_{CYST}: Individual classification accuracy of cyst class, ICA_{HEM}: Individual classification accuracy of HEM class, ICA_{HCC}: Individual classification accuracy of HCC class, ICA_{MET}: Individual classification accuracy of MET class. OCA and ICA values are expressed in %age.

The ratio of GLCM range statistics and GLCM mean statistics derived from IROI and SROI yield maximum OCA value of 74.4 % and ICA values of 83.3 %, 85.7 %, 50 % and 93.3 % at '*d'* = 1 for Cyst, HEM, HCC and MET classes, respectively.

5.3.2.5 ***Experiment 2 (e):*** Evaluating the efficacy of GLCM-M and GLCM-R additive, ratio feature vector ARFV using SVM classifier.

In this experiment addition of GLCM-M and GLCM-R features are extracted from each LROIs and DROIs by varying the inter-pixel distance '*d*' from 1 to 10 is reported in Table 5.13. The extracted features are passed to SVM classifier and the performance of the proposed CAC system is evaluated.

Table 5.13 Performance of ARFV computed for inter pixel distance '*d'* from 1 to 10 using SVM classifier.

FV (*l*)	*d*	OCA	ICA_{CYST}	ICA_{HEM}	ICA_{HCC}	ICA_{MET}
ARFV (17)	1	60.4	50.0	66.6	42.8	86.6
	2	46.5	66.6	42.8	57.1	33.3
	3	48.8	66.6	28.5	35.7	66.6
	4	53.4	16.6	14.2	64.2	80.0
	5	46.5	33.3	0,0	57.1	66.6
	6	53.0	66.6	0.0	42.8	86.6
	7	53.4	50.0	28.5	50.0	73.3
	8	53.4	20.0	14.2	57.1	86.6
	9	58.1	83.3	14.2	57.1	73.3
	10	46.5	16.6	14.2	71.4	53.3

Note: *d*: Inter-pixel distance, OCA: Overall classification accuracy; ICA_{CYST}: Individual classification accuracy of cyst class, ICA_{HEM}: Individual classification accuracy of HEM class, ICA_{HCC}: Individual classification accuracy of HCC class, ICA_{MET}: Individual classification accuracy of MET class. OCA and ICA values are expressed in %age.

The addition of GLCM-R statistics and GLCM-M statistics derived from IROI and SROI yield maximum OCA value of 60.4 % and ICA values of 50 %, 66.6 %, 42.8 % and 86.6 % at '*d*' = 1 for Cyst, HEM, HCC and MET classes, respectively.

From experiment 2, it is observed that for feature extracted using statistical method, maximum OCA value of 74.4 % is obtained with ratio of GLCM-R and GLCM-M statistics derived from IROI and SROI (CRFV2) computed at inter-pixel distance 'd' = 1 along with ICA values of 83.3 %, 85.7 %, 50 % and 93.3 % for Cyst, HEM, HCC and MET classes, respectively. The detailed result obtained from GLCM-M and GLCM-R statics is given in Table 4.14.

Table 5.14 Description of FVs yielding the best classification accuracy values in experiments 2 (*a*) to 2 (*e*) using SVM classifier.

FVs (*l*)	***d***	**OCA**	**ICA_{CYST}**	**ICA_{HEM}**	**ICA_{HCC}**	**ICA_{MET}**
RFV1 (17)	3	58.1	66.6	16.6	57.1	80.0
RFV2 (17)	9	60.4	50.0	14.2	64.2	86.6
CRFV1 (17)	1	62.7	83.3	14.2	57.1	86.6
CRFV2 (17)	1	74.4	83.3	85.7	50.0	93.3
ARFV (17)	1	60.4	50.0	66.6	42.8	86.6

Note: *d*: Inter-pixel distance, OCA: Overall classification accuracy; ICA_{CYST}: Individual classification accuracy of cyst class, ICA_{HEM}: Individual classification accuracy of HEM class, ICA_{HCC}: Individual classification accuracy of HCC class, ICA_{MET}: Individual classification accuracy of MET class. OCA and ICA values are expressed in %age.

5.3.4 SVM based CAC System for Classification of Focal Liver Lesions (with feature selection)

Optimization is a process which makes something as fully as perfect by finding the maximum value of function involved in it. Different types of optimization techniques are used for feature selection in image processing. In this study, GA-*k*NN feature selection technique has been used [42,114,115].

In the present study population size = 20, mutation rate = 0.05, crossover rate= 0.7 has been used.

The features selected after applying GA-*k*NN feature selection technique are angular second moment-mean, contrast-mean, sum of squares variance, sum entropy-mean and difference entropy-mean.

The ratio of GLCM range statistics and GLCM mean statistics derived from IROI and SROI yield maximum classification accuracy value of 74.4 % and ICA values of 83.3 %, 85.7 %, 50 % and 93.3 % at '*d*' =1 for Cyst, HEM, HCC and MET classes, respectively. After optimization using GA-*k*NN, overall classification accuracy increase to 78.37 % and ICA values of 100.0 %, 44.0 %, 100.0 % and 80.0 % for Cyst, HEM, HCC and MET classes.Optimized focal liver features for classification of focal liver lesions are shown in Fig 5.7.

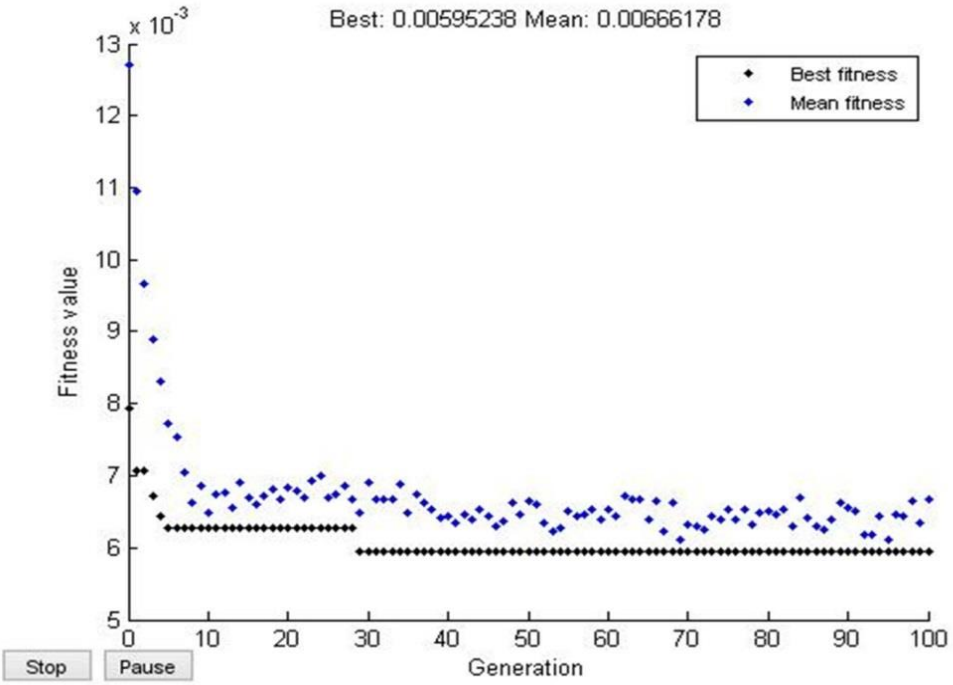

Fig 5.7: Optimized GLCM features for classification of focal liver lesions

5.3.4.1 Experiment 3: *Evaluating the efficacy of GLCM-M and GLCM-R ratio, Reduced feature vector (Reduced-CRFV2) using SVM classifier*

In this experiment ratio of GLCM-R and GLCM-M statistics derived from IROIs and SROIs by taking the inter-pixel distance '*d*' = 1 is reported in Table 5.15. The extracted features are passed to GA-*k*NN classifier and the performance of the proposed CAC system is evaluated.

From experiment 3, it is observed that the ratio of GLCM-R statistics and GLCM-M statistics derived from IROI and SROI after applying GA-kNN feature selection technique yield maximum OCA value of 78.3 % and ICA values of 83.3 %, 85.7 %, 50 % and 93.3 % at d=1 for Cyst, HEM, HCC and MET classes, respectively.

Table 5.15 Performance of Reduced-CRFV2 for inter-pixel distance '*d*' = 1 using SVM classifier.

FV (*l*)	**CM**					**OCA**	**ICA_{CYST}**	**ICA_{HEM}**	**ICA_{HCC}**	**ICA_{MET}**
		CYST	**HEM**	**HCC**	**MET**					
Reduced CRFV2 (5)	CYST	6	0	0	0	78.37	83.3	85.7	50	93.3
	HEM	1	4	0	4					
	HCC	0	0	7	0					
	MET	1	1	1	12					

Note: '*l*': Length of feature vector, CM: Confusion matrix, HEM: Hemangioma, HCC: Hepatocellular carcinoma, MET: Metastatic carcinoma, OCA: Overall classification accuracy, ICA: Individual classification accuracy, GA: Genetic algorithm, The ICA and OCA values in %.

The proposed CAC system for classification of focal liver classes using GA-*k*NN is shown in Fig 5.8.

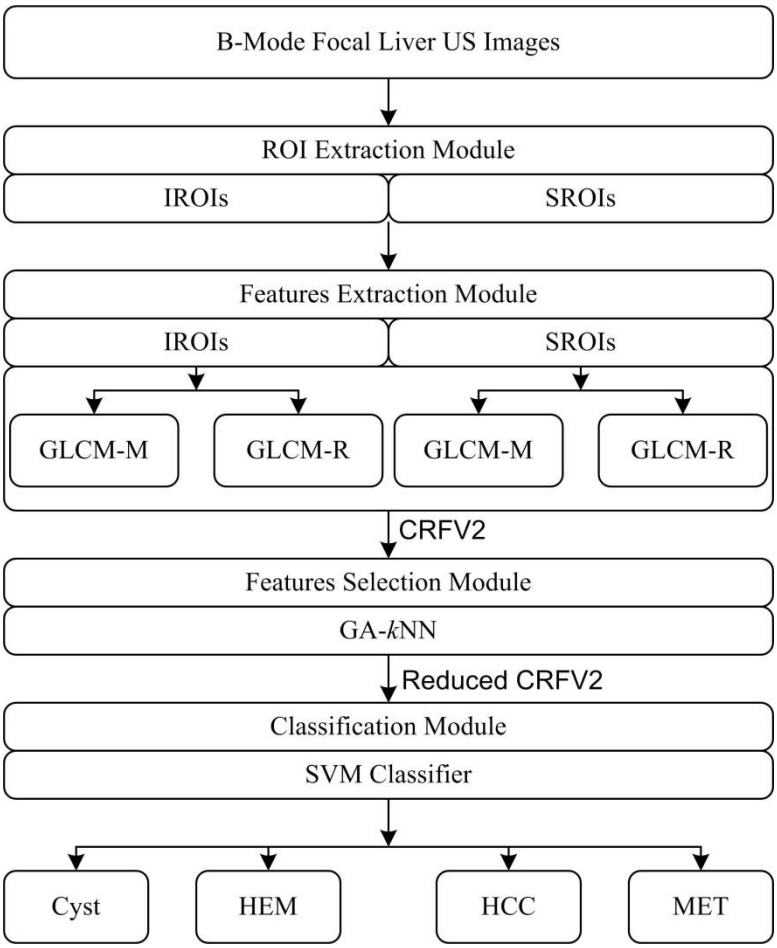

Fig 5.8 SVM based CAC system for classification of focal liver lesions (with feature selection)

5.4 Concluding Remarks

In the present work, to classify the instances of the testing data set of focal liver classes into one of the four classes namely Cyst, HEM, HCC and MET. The SVM classifier is used to classify the focal liver diseases. The reduced combined ratio feature vector (CRFV2) yielding the best overall maximum classification accuracy value of 78.37 % and ICA values of 100.0 %, 44.0 %, 100.0 % and 80.0 % for Cyst, HEM, HCC and MET classes.

Table 5.16 Classification performance of experiment 1, 2 and 3.

CAC System Designs	*FV (l)*	*Classes*	*OCA*	*ICA*
Experiment 1	CFV1 (17)	Cyst	55.8	83.3
		HEM		14.2
		HCC		42.8
		MET		80.0
Experiment 2	RFV1 (17)	Cyst	74.4	83.3
		HEM		85.7
		HCC		50.0
		MET		93.3
Experiment 3	Reduced RFV1 (5)	Cyst	78.3	100
		HEM		44.0
		HCC		100
		MET		80.0

Note: OCA: Overall classification accuracy (%), ICA: Individual class accuracy (%), CFV: Combined feature vector, RFV: Ratio feature vector, Reduced RFV: Reduced ratio feature vector.

Efficiency contribution of different proposed CAC system design is given in the next chapter. The present work future scope is also discussed.

Chapter 6

Conclusion and Future Scope

This dissertation presents the classification of diffused and focal liver using texture analysis. The fatty liver ROIs 221 in number, are classified into mild, moderate and severe fatty liver. Further, 168 focal liver ROIs are classified into Cyst, HEM, HCC and MET. In total, 17 features are extracted for texture analysis. The type of classifier which has been used for both studies is SVM. The conclusions of the work are listed below.

6.1 Module 1: SVM based CAC system for Grading of Fatty Liver Disease (without feature selection)

The extensive experimentation carried out in the present work. Indicated that the ratio feature vector (RFV1) computed using GLCM mean statistics derived from LROI and DROI for fatty liver problems, the best overall accuracy produces in fatty liver problem is 64.4 % and individual classification accuracy of 66.6 %, 53.1 % and 73.2 % of mild, moderate and severe classes. The developed CAC system for grading of fatty liver disease using SVM classifier is shown in Fig 6.1.

The results obtained from GLCM-M and GLCM-R features for grading of fatty liver disease and classification of focal liver lesions are used to develop a proposed CAC system.

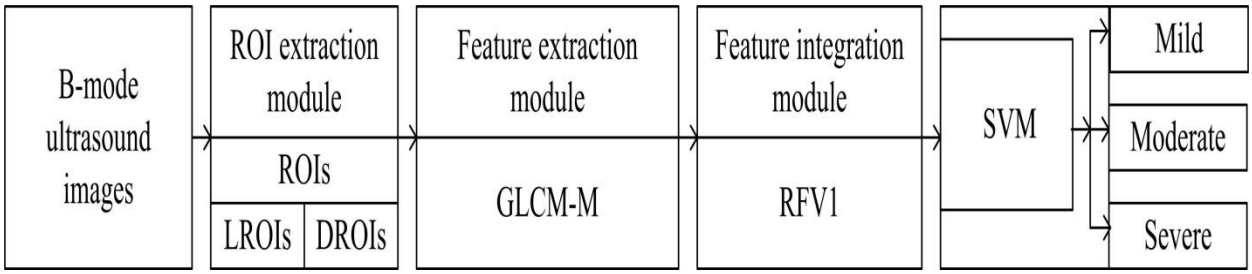

Fig 6.1 Generalized Proposed CAC system for grading of fatty liver disease using the SVM classifier (with feature selection)

6.2 Module 2: SVM based CAC system for grading of fatty liver disease (with feature selection)

The extensive experimentation carried out in the present work, indicate that the RFV1 computed using GLCM mean statistics derived from the liver region of interest (LROI) and diaphragm region of interest (DROI) for fatty liver problems, after applying optimization

technique overall classification accuracy increased to 66.6 % and ICA values of 68.8 %, 60.0 % and 73.2 % for mild, moderate and severe classes respectively. The CAC system developed for grading of fatty liver disease using SVM classifier is shown in Fig 6.2.

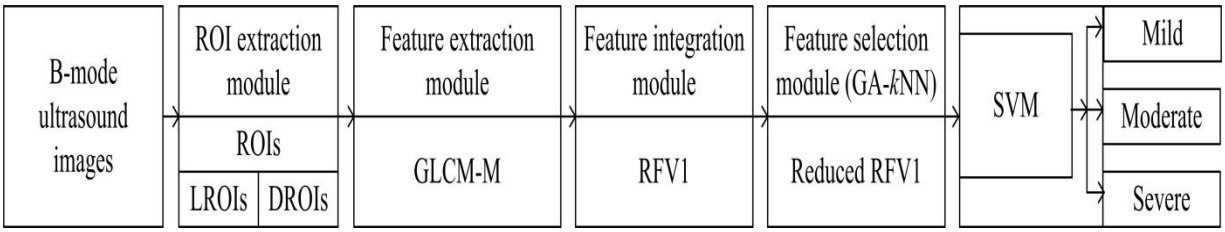

Fig 6.2: Generalized proposed CAC system for grading of fatty liver disease using the SVM classifier (with feature selection)

6.3 Module 3: SVM based CAC system for classification of focal liver lesions (without feature selection)

The extensive experimentation carried out in the present work, indicates that the CRFV2 computed using GLCM mean and GLCM range statistics derived from IROI and SROI from focal liver problem, the best overall accuracy produce in focal liver problem is 74.4 % and individual classification accuracy of 83.3 %, 85.7 %, 50 % and 93.3 % for Cyst, HEM, HCC and MET classes is achieved using the SVM classifier. The CAC system developed for classification of focal liver lesions using SVM classifier is shown in Fig 6.3.

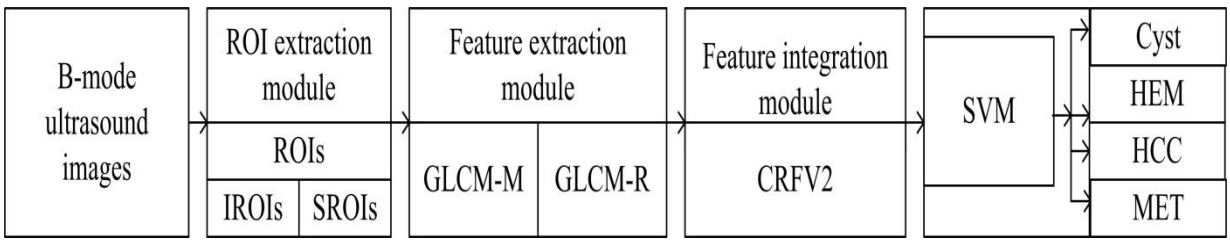

Fig 6.3: Generalized Proposed CAC system for classification of focal liver lesions using the SVM classifier (without feature selection)

6.4 Module 3: SVM based CAC system for classification of focal liver lesions (with feature selection)

The extensive experimentation carried out in the present work, indicate that the combined ratio feature vector (CRFV2) computed using GLCM mean and GLCM range statistics derived from IROI and SROI for focal liver lesions, after applying optimization technique accuracy increased to 78.37 % and ICA values of 100.0 %, 44.0 %, 100.0 % and 80.0 % for Cyst,

HEM, HCC and MET classes respectively. The CAC system developed for classification of focal liver lesions using SVM classifier is shown in Fig 6.4.

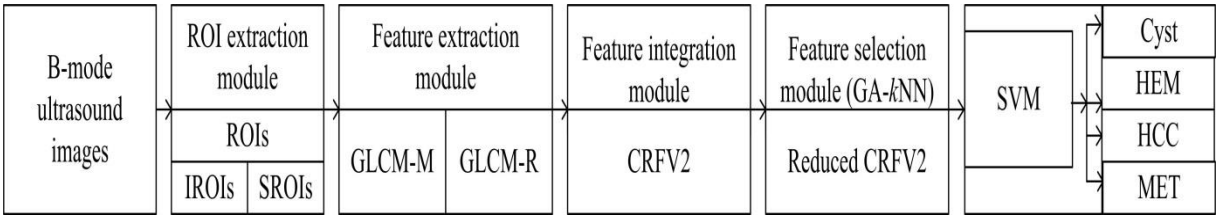

Fig 6.4: Generalized proposed CAC system for classification of focal liver lesions using the SVM classifier (with feature selection)

It is observed from the above results that the four modules, i.e., module 1, module 2, module 3, and module 4 developed for grading of fatty liver disease and classification of focal liver lesions can be effectively used for prognosis. This is further concluded that the data mining algorithm is much more reliable.

A brief comparison of performance obtained by different implemented modules for grading of fatty liver disease and classification of focal liver lesions using B-Mode US images are depicted in Table 6.1.

Table 6.1 Classification performance of different CAC systems

CAC System Designs	*FVs (l)*	*Classes*	*OCA*	*ICA*
Module 1: SVM based CAC system for grading of fatty liver disease (without feature selection).	RFV1 (17)	Mild Moderate Severe	64.4	66.6 53.1 73.2
Module 2: GA-*k*NN based CAC system for grading of fatty liver disease (with feature selection).	Reduced RFV1 (6)	Mild Moderate Severe	66.6	68.8 60.0 73.2
Module 3: SVM based CAC system for classification of focal liver lesions (without feature selection).	CRFV2 (17)	Cyst HEM HCC MET	74.4	83.3 85.7 50.0 93.3
Module 4: GA-*k*NN based CAC system for classification of focal liver lesions (with feature selection).	Reduced CRFV2 (5)	Cyst HEM HCC MET	78.3	100 44.0 100 80.0

Note: HEM: Hemangioma, HCC: Hepatocellular carcinoma, MET: Metastatic carcinoma, OCA: Overall classification accuracy (%), ICA: Individual classification accuracy (%)

6.5 Limitations and Future Scope

Even though it is demonstrated that texture analysis is a very adequate tool for classifying the diffused and focal liver disease into various classes, it does not discriminate completely. Also, a

limitation of the present work is that it has been carried out on a limited dataset. Following are the recommendations for future work:

(*i*) In the present work, 42 digital B-mode renal US images recorded by Siemens ACUSON X300 ultrasound machine have been used. The efficacy of the proposed CAC system designs should also be tested on the images recorded by different US machines.

(*ii*) Performance of some transform domain feature extraction methods (such as Fourier power spectrum, select transform, non-subsampled contourlet transform etc.) for grading of fatty liver disease and classification of focal liver lesions should be investigated.

References

[1] http://www.webmd.com/digestive-disorders/.

[2] http://www.hopkinsmedicine.org/healthlibrary/.

[3] http://www.medscape.org/noscan/.

[4] G.Li, Y.Luo, W.Deng, X.Xu, A.Liu, and E.Song, "Computer Aided Diagnosis of Fatty Liver Ultrasonic Images Based on Support Vector Machine," Proc. IEEE Eng. Med. Biol. Soc., IEEE Press,vol.2008, Aug. 2008, pp. 4768–4771.

[5] B.K. Raja, M. Madheswaran and K. Thyagarajah, "A Hybrid Fuzzy-Neural System for Computer-Aided Diagnosis of Ultrasound Kidney Images using Prominent Features," J. Med. Syst., vol.32, Feb 2008, pp. 65–83.

[6] W.contributors, 'Liver', [Online]. Available: http://en.wikipedia.org/wiki/Liver. [Accessed 30 May 2014].

[7] G.Bedogni, L.Miglioli, F.Masutti, C.Tiribelli, G.Marchesini, S.Bellentani, "Prevalence of and risk factors for non-alcoholic fatty liver disease", the Dionysos nutrition and liver study. Hepatology, vol. 42, 2005, pp. 44-52.

[8] H.Y.Ma, Z.Zhou, S.Wu, Y.L.Wan, and P.H.Tsui, "A Computer-Aided Diagnosis Scheme for Detection of Fatty Liver In Vivo Based on Ultrasound Kurtosis Imaging," J. Med. Syst, vol. 40, 2016, doi: 10.1007/s10916-015-0395-z.

[9] U.R.Acharya, H.Fujita, V.K.Sudarshan, M.R.K.Mookiah, J.E.W. Koh, J.H. Tan, Y. Hagiwara, C.K.Chua, S.P. Junnarkar, A. Vijayananthan, and K.H. Ng, "An Integrated Index for Identification of Fatty Liver Disease using Radon Transform and Discrete Cosine Transform Features in Ultrasound Images", J. of Information Fusion, vol. 31, 2016, pp. 43-53.

[10] T.Akiyama,. M .Saito, N.Taniguchi, K.Itoh, "Tissue Characterization by using Fractal Dimension of B-Scan Image", Proc. IEEE Ultrasonics Symp, IEEE Press, vol. 3, Dec. 1990, pp. 1353-1355.

[11] Y.M. Kadah, A.A. Farag, J.M. Zurada, A.M. Badawi, and A.M. Youssef, "Classification Algorithms for Quantitative Tissue Characterization of Diffuse Liver Disease from Ultrasound Images", IEEE Trans. Med. Imaging, vol. 15, 1996, pp. 466–478.

[12] J.W. Jeong, S. Lee, J. Won Lee, D.S. Yoo and S. Kim 2004, "Computer-Assisted Sonographic Analysis of the Hepatorenal and Textural Features for the Diagnosis of the

Fatty Liver," Proc. IEEE Eng. Med. Biol. Soc., IEEE Press, vol.3, Sep. 2005, pp. 3348–3350.

[13] G. Li, Y. Luo, W. Deng, X. Xu, A. Liu, and E. Song, "Computer Aided Diagnosis of Fatty Liver Ultrasonic Images Based on Support Vector Machine", Proc. IEEE Eng. Med. Biol. Soc., IEEE Press, vol.2008, Aug. 2008, pp. 4768–4771.

[14] R. Ribeiro and J. Sanches, "Fatty liver characterization and classification by ultrasound in Pattern Recognition and Image Analysis", H. Araujo, A.M. Mendonca, A.J. Pinho, M.I. Torres, Eds. Berlin Heidelberg: Springer, vol. 5524, 2009, pp. 354–361.

[15] B.A. Neuschwander-Tetri, S.H.Caldwell, "Nonalcoholic steatohepatitis: summary of an AASLD", Single Topic Conference. Hepatology, vol. 37, 2003, pp. 1202–1219.

[16] D.G. Tiniakos, M.B. Vos, E.M. Brunt, "Nonalcoholic fatty liver disease: pathology and pathogenesis", Annu Rev Pathol, vol.5, 2010, pp. 145–171.

[17] G.Targher, G.Arcaro, "Non-alcoholic fatty liver disease and increased risk of cardiovascular disease", Atherosclerosis, vol.191, 2007, pp.235–240.

[18] A.Kotronen, H.Yki-Jarvinen, "Fatty liver, A novel component of the metabolic syndrome", Arterioscler Thromb Vasc Biol, vol.28 , 2008, pp. 27– 38.

[19] J.D.Browning, L.S. Szczepaniak, R.Dobbins, P.Nuremberg, J.D.Horton, J.C.Cohen, S.M. Grundy, H.H.Hobbs, "Prevalence of hepatic steatosis in an urban population in the United States: impact of ethnicity",. Hepatology, vol 40, 2004, pp.1387–1395.

[20] S.Mottillo, K.B.Filion, J.Genest, L.Joseph, L.Pilote, P.Poirier, S.Rinfret, E.L.Schiffrin, M.J.Eisenberg, "The metabolic syndrome and cardiovascular risk a systematic review and meta-analysis", J of Am Coll Cardiol, vol.56, 2010, pp.1113–1132.

[21] G.Targher, F.Marra, G. Marchesini, "Increased risk of cardiovascular disease in non-alcoholic fatty liver disease: causal effect or epiphenomenon", Diabetologia, vol.51,2008, pp.1947– 1953.

[22] S. Strauss, E. Gavish, P. Gottlieb and L. Katsnelson, "Interobserver and Intraobserver Variability in the Sonographic Assessment of Fatty Liver", J of Am. J. Roentgenol., vol. 189, Dec. 2007, pp. W320–W323.

[23] K.R .Reddy, E.Schiff , "Approach to a liver mass", Seminars in liver disease, vol.13, 1993, pp. 423-435.

[24] J.Virmani, V.Kumar, N. Kalra and N. Khandelwal, "A rapid approach for prediction of liver cirrhosis based on first order statistics", Proceedings of the IEEE International Conference on Multimedia, Signal Processing and Communication Technologies, IMPACT-2011, Aligarh Muslim University, AMU, Aligarh, India 2011, pp. 212–215.

[25] J.Virmani, V.Kumar, N. Kalra and N. Khandelwal, "Prediction of liver cirrhosis based on multiresolution texture descriptors from B-mode ultrasound", International Journal of Convergence Computing, 1, In Press, (forthcoming). [Epub Ahead of print], 2013,.

[26] J.A.Bates, "Abdominal ultrasound how why and when", 2nd edn. (Philadelphia, USA: Chrchill Livingstone, An imprint of Elsevier Limited), vol.193, 2004, pp. 80–107.

[27] J.A Soye, C..P.Mullan, S.Porter, H.Beattie, A.H.Barltrop, and W.M.Nelson, "The use of contrast-enhanced ultrasound in the characterisation of focal liver lesions", J of Ulster Medical, vol.76, 2007, pp. 22–25

[28] A.L.Baert, K.Sartor, "Focal liver lesions -detection, characterization, ablation", (New York: Springer Berlin Heidelberg), 2005, pp. 167–177.

[29] J.Hardling and Callaway, "Ultrasound of focal liver lesions", Rad Magazine, vol.36, 2010, pp. 33–34.

[30] R.B.Jeffery and P.W.Ralls, "Sonography of abdomen", (New York: Raven Press), (1995),.

[31] S.Namasivayam, K.Salman, P.K.Mittal, D.Martin and W.C.Small, "Hypervascular hepatic focal lesions: spectrum of imaging features",. Current Problems in Diagnostic Radiology, vol.36, 2007, pp.107–123.

[32] S.G. Mougiakakou, I.K.Valavanis, A.Nikita, and K.S.Nikita, "Differential diagnosis of CT focal liver lesions using texture features, feature selection and ensemble driven classifiers", Artificial Intelligence in Medicine, vol.41, 2007, pp. 25–37.

[33] J.H.Pen, P.A.Pelckmans, Y.M.V.Maercke, H.R.Degryse, and A.M.D.Schepper, "Clinical significance of focal echogenic liver lesions", Gastrointestinal Radiology, vol.11, 1986, pp. 61–66.

[34] F. Minhas, D.Sabih, and M.Hussain, "Automated classification of liver disorders using ultrasound images", Journal of Medical Systems, vol.36, 2012, pp. 3163–3172.

[35] J.Virmani, V.Kumar, N. Kalra and N. Khandelwal, "SVM based characterization of Liver cirrhosis by singular value decomposition of GLCM matrix", International Journal of Artificial Inteligence and Soft Computing, vol.3, 2013, pp. 276–296.

[36] J.Virmani, V.Kumar, N. Kalra and N. Khandelwal, "SVM based characterization of liver ultrasound images using wavelet packet texture descriptors", Journal of Digital Imaging, vol.25, 2012, pp.No. 5, DOI 10.1007/s10278-012-9537-8, [Epub Ahead of print].

[37] M.Tsurusaki, R.Kawasaki, M.Yamaguchi, K.Sugimoto, T. Fukumoto, Y.Ku, and K.Sugimura, "Atypical hemangioma mimicking hepatocellular carcinoma with a special note on radiological and pathological findings", J of Radiology, vol.27, 2009, pp.156–160.

[38] J.I.Marsh, R.G.Gibney, and K.B.David, "Hepatic hemangioma in the presence of fatty infiltration: An atypical sonographic appearance", Gastrointestinal Radiology, vol.14, (1989), pp. 262–264.

[39] Y.Kimura, R.Fukada, S. Katagiri, and Y.Matsuda, "Evaluation of hyperechoic liver tumors in MHTS. Journal of Medical Systems", vol.17, 1993, pp. 127–132.

[40] R.Sekiguchi, A.Kuwajima, M.Nagamoto, H. Ohno, and M.Tamura, "Hepatocellular carcionoma: The diagnostic difficulties of ultrasonography and analysis of risk factors in MHTS", J of Medical Systems, vol.17, 1993, pp.133–137.

[41] W.Scheible, B.B.Gosink, G.R. Leopold, "Gray scale echographic patterns of hepatic metastatic disease", J of Roentgenology, vol.129, 1977, pp. 983–987.

[42] J.Virmani, V.Kumar, N. Kalra, and N. Khandelwal, "Characterization of primary and secondary malignant liver lesions from B-mode ultrasound", J of Digital Imaging, vol.26, 2013, pp. No.1, DOI 10.1007/s10278-013-9578-7. [Epub Ahead of print].

[43] D.Mittal, V.Kumar, S.C.Saxena, and N.Khandelwal, "Neural network based focal liver lesion diagnosis using ultrasound images", Computerized Medical Imaging and Graphics, vol.35, 2011, pp. 315–323.

[44] H.Yoshida, D.D.Casalino,B.Keserci, "Wavelet packet based texture analysis for differentiation between benign and malignant liver", J of Physics in Medicine & Biology, vol.48, 2003, pp.3735–3753.

[45] A.M.Badawi, A.S.Derbala, and A.M.Youssef, "Fuzzy logic algorithm for quantitative tissue characterization of diffuse liver diseases from ultrasound images", J of Medical Informatics, vol.55, 1999, pp.135–147.

[46] K.M.Horton , D.A .Bluemke ,R.H. Hruban, "CT and MR imaging of benign hepatic and biliary tumors", J of Radiographics vol.19, 1999, pp. 431-51

[47] A.S.Fulcher, R.K.Sterling, "Hepatic Neoplasms", J of Clin Gastroenteol, vol.34, 2002,pp. 463-71.

[48] S.Namasivayam, K.Salman, P.K.Mittal, D.Martin, W.C.Small, "Hypervascular hepatic focal lesions: spectrum of imaging features", Current Problems in Diagnostic Radiology, vol.36, 2007, pp. 107–123.

[49] H.Sujana, S.Swarnamani, and S.Suresh, "Application of artificial neural networks for the classification of liver lesions by image texture parameters", J of Ultrasound in Medicine & Biology, vol.22, 1996, pp.1177–1181.

[50] S.Poonguzhali, B.Deepalakshmi, and G.Ravindran, "Optimal feature selection and automatic classification of abnormal masses in ultrasound liver images", IEEE-ICSCN, MIT Campus, Anna University, Chennai, India, vol.25, 2007, pp.67–70.

[51] J.A.Soye, C.P.Mullan, S. Porter, H.Beattie, A.H.Barltrop, and W.M.Nelson, "The use of contrast-enhanced ultrasound in the characterisation of focal liver lesions", The Ulster Medical Journal, vol.76, 2007, pp.22–25.

[52] S.G.Mougiakakou, I.K.Valavanis, A.Nikita, K.S.Nikita, "Differential diagnosis of CT focal liver lesions using texture features, feature selection and ensemble driven classifiers", Artificial Intelligence in Medicine, vol.41, 2007, pp. 25–37.

[53] J.Harding, M.Callaway, "Ultrasound of focal liver lesions", RAD Magazine, vol.36, 2010, pp.33–34.

[54] D.Mittal, V.Kumar, S.C.Saxena, and N.Khandelwal, "Neural network based focal liver lesion diagnosis using ultrasound images", J of Computerized Medical Imaging and Graphics, vol.35, 2011, pp.315–323.

[55] A. Ahmadian, A. Mostafa, M. Abolhassani, N. Alam, and . Gitti, "An Efficient Texture Feature Extraction Method for Classification of Liver Sonography Based on Gabor Wavelet", Medicon, vol.2, 2004, pp.73-80.

[56] S.H.Kim, J.M. Lee, K.G.Kim, J.H.Kim, J.Y.Lee, J.K.Han, B.I.Choi , "Computer-aided image analysis of focal hepatic lesions in ultrasonography", preliminary results. Abdom Imaging , vol.34(2) , 2009, pp.183–91.

[57] C.Lee, S.H.Chen, "Gabor wavelets and SVM classifier for liver diseases classification from CT images", In: Proceedings of IEEE International Conference on Systems, Man, and Cybernetics, 2006, pp.548– 552

[58] Y.M.Kadah, A.A.Farag, J.M.Zurada, A.M.Badawi, and A.M.Youssef, "Classification algorithms for quantitative tissue characterization of diffuse liver disease from ultrasound images," IEEE Transactions on Medical Imaging, vol.15, 1996, pp. 466–478.

[59] A. Wieckowska, A.E. Feldstein, "Diagnosis of non-alcoholic fatty liver disease: invasice versus noninvasive", J of Semin Liver Dis, vol.28, 2008, pp.386-395.

[60] K.Fukunaga, "Introduction to statistical pattern recognition", (New York: Academic Press), vol.22, 1990, pp. 833-834.

[61] M. B. Subramanya, V. Kumar, S. Mukherjee, and M. Saini, "A CAD System for B-Mode Fatty Liver Ultrasound Images Using Texture Features", J.of Med. Eng. Technol., vol. 39, Feb.2015, pp. 123-130

[62] J.M.Thijssen, A.Starke, G.Weijers, A.Haudum, K. Herzog, P. Wohlsein, J. Rehage, C.L.D Korte, "Computer-aided Bmode ultrasound diagnosis of hepatic steatosis: a feasibility study", IEEE Trans Ultrason Ferroelectric Freq Control, vol.55(6), 2008, pp. 1343–1354.

[63] M.K. Yasser, A.F. Aly, M.Z. Jacek, M.B. Ahmed, Abou-Bakr MY. "Classification algorithms for quantitative tissue characterization of diffuse liver disease from ultrasound images", IEEE transaction on medical imaging vol.15, 1996, pp.466-477.

[64] W.C. Yeh, Y.M. Jeng, C.H. Li, P.H. Lee, P.C. Li., "Liver fatty change classification using 25MHz high frequency ultrasound", IEEE ultrasonics symphosium vol.3, 2004, pp.2169-2172.

[65] S.Mukherjee, A.Chakravorty, K.Ghosh, M.Roy, A.Adhikari, S.Mazumdar, "Corroborating the subjective classification of ultrasound images of normal and fatty human livers by the radiologist through texture analysis and SOM", IEEE 15th International Conference on Advanced Computing and Communications , 2007, pp. 197-202.

[66] R.Ricardo, S. Joao. "Fatty liver characterisation and classification by ultrasound. Pattern recognition and image analysis", Lecture notes in computer science vol.5524, 2009, pp.354-361.

[67] A.Andreia, S.S. Jose, S.Jaime, B.S. Pedro. "Classifier approaches for liver steatosis using ultrasound images", J of Procedia technology, vol.5, 2012, pp.763-770.

[68] M. Singh, S. Singh, S. Gupta. "A new quantitative metric for liver classification from ultrasound images", J of computer and electrical engineering, vol.4, 2012, pp.605-607.

[69] L.A. Adams, J.A. Talwalkar, "Diagnostic evaluation of non-alcoholic fatty liver disease", J of clin Gastroenterolo, vol.40, 2006, pp.S34-S38.

[70] J.W.Jeong,S.Lee, J.Won Lee, D.S.Yoo, S.Kim, "Computer assisted Sonographic Analysis of the Hepatorenal and Textural Features for the Diagnosis of the Fatty Liver," Proceedings of the 2005 IEEE Engineering in Medicine and Biology, 2005, pp.1-4.

[71] F. Minhas, D. Sabih, M. Hussain. "Automated classification of liver disorders using ultrasound images", J of Med Syst vol.36, 2012, pp.3163-3172.

[72] U.R. Acharya, S.V. Sree, R. Ribeiro, G. Krishnamurthi, R.T. Marinho, J. Sanches, J.S. Suri. "Data mining framework for fatty liver disease classification in ultrasound: a hybrid feature extraction paradigm", J of Med Phys, vol.39, 2012, pp.4255-4264.

[73] M.M. Dan, G. Vasile, I.T. Corneliu, P. Alina, S. Ioan. "Computer aided diagnosis method for steatosis rating in ultrasound images using random forests", J of Med Ultrason vol.15, 2013, pp 184-190.

[74] U.R.Acharya, H.Fujita, S.Bhat, U.Raghaventra, A.Gudigar, F.Molinari, A.Vijayanathan, K.H. Ng. "Decision support system for fatty liver disease using GIST descriptors extracted from ultrasound images", J of Information Fusion, vol.29, 2016, pp.32-39.

[75] X.Wang, X, J.Wang, D.Li, T.Wang, C. Zheng, and Y.Cheng, "B-scan ultrasonic image recognition of fatty liver based on texture analysis", J of Space Med Eng, vol. 17, 2004, pp.144–148.

[76] I.Akiyama, T.Saito, M.Nakamura, N. Taniguchi, and K.Itoh, "Tissue characterization by using fractal dimension of B-scan image", Ultrasonics symposium, vol.3, 1990, pp. 1353-1355.

[77] S. Yatsuji, E. Hashimoto, M. Tobari, M. Taniai, K. Tokushige, K. Shiratori, "Clinical features and outcomes of cirrhosis due to non-alcoholic steatohepatitis compared with cirrhosis caused by chronic hepatitis C", J.of Gastroenterol. Hepatol, vol.24 (2), 2009, pp. 248–254.

[78] I.Guyon, J.Weston, S.Barnhill, V.Vapnik, "Gene selection for cancer classification using support vector machines", J of Machine Learn , vol.46, 2002, pp.1–39.

[79] D.Mittal, V.Kumar, S.C.Saxena, and N.Khandelwal, "Neural network based focal liver lesion diagnosis using ultrasound images", J of Computerized Medical Imaging and Graphics, vol.35, 2011, pp.315–323.

[80] A.J.Sanyal "American gastroenterological association. AGA technical review on non-alcoholic fatty liver disease", Gastroenterology, vol.123, 2002, pp.1705-1725.

[81] J.Virmani, V.Kumar, N.Kalra and N.Khandelwal, "Prediction of Cirrhosis Based on Singular Value Decomposition of Gray Level Co-Occurrence Matrix and a Neural Network Classifier", Proc. IEEE Developments in E-Systems Engineering (DeSE), IEEE Press, 2011, pp. 146–151.

[82] D.Amarapurkar, P.Kamani, N.Patel, P.Gupte, P.Kumar, S.Agal, R.Baijal, S.Lala, D.Chaudhary, A.Deshpande, "Prevalence of non-alcoholic fatty liver disease population based study",.J of Ann Hepatol , vol.6, 2007, pp.161-163.

[83] S.A.Harrison, S.Torgerson, P.H.Hayashi, "The natural history of non-alcoholic fatty liver disease, a clinical histopathological study", J of Am J Gastroenterol, vol.98, 2003, pp.2042- 2047.

[84] H.Hyogo, K.Chayama, S.I.Yamagishi, "Nonalcoholic fatty liver disease and cardiovascular disease", J of Curr. Pharm. Des, vol.20(14), 2013, pp.2403–2411.

[85] G.Targher, A.Mantovani, I.Pichiri, et al., “Non-alcoholic fatty liver disease is associated with an increased prevalence of atrial fibrillation in hospitalized patients with type 2 diabetes”, J of Clin. Sci, vol.125, 2013, pp.301–309.

[86] L.S. Bhatia, N.P. Curzen, P.C. Calder, C.D. Byrne, “Non-alcoholic fatty liver disease: a new and important cardiovascular risk factor?”, J of Eur. Heart, vol.33(10), 2012, pp. 1190–1200.

[87] G. Calori, G. Lattuada, F. Ragogna, et al., “Fatty liver index and mortality: the Cremona study in the 15th year of follow-up”,J of Hepatology, vol.54(1), 2011, pp.145–152.

[88] J.S.Ahn, D.H.Sinn, G.Y.Gwak, et al., “Steatosis among living liver donors without evidence of fatty liver on ultrasonography: potential implications for preoperative liver biopsy”, Transplantation , vol.95(11), 2013, pp.1404–1409.

[89] L.A.Adams, J.F.Lymp, J.Sauver, et al., “The natural history of nonalcoholic fatty liver. disease: a population based cohort study”, J of Gastroenterology, vol.129(1), 2005, pp.113–121.

[90] J.R.Lewis, S.R.Mohanty, “Nonalcoholic fatty liver disease: a review and update”, J of Dig. Dis. Sci, vol.55 (3), 2010, pp.560–578.

[91] A.E.Feldstein, P.Charatcharoenwitthaya, S.Treeprasertsuk, J.T.Benson, F.B.Enders, P. Angulo, “The natural history of non-alcoholic fatty liver disease in children: a follow-up study for up to 20 years”, J of Gut ,vol.58(11) , 2009, pp.1538–1544.

[92] M.Stepanova, N.Rafiq, H.Makhlouf, et al., “Liver-related mortality in patients with non-alcoholic fatty liver disease (NAFLD)”, J of Dig. Dis. Sci, vol.58(10), 2013, pp.3017–3023.

[93] K.Mala, V.Sadasivam, “Classification of fatty and cirrhosis liver using waveletbased statistical texture features and neural network classifier”, J.of Softw.Inform, vol. 4(2), 2010, pp. 151–163.

[94] M.S. Ascha, I.A. Hanounch, R. Lopez, T.A.R. Tamini, A.F. Feldstein, N.N. Zein, “The incidence and risk factors of hepatocellular carcinoma in patients with non-alcoholic steatohepatitis”, J of Hepatology, vol.51, 2010, pp.1972-1978.

[95] S.H. Kim, J.M.Lee, K.G.Kim, J.H.Kim, J.Y.Lee, J.K.Han, B.I.Choi, “Computer-aided image analysis of focal hepatic lesions in ultrasonography, preliminary results”, J of Abdom Imaging , vol.34(2), 2009, pp.183–191.

[96] S.Singh, V.Kumar, H.K.Verma, D.Singh, “SVM based system for classification of microcalcifications in digital mammograms”,. In: 28th annual international conference of the IEEE engineering in medicine and biology society EMBS, vol.06, 2006, pp. 47-54.

[97] Y.L Huang, K.L Wang, D.R Chen: “Diagnosis of breast tumors with ultrasonic texture analysis using support vector machines”, Neural Comput & Applic, vol.15, 2006, pp.164–169.

[98] J. Virmani, V. Kumar, N. Kalra, and N. Khandelwal, “Characterization of Primary and Secondary Malignant Liver Lesions from B-Mode Ultrasound”, J.of Digit. Imaging, vol. 26, Dec. 2013, pp. 1058–1070.

[99] T Poynard, F Imbert-Bismut, V Ratziu, S.Chevret, C .Jardel, et al.“Biochemical markers of liver fibrosis in patients infected by hepatitis C virus: longitudinal validation in a randomized trial”, J of Viral Hepatitis, vol.9, 2002, pp. 128-133.

[100] S. Nawaz and A.H. Dar, “Hepatic Lesions Classification by Ensemble of SVMs Using Statistical Features Based on Co-Occurrence Matrix”, Proc. 4th IEEE International Conference on Emerging Technologies, IEEE Press, Oct. 2008, pp. 21–26.

[101] Y.L.Huang, D.R.Chen, Y.R.Jiang, J.Kuo, H.K.Wu, W.K.Moon, “Computer-Aided Diagnosis using Morphological Features for Classifying Breast Lesions on Ultrasound”, J of Ultrasound Obstet. Gynecol, vol. 32, Sep. 2008, pp. 565–572.

[102] N.Manth, J.Virmani, V.Kumar, N.Kalra, N.Khandelwal, “Application of texture features for classification of primary benign and primary malignant focal liver lesions”, Image Feature Detectors and Descriptors, A.A.Awad and M.Hassaballah, Eds. Berlin Heidelberg: Springer, vol. 630, 2016, pp. 385-409.

[103] Y.L.Huang, K.L.Wang and D.R.Chen, “Diagnosis of Breast Tumors with Ultrasonic Texture Analysis using Support Vector Machines”, J of Neural Computing and Applications, vol. 15, 2006, pp. 164–169.

[104] E. Akbal, S. Koklu, E. Kocak, et al., “Liver fatty acid-binding protein is a diagnostic marker to detect liver injury due to chronic hepatitis C infection”, J of Arch. Med. Res,.vol. 44(1), 2013, pp. 34–38.

[105] A.M.Zaitoun, H.A.Mardini, S.Awad, S.Ukabam, S.Makadisi, C.O.Record, “Quantitative assessment of fibrosis and steatosis in liver biopsies from patients with chronic hepatitis C”, J.of Clin. Pathol. vol.54, 2001, pp. 461–465.

[106] A.M.Youssef, D.Schlaps, W.J.Lorenz, “Ultrasound textural synthesis using 2-D autoregressive models for pathology characterization”, J of Proc. SPIE-87, vol.768, 1987, pp. 201-206.

[107] C.D.Williams, J.Stengel, M.I.Asike et al., “Prevalence of non-alcoholic fatty liver disease and non-alcoholic steatohepatitis among a largely middle-aged population utilizing

ultrasound and liver biopsy", a prospective study Gastroenterology, vol.140, 2011, pp. 124-131.

[108] J.Virmani, V.Kumar, N.Kalra, N.Khandelwal, "Characterization of Primary and Secondary Malignant Liver Lesions from B-Mode Ultrasound", J.of Digit. Imaging, vol. 26, Dec. 2013, pp. 1058–1070.

[109] J. Virmani, V. Kumar, N. Kalra and N. Khandelwal, "Prediction of Liver Cirrhosis Based on Multiresolution Texture Descriptors from B-Mode Ultrasound", J. of Convergence Computing, vol. 1, Jan. 2013, pp. 19–37.

[110] A.M. El-Badry, S. Breitenstein, W. Jochum, et al.," Assessment of hepatic steatosis by expert pathologists: the end of a gold standard", Ann. Surg, vol.250 (5), 2009, pp. 691–697.

[111] T.Zielke, P.Nauth, N.Stein, W.V Seelen, E. G.Loch, A. Gaca, "Quantitative techniques in ultrasonic diagnosis", J of Radiologe, vol. 25, 1985, pp. 486-73.

[112] U.Reath, D.Schlaps, B.Limberg, "Diagnostic Accuracy of computerized B-Scan texture analysis and conventional ultrasonography in diffuse parenchymal and malignant liver disease", J of Clinical Ultrasound, vol. 13, 1985, pp. 87-89.

[113] Y.L. Huang, K.L. Wang and D.R. Chen, "Diagnosis of Breast Tumors with Ultrasonic Texture Analysis using Support Vector Machines", J of Neural Computing and Applications, vol. 15, Apr. 2006, pp. 164–169.

[114] C.C.Chang, C.J. Lin, LIBSVM, a library of support vector machines. Software available at http://www.csie.ntu.edu.tw/~cjlin/libsvm. [Accessed 15 June 2012].

[115] R.J.Nandi, A.K.Nandi, R.M.Rangayyan, D.Scutt, "Classification of breast masses in mammograms using genetic programming and feature selection", J of Med Biol Eng Comput, vol.44(8), 2006, pp.683–694.

[116] B.Oluleye, A.Leisa, J.Leng, D.Dean, "Zernike Moments and Genetic Algorithm : Tutorial and Application", J of Mathematics & Computer Science, vol.4(15), 2014, pp.2217-2236.

Appendix A

List of Publications

[1] **H.Kothari, J.Virmani, N.J.Singh,** "Evaluating the efficacy of second order statistical features for classify of fatty liver diseases" in Proceedings of IEEE international conference CSNT-2016, Chitkara university, Chandigarh. [Status: Accepted]

Appendix B

Originality Report